

A spectral line survey in the $\lambda 2$ and $\lambda 1.3$ mm windows toward the carbon rich envelope of IRC +10216

J. H. He^{1,2}, Dinh-V-Trung¹, S. Kwok^{3,1}, H. S .P. Müller⁴, Y. Zhang³, T. Hasegawa¹, T. C. Peng¹ and Y. C. Huang¹

ABSTRACT

We present the results of our spectral line surveys in the 2 mm and 1.3 mm windows toward the carbon rich envelope of IRC +10216. Totally 377 lines are detected, among which 360 lines are assigned to 57 known molecules (including 29 rare isotopomers and 2 cyclic isomers). Only 17 weak lines remain unidentified. Rotational lines of isotopomers ^{13}CCH and $c\text{-}^{13}\text{CCCH}$ are detected for the first time in IRC +10216. The detection of the formaldehyde lines in this star is also confirmed. Possible abundance difference among the three ^{13}C substituted isotopic isomers of HC_3N is reported. Isotopic ratios of C and O are confirmed to be non-solar while those of S and Si to be nearly solar. Column densities have been estimated for 15 molecular species. Modified spectroscopic parameters have been calculated for NaCN , Na^{13}CN , KCN and SiC_2 . Transition frequencies from the present observations were used to improve the spectroscopic parameters of Si^{13}CC , $^{29}\text{SiC}_2$ and $^{30}\text{SiC}_2$.

Subject headings: line: identification — radio lines: ISM — stars: AGB and post-AGB — stars: individual (IRC +10216) — surveys

1. Introduction

IRC +10216 (CW Leo) is a nearby AGB star with heavy mass loss of about $3 \times 10^{-5} M_{\odot} \text{yr}^{-1}$. The distance to IRC +10216 is estimated to be in the range of 120-150 pc

¹Institute of Astronomy and Astrophysics, Academia Sinica, P.O. Box 23-141, Taipei 10617 Contact author: J.H. He, email: jhhe@asiaa.sinica.edu.tw

²National Astronomical Observatories/Yunnan Observatory, Chinese Academy of Sciences, PO Box 110, Kunming, Yunnan Province 650011, PR China

³Department of Physics, Faculty of Science, University of Hong Kong, Pokfulam Road, Hong Kong

⁴I. Physikalisches Institut, Universität zu Köln, Zùlpicher Str. 77, 50937 Köln, Germany

(Groenewegen et al. 1998; Lucas & Guélin 1999). The combination of proximity and the massive expanding envelope created by the high mass loss rate makes IRC+10216 one of the strongest sources of continuum and molecular line emission in the radio sky. Over 60 molecular species have been identified in IRC +10216, some of which are unique to this source. The rich molecular inventory is the result of active photochemistry and molecule-radical reactions initiated by the penetration of interstellar UV photons into the outer envelope of IRC +10216 (Cherchneff et al. 1993; Millar & Herbst 1994; Millar et al. 2000).

Due to the expansion of the envelope, the physical conditions (i.e., temperature, gas density, and infrared radiation field) vary greatly within the envelope of IRC +10216. Such condition allows the excitation of many different molecular species by collisions with hydrogen molecules. We expect that line emission from not too heavy molecules such as diatomic or triatomic molecules and simple carbon chains to be strong in the millimeter region.

Several spectral line surveys have been carried out toward IRC +10216. The most comprehensive and most sensitive surveys to date are those of Cernicharo, Guélin, & Kahane (2000) (CGK survey) in the 2 mm window (129 – 172.5 GHz) with the IRAM 30 M telescope and Kawaguchi et al. (1995) in the 30 – 50 GHz range with Nobeyama 45 M telescope. In other wavelength regions, the other surveys (Avery et al. 1992 and Groesbeck et al. 1994 in the 230 and 345 GHz bands, respectively, Johansson et al. 1985 in the 70 – 115 GHz band) have lower sensitivity.

The advent of millimeter and sub-millimeter radio interferometers with wide frequency coverage such as the SMA (Sub-Millimeter Array), CARMA and PdBI highlights the need for sensitive spectral line survey in these wavelength regions to serve as a guide for future interferometric observations of circumstellar envelopes. In this paper we present sensitive spectral line surveys toward IRC +10216 in the 2 mm (130 – 160 GHz) and 1.3 mm (219.5 – 267.5 GHz) regions using the radio telescopes of the Arizona Radio Observatory (ARO).

2. Observations and data reduction

The surveys were carried out using the λ 2 mm receiver of the Arizona Radio Observatory (ARO) 12M Telescope (KP12M) at Kitt Peak (April 26, 2005 to April 29, 2006) and the λ 1.3 mm JT receiver of the Heinrich Hertz submillimeter Telescope (SMT) at Mt. Graham (October 31, 2005 to January 24, 2007). Observed frequency ranges are 131.2-160.3 GHz for the λ 2 mm survey, 219.5-245.5 and 251.5-267.5 GHz for the λ 1.3 mm survey. The sky subtraction was made with beam switch with a beam throw of 2 arcmin in azimuth at a rate of 1.25 Hz (KP12M) or 1 Hz (SMT). The receivers were configured in single sideband (SSB)

dual polarization mode. At the KP12M telescope, the image sideband signal was rejected by tuning the backshots, while for the SMT telescope, Martin-Pupplet filter was used to reject the image sideband. The image rejection ratio was usually better than 20 dB. Millimeter Auto-Correlators (MAC, 3072 channels, 0.195 MHz per channel) were used for the $\lambda 2$ mm survey, while Forbes Filterbanks (FFBS, 1024 channels, 1 MHz per channel) were used for the $\lambda 1.3$ mm survey. The antenna temperature scale was determined by vane calibration. Typical system temperature T_{sys} was 250 K for the $\lambda 2$ mm data and 400 K for the $\lambda 1.3$ mm data (below 300 K and 500 K for 44% and 88% of all data, respectively). An integration of one hour resulted in a typical sensitivity in T_{R}^* or T_{A}^* of about 10-20 mK for a resolution of 1 MHz in both surveys. The atmospheric opacity was better than 0.2 and 0.4 for 60% and 90% of our data (in both 1.3 mm and 2 mm ranges), respectively. Both repeated observations by engineer and the analysis of the $T_{\text{sys}} - e^{-\tau_0 A}$ relation of our data (τ_0 is zenith atmospheric opacity, A is airmass) demonstrate a relative calibration uncertainty (repeatability) within 10% (adopted in the determination of excitation temperatures and isotopic ratios). However, the absolute calibration error could be higher than this (we adopt 20% for the determination of column density).

The data were reduced using the Gildas software package CLASS. Bad scans were discarded and bad channels were removed. Baseline was removed by fitting low order (typically 1-2 order) of polynomial to it. With the fixed LO and IF (IF = 5 and 1.5 GHz for the 1.3 mm and 2 mm surveys respectively), we identified several mirror line features of strong lines from the image sideband that leaked through the image rejection filters, using our spectra observed 10 or 3 GHz apart. For several scans near the higher and lower ends of our surveyed frequency ranges, strong lines found by other surveys (Cernicharo et al. 2000; Avery et al. 1992) were used to check possible image sideband contamination. The image sideband contamination features have been marked in the spectral plots in Fig 3.

The $\lambda 2$ mm survey data were recorded in T_{R}^* , the antenna temperature corrected for atmospheric attenuation, Ohmic loss and rearward and forward scattering and spillover. A corrected mainbeam efficiency of $\eta_{\text{m}}^* = 0.75$ (from the KP12M telescope manual) was used to derive the mainbeam temperature through $T_{\text{mb}} = T_{\text{R}}^*/\eta_{\text{m}}^*$. The FWHM beam size of the KP12M is $43''$ at 145 GHz.

The $\lambda 1.3$ mm survey data were recorded in T_{A}^* , the antenna temperature corrected for atmospheric attenuation, Ohmic loss and rearward scattering and spillover. A special main beam efficiency of η_{m} was used to calculate the mainbeam temperature through $T_{\text{mb}} = T_{\text{A}}^*/\eta_{\text{m}}$, where $\eta_{\text{m}} = 0.65$ for polarization channel A and 0.55 for channel B (private communication with Dr. William Peters at ARO). The FWHM beam size of the SMT is $31''$ at 240 GHz.

3. Line identification

Line identification was performed by using Cologne Database for Molecular Spectroscopy (CDMS, see Müller et al. 2001, 2005)¹ and the Molecular Spectroscopy database of Jet Propulsion Laboratory (JPL, see Pickett et al. 1998)². The online Lovas line list (Lovas 2004)³ was also frequently consulted to help verify the line identities. We first identified clearly-detected lines. Weaker lines of the identified species (particularly those asymmetric rotors) are then checked by comparing the predicted LTE line intensities from CDMS or JPL catalogues with the spectral data. Especially the line frequency predictions of SiCC isotopologues computed during this work (see details below) helped us identify many unidentified or weak lines. To implement the CDMS and JPL catalogues, we developed several scripts on the basis of CLASS to automate the line identification. Our scripts also invoke the truncated parabolic profile fitting procedure of CLASS to fit the line profiles with an truncated parabolic profile to determine line center frequency and line center antenna temperature. Integrated intensities of blended lines were determined by the profile fitting as well, while those of isolated lines were obtained by direct integration of the observed line profiles.

In the course of the present investigation, entries for a number of molecular species were created for the CDMS as comprehensive predictions were missing in either the CDMS or JPL catalogues. The species are NaCN/NaNC, Na¹³CN/NaN¹³C, KCN/KNC, Si¹³CC, ²⁹SiC₂, and ³⁰SiC₂. In addition, an entry was also provided for the main isotopic species ²⁸SiC₂. The alkali metal cyanides are nearly T-shaped molecules in the gas phase with the M-C bond slightly longer than the M-N bond (van Vaals et al. 1984a,b). Therefore, these species should be considered more as alkali metal isocyanides. However, following the current convention, we still use the designation of cyanides.

NaCN (van Vaals et al. 1984a) and KCN (Kuijpers et al. 1976; Törring et al. 1980; van Vaals et al. 1984b) have been characterized by microwave spectroscopy; the latter also by millimeter-wave spectroscopy. Ab initio calculations (H. S. P. Müller, unpublished) yield very large *a*-dipole moment components of about 8.85 and 9.96 D for NaCN and KCN, respectively, while the *b*-components are only of order of 0.2 D. Laboratory investigations employing molecular beams (van Vaals et al. 1984a,b) permitted *b*-type transitions to be observed despite the small dipole moment component for each molecule. These transitions ensure reasonably good predictions into the millimeter-wave region. Predictions in the upper

¹The CDMS catalogue at <http://www.ph1.uni-koeln.de/vorhersagen/>

²The JPL catalogue at <http://spec.jpl.nasa.gov/home.html>

³The Lovas line list at <http://physics.nist.gov/PhysRefData/Micro/Html/contents.html>

millimeter-wave region or at higher values of K_a should be viewed with caution because of the fairly small datasets, especially in the cases of NaCN and Na¹³CN. Earlier fit of the rotational spectra of these molecules only involved four quartic centrifugal distortion terms (planar reduction). New fits with five such terms from Watson’s S reduction were performed in this work, which was an obvious choice for these asymmetric molecules very close to the prolate limit. The inclusion of NaCN transition frequencies determined through radioastronomical observations have negligible effects on the spectroscopic parameters and their uncertainties. These frequencies were thus omitted from the final fits. The fitted results are given in Table 1. Predictions of the rotational spectra as well as input files to generate these are available in the CDMS.

The rotational spectrum of the main isotopic species of SiC₂ had been studied by Suenram et al. (1989) and Gottlieb et al. (1989). The derived spectroscopic parameters yield sufficiently good predictions for the transitions observed toward IRC +10216 thus far. However, at higher frequencies the predictions become imprecise. The discrepancies between the earlier predictions and observed frequencies reached four times the quoted uncertainties, even though the number of parameters (15) was comparatively large with respect to the number of transition frequencies (34). Trial fits with different sets of spectroscopic parameters showed that a significant improvement was possible if Watson’s S reduction was used instead of the A reduction. But even with two more parameters used in the fit of now 35 lines, the transition frequencies from Gottlieb et al. (1989) could be reproduced to slightly worse than the quoted uncertainties. Therefore, these uncertainties have been increased by 50%. The high order term P_{KKKJ} was estimated from the lower order terms L_{KKJ} , H_{KJ} , and D_{JK} . This parameter set was the starting point for the other isotopic species. The initial data set for Si¹³CC consisted of transition frequencies determined in the laboratory around 350 GHz as well as frequencies from astronomical observations at lower frequencies (Cernicharo et al. 1991). Some Si¹³CC parameters were estimated from those of SiC₂. In the cases of ²⁹SiC₂ and ³⁰SiC₂, transition frequencies were available almost exclusively from astronomical observations (Cernicharo et al. 1991); the $1_{01} - 0_{00}$ transitions had been measured in the laboratory (Suenram et al. 1989). Several spectroscopic parameters were kept fixed to those estimated from SiC₂, because the input data sets are rather small. The $A - (B + C)/2$ were determined by assuming substitutions of the Si atom do not change A , an assumption that usually holds well under similar circumstances. In the final fits for Si¹³CC, ²⁹SiC₂, and ³⁰SiC₂, transition frequencies from the current study were also used. The final sets of spectroscopic parameters have been gathered in Table 2. Predictions of the rotational spectra as well as input files to generate these are available in the CDMS. Because of the limited number of transition frequencies used in the fits all predictions should be taken with great caution.

4. Results

A total of 377 line features are detected in our surveys. Among them, 360 are assigned to 57 known molecules (including 29 rare isotopomers and 2 cyclic isomers). Only 17 weak lines remain unidentified and need further observations to confirm. The two rotational lines from formaldehyde (H_2CO) that were first identified by Ford et al. (2004) in this carbon star are confirmed by our observation. The fact that the $2_{1,2} - 1_{1,1}$ (140840 MHz) line is the strongest line of H_2CO indicates that its excitation temperature could be lower than 10 K.

Overview plots of the λ 1.3 mm and λ 2 mm spectral survey results are shown separately in the two panels of Fig. 1, with all spectra smoothed to a resolution of about 3 MHz. Line features with main beam temperature $T_{\text{mb}} > 0.5$ K in the λ 1.3 mm survey and $T_{\text{mb}} > 0.3$ K in the λ 2 mm survey have been labeled. Weaker features are enlarged in the insets of each panel. The λ 1.3 mm survey results are dominated by strong lines from 11 species: CO, HCN and H^{13}CN with $T_{\text{mb}} > 10$ K; CS, SiS, SiO, CCH, CN and ^{13}CO with $T_{\text{mb}} > 1$ K; SiCC and C^{34}S with $T_{\text{mb}} > 0.5$ K. The λ 2 mm survey results are dominated by strong lines from 7 species: CS, SiS and HC_3N with $T_{\text{mb}} > 1$ K; SiCC and C_4H with $T_{\text{mb}} > 0.5$ K; C_3N and C^{34}S with $T_{\text{mb}} > 0.3$ K.

The overview plot of the λ 2 mm survey in Fig. 1 resembles that of CGK survey, except C^{34}S . But the relative intensity of lines are significantly different. The integrated line intensity ratios between the CGK and our surveys for the strong lines labeled in Fig. 1 have been roughly estimated. All these ratios are larger than 1 because our λ 2 mm survey has larger beam size and so weaker line intensities due to beam dilution. Although the CS, HC_3N and SiCC line intensity ratios are all roughly equal to 3, the average ratios of C_4H and C_3N line ratios are obviously smaller (roughly 1.8 and 2.6, respectively), while that of SiS and C^{34}S are obviously larger (around 5.8 and 3.7, respectively). The smaller line ratios of C_4H and C_3N indicate that their spatial distribution might be more extended than the other species. Although the hollow shell distribution detected by interferometry for C_4H (Guélin et al. 1993) and C_3N (Bieging & Tafalla 1993) showed similar radius of about $15''$ as other extended species such as SiCC (Lucas et al. 1995) and HC_3N (Bieging & Tafalla 1993), the smaller line intensity ratios of C_4H and C_3N might indicate additional extended emission component not detected by interferometry observations. The larger line intensity ratios of SiS and C^{34}S indicate that their spatial distribution might be more compact than the other species. This result of SiS agrees with the interferometry observation by Lucas et al. (1995) in which they found a strongly centrally peaked distribution of SiS line emission. The slightly higher compactness of C^{34}S can be interpreted by its centrally peaked spatial distribution and much lower abundance than CS.

The full resolution spectra of both the λ 1.3 mm and 2 mm surveys are present in Fig. 3.

The shown temperature is T_{R}^* for the 131.2-160.3 GHz range and T_{A}^* for the 219.5-245.5 and 251.5-267.5 GHz ranges. All spectra in Fig. 3 have been smoothed to roughly 1 MHz resolution by box averaging. Temperature is plotted usually in -0.1 to 0.3 K range, with exceptional plots marked by a solid square to the upper-right corner. Vertical arrows are used to mark the catalogue frequencies. The Quantum number (Qn) convention conforms to that of the CDMS and JPL catalogues. The involved Qns are: primary Qns N, K, Ka, Kc, Λ , ℓ , v, and ν_n ; spin involved Qns J and F; J_{K} for symmetric tops; $J_{\text{Ka,Kc}}$ or in rare cases $N_{\text{Ka,Kc}}$ for asymmetric tops; ν_n^ℓ for the excited bending mode ν_n of a linear molecule with its projection ℓ along the molecular axis; e/f for the parity of upper level, according to the convention of Brown et al. (1975). For the special case of $l\text{-C}_3\text{H}$ and its isotopic species, the projection of electronic orbital angular momentum on the molecular axis has a quantum number $\Lambda = 1$. So its ground level is $X^2\Pi$. In the excited bending mode ($\nu_4 = 1$, with a projection quantum number $\ell = +1$ on the molecular axis), only the lower component of the Λ doublets is detected and this component is denoted as $\mu^2\Sigma$ in which μ means the lower component. An online color version of the paper is available in which blue, magenta and red labels are used to differentiate identified, unidentified and image sideband contamination lines respectively, and zoom-in plots are shown in red boxes.

All identified species are summarized in Table 3 which gives the number of detected transitions and the index of the tables (Table 6 - 11) that contain the relevant line parameters. Table 4 gives line parameters of all detected lines (with its format explained below). The identified lines are divided into 6 groups with their line parameters extracted from Table 4 into six dedicated tables 6 - 11: Si containing species (Table 6), SiCC (Table 7), metal containing species (Table 8), C and H compounds (Table 9), Nitrogen containing species (Table 10), O and S containing species (Table 11). Unidentified lines are present in Table 5.

The columns in Tables 4 - 11 are as follows: species name, transition, line frequency and uncertainty in MHz from fitting, catalogue frequency from CDMS/JPL in MHz, integrated main beam temperature and 1σ uncertainty in K km s^{-1} , main beam line center temperature T_{mb} and 1σ uncertainty in mK from fitting, envelope expansion velocity and 1σ uncertainty in km s^{-1} , and the coding for the line blending status. If the fitted line frequency and expansion velocity are given without uncertainty, they are set at catalogue frequency and 14.5 km s^{-1} respectively for line profile fitting. This is often the case when a line is either too weak or blended with other lines. The line frequency uncertainty given by the truncated parabolic profile fitting method in CLASS was found to be too small. Therefore, we merely present spectral resolution as the uncertainty of most frequencies in Tables 4 - 11. However, the frequency uncertainty of some weak lines and all unidentified lines (also weak) were estimated by eye, and hence is usually worse than the spectral resolution. The one-letter mark that follows the catalogue frequency of some entries means the frequency is

an average of several blended (hyper)fine structure components. Most of the integrated line intensities were derived by direct integration of the line spectrum, except for those entries with their integrated intensity followed by a star symbol in the tables where the integrated line intensities were derived by line profile fitting in CLASS.

Two species, ^{13}CCH and HN^{13}C , are of the first detection in IRC +10216. The isotopic hydrogen isocyanide HN^{13}C has four rotational lines below 400 GHz, namely, $J = 1 - 0$ (87 GHz), $2 - 1$ (174 GHz), $3 - 2$ (261 GHz) and $4 - 3$ (348 GHz). Due to the limited sensitivity of the earlier surveys, the $J = 1 - 0$ line was not detected by Johansson et al. (1985) and the $J = 4 - 3$ line not detected by either Avery et al. (1992) or Groesbeck et al. (1994). The $J = 2 - 1$ line was out of the frequency coverage of the CGK survey. The $J = 3 - 2$ line at 261.263 GHz is clearly detected in our survey, with the integrated line intensity larger than 7σ . Similarly, the isotopic ethynyl ^{13}CCH has 4 groups of fine and hyperfine structure lines below 400 GHz, namely, $N = 1 - 0$ (84 GHz), $2 - 1$ (168 GHz), $3 - 2$ (252 GHz) and $4 - 3$ (336 GHz) groups. The $N = 1 - 0$ line group was covered by the survey of Johansson et al. (1985) but not detected. The $N = 2 - 1$ line group was within the frequency range of CGK survey but not detected, due to the weakness of the lines and limited S/N ratio of that portion of data and perhaps too small beam of the IRAM 30M telescope (because ^{13}CCH may follow its main isotopic species CCH to show the hollow spherical distribution as given by Guélin et al. 1996). The $N = 4 - 3$ line group was covered by the survey of Groesbeck et al. (1994). Actually, their spectrum did show some unusual features around the frequency 336.6 GHz, but the limited S/N ratio made the identification inconclusive. The $N = 3 - 2$ line group between 252.4 – 252.6 GHz in our survey data shows clear detection of its partially blended fine and hyperfine structure components.

5. Discussions

The line frequencies of all identified lines generally agree well with the predicted frequencies from CDMS or JPL. The LSR velocity of IRC +10216 calculated from the uncertainty weighted average over 49 double horn strong lines (better than 10σ detection) is $V_{\text{LSR}} = -26.404 \pm 0.004 \text{ km s}^{-1}$, close to the value of -26.5 km s^{-1} from CGK survey. The standard value of $V_{\text{LSR}} = -26.5 \text{ km s}^{-1}$ was adopted for other parts of this work. The expansion velocity of the circumstellar envelope calculated from the same sample of lines is $V_{\text{exp}} = 13.61 \pm 0.05 \text{ km s}^{-1}$, a little different from the value of 14.5 km s^{-1} from CGK survey. The difference might not be significant, because the line profile is usually not perfectly truncated parabola even in the optically thin case. The measurements given here were derived by truncated parabolic profile fitting in CLASS and should be taken as FWHM of the lines.

5.1. A brief comparison with the survey of Cernicharo et al.

The whole $\lambda 2$ mm part of our survey (131.2-160.3 GHz) overlaps with the survey by CGK. The main differences of the two surveys lie in following facts: 1) Our survey were performed in a relatively short duration (within one year) while CGK survey were done in 11 years. 2) Our survey has more homogeneous data quality than CGK survey because the IRAM 30M telescope experienced major technical updates during those 11 years. 3) Although our telescopes are smaller than the IRAM 30M telescope, we used longer integration time, so that the S/N is higher than CGK survey in a number of wavelength ranges. For example, we have detected CCS, $N = 11 - 10, J = 12 - 11$ around 144246 MHz and c -C₃H_{2,2,0} - 1_{1,1} around 150437 MHz, while these lines were buried in the high noise of the CGK survey spectra. 4) Our surveys have larger beam sizes (30'' - 40'') than CGK survey (15''), which means the two surveys were looking at slightly different regions of the circumstellar envelope. The large beam size in our survey has advantage in detecting molecular species with extended distribution. For example, the inner edge of the shell-like C₄H distribution region had been resolved by the small beam of the IRAM 30M telescope in the CGK survey, so that all the the C₄H emission lines became narrow double peaks in their spectra, while in our survey, they take a look of typical broad and strong double peak profile. Another consequence of different beams is that the column densities of C₃H, C₄H and C₃N determined from our survey data are all larger than that from CGK survey by a factor of two (see the details in next section and in Table 12), which can be interpreted by the inclusion in our larger beams the bright molecular emission ring at the radius of 15''.

Compared with the CGK survey results, lines from 18 species (or isotopomers or vibrational states) were not detected. They are CP, CS($v = 1$), ¹³CCCN, C¹³CCN, CC¹³CN, C₅H, HC₂N, HC₃N($\nu_7 = 1$), HC₅N, KCl, K³⁷Cl, ²⁶MgNC, ²⁵MgNC, SiCC($\nu_3 = 1$), SiC₃, SiS($v = 2, 3$), ²⁹Si³⁴S, ³⁰Si³⁴S. The species SiS, CS and KCl are known to show centrally peaked emission distribution (Lucas et al. 1995; Cernicharo & Guélin 1987), hence the non-detection of ²⁹Si³⁴S, ³⁰Si³⁴S, SiS($v = 2, 3$), CS($v = 1$), KCl and K³⁷Cl can be explained by larger beam dilution in our survey. Another three species, C₃³⁴S, H₂S and ²⁹SiO, had been detected by CGK survey, but the frequencies were not covered by our survey.

In the $\lambda 1.3$ mm survey, we detected 17 more species (or isotopomers or vibrational states): CCH, ¹³CCH, C¹³CH, CN, CO, ¹³CO, C¹⁷O, C¹⁸O, H₂CO, ¹³CCCH, c -¹³CCCH, H¹³CN, H¹³CN($\nu_2 = 1$), HC¹⁵N, HN¹³C, SiO($v = 1$), compared to the CGK $\lambda 2$ mm survey. The main isotopic species of these molecules are all already known in IRC +10216, according to the attached molecule list in the end of Table 1 of CGK. However, according to our knowledge, it is the first time to detect the isotopic species ¹³CCH and HN¹³C in IRC +10216, as discussed in Sect. 4. The molecules C₃H₂ and ¹³CCCH₂ detected by both CGK

and our surveys are cyclic isomers $c\text{-C}_3\text{H}_2$ and $c\text{-}^{13}\text{CCCH}_2$, according to the CDMS line list of $l\text{-C}_3\text{H}_2$ and $l\text{-}^{13}\text{CCCH}_2$ and the JPL line list of $c\text{-C}_3\text{H}_2$ and $c\text{-}^{13}\text{CCCH}_2$.

5.2. Column densities and rotational temperatures

Rotational temperatures and column densities were determined for those molecules that show extended spatial distribution in interferometry observations. The standard formula for the rotation analysis of optically thin lines from a homogeneous medium is as follows (see, e.g., the deduction of the formula in Kawaguchi et al. 1995; Cummins et al. 1986):

$$\log\left(\frac{3kW}{8\pi^3\nu S\mu_i^2}\right) = \log\frac{N(T_{\text{ex}} - T_{\text{bg}})}{QT_{\text{ex}}} - \frac{E_{\text{up}} \log e}{kT_{\text{ex}}},$$

where k is Boltzmann constant, W is integrated line intensity, S is the transition strength, μ_i is the permanent dipole moment along molecular axis i ($=a, b$ or c), N is the column density, T_{ex} and T_{bg} are the excitation temperature and background brightness temperature respectively, Q is the partition function, and E_{up} is the energy of the upper level of the transition. The unit of W is K cm s^{-1} , while all other quantities are in normal cgs units. The value of Q at different temperatures and μ_i can be found in the documentation entries of the CDMS or JPL catalogues. The integrated line intensity W has been corrected for beam dilution by using source sizes from literature (see in Table 12) and assuming gaussian source shape. For the expanding shell around evolved stars, this formula gives a gross estimate of the column density through the whole circumstellar envelope (i.e., two times of the radial column density). Almost all molecules involved in this work were present in either CDMS or JPL or both, except metal cyanides and SiC_2 isotopologues that were computed during this work.

The derived excitation temperatures (T_{ex}) and column densities (N_{col}), together with some results from the literature, are summarized in Table 12. The agreement of the column densities with literature results is generally good. Larger discrepancy is found for $c\text{-C}_3\text{H}_2$ and SiCC . There are several major sources of uncertainty in T_{ex} and N_{col} . Although in the rotation diagram analysis we have excluded several lines that are obviously weaker than expected from optically thin case (low transitions) or from LTE condition (high transitions), weaker opacity effect or non-LTE effect are still very difficult to identify and remove. The non-gaussian source brightness distribution (e.g., ring-like pattern) will result in a beam dilution behavior different from gaussian source if observations are done with different beam sizes. Furthermore, the source size variation from transition to transition has been neglected. Another source of uncertainty is related to the fact that our beam size is comparable to the source sizes. Our beam size in 1.3 mm survey is about $30''$ (comparable to the size of most of

the ring-like distributions) while our 2 mm survey has larger beam size of $40''$. This difference means that the 2 mm survey may have covered most of the ring-like emission region while the 1.3 mm survey may have missed a significant part of it, which may introduce additional uncertainty into T_{ex} and N_{col} in some cases.

The derived ortho/para ratio of $c\text{-C}_3\text{H}_2$ is roughly 4, close to the expected theoretical value of 3. The column densities of C_4H in the vibrationally excited states $\nu_7 = 1$ and 2^0 are only slightly lower than in the ground state, which indicates strong over-population in the vibrational states because all the vibrational levels have energy (about 300 K) well above the typical kinematic temperature (around 50 K) in the circumstellar envelope of IRC +10216. This could be explained by infrared radiation excitation of the vibrational levels.

The rotation diagram of the slightly asymmetric molecule SiCC is unusual. The different transitions with lower and higher J_{up} or with different quantum number K_a are located along different more or less parallel straight line segments (See Fig. 2). The unusual rotation diagram pattern of this molecule was first addressed by Thaddeus et al. (1984), and later elaborated by Avery et al. (1992) with more high frequency observations. The latter authors argued that there might be three different temperature components in the rotation diagram of SiCC: $T_{\text{ex}} = 14$ K in lower K_a ladders, 60 K in higher K_a ladders, and 145-227 K across K_a ladders. The reason for the quite different intra- K_a -ladder and inter- K_a -ladder rotational temperatures is that the radiation transition probability between the K_a ladders is much weaker than within each K_a ladders, so that the relative population between the K_a ladders might be controlled by collision, while that within each K_a -ladder might be controlled by spontaneous radiation decay. However, a kinematic temperature of > 140 K seems to be too high for the gas at the large radius where SiCC appears. So the infrared excitation mechanism suggested by Avery et al. (1992) might be a better interpretation of the high excitation temperature across K_a ladders than collisional excitation. This is supported by the tentative detection rotational of transitions in the vibrationally excited $\nu_3 = 1$ antisymmetric mode of SiCC in IRC +10216 by Gensheimer & Snyder (1997) using the transition frequency list from Bogey et al. (1991). The different rotation temperatures in the lower and higher K_a ladders could be interpreted by two components in the density distribution: a ring-like extended component and a centrally peaked compact component (see the map in Lucas et al. 1995). There are some other papers (e.g., Groesbeck et al. 1994; Kawaguchi et al. 1995) that gave quite different rotation temperatures and column densities (see in Table 12). Our results are also different from the earlier results. Particularly, we have some points in the transitional region between the low and high energy levels (around $E/k = 70$ K in Fig. 2). These points (with $K_a = 0, 2, 4$ and $J_{\text{up}} = 9, 10, 11, 12$) roughly align along the same straight line, which indicates that the inter- K_a ladder temperatures may not be so different from the intra- K_a ladder temperatures among these energy levels. More detailed analysis is

needed to interpret this phenomenon.

5.3. Isotopic ratios

Elemental isotopic ratio can be determined from intensity ratio of optically thin lines of isotopic species pairs (see discussions by Kahane et al. 1988, 1992). But the poorly known effects of opacity, beam dilution, excitation and isotopic fractionation on the line intensity ratios make the accurate determination of isotopic ratio difficult. Here, for most lines, we simply neglect these effects, and take the integrated line intensity ratio of possibly optically thin lines, after correction for the frequency dependence of ν^2 (for both line intensity in unit of K and integrated line intensity in unit of K km s⁻¹), as the isotopic ratio. However, for the case of ¹³CO, $J = 2 - 1$ line, opacity effect has been checked by channel-by-channel profile comparison (see details below). The relative calibration uncertainty of 10% has been taken into account in these calculations.

5.3.1. Oxygen and carbon isotopes

Table 13 shows that our ¹²C/¹³C ratio (34.7 ± 4.3) determined from [SiCC]/[Si¹³CC] is slightly smaller than the best value of 47(+6, -5) from Kahane et al. (1988). We have noticed that the SiCC lines are strong and hence may suffer from opacity effect. But the Si¹³CC lines are too noisy to allow channel-by-channel comparison. Therefore, our smaller ¹²C/¹³C ratio could be attributed to opacity effect. The opacity effect in ¹³CO line profile is also obvious. A channel-by-channel comparison introduced by Kahane et al. (1992) is performed between the $J = 2 - 1$ line profile of ¹³CO and that of C¹⁷O and C¹⁸O (see Fig. 4). The drop-down trend near both edges of the line profiles demonstrates the opacity effect near the line edges of ¹³CO $J = 2 - 1$ line. Therefore, only the central portion between (-5,+5) km s⁻¹ is averaged to compute the line intensity ratios. In the calculation of ¹⁶O/¹⁷O and ¹⁶O/¹⁸O ratios from double ratios [¹³CO]/[C¹⁷O] and [¹³CO]/[C¹⁸O], we do not use our ¹²C/¹³C value, but use 47 ± 5.5 from Kahane et al. (1988). Eventually, with the opacity effect removed, our ¹⁶O/¹⁷O and ¹⁶O/¹⁸O ratios agree quite well with that of Kahane et al. (1992). Therefore, our results confirm the conclusion that the isotopic ratios of S and Si are nearly solar while that of C and O are non-solar in CW Leo (see the comparison with solar values in Table 13).

5.3.2. Sulfur and silicon isotopes

The abundance ratios of the rare isotopes of sulfur and silicon, ^{33}S , ^{34}S , ^{29}Si and ^{30}Si , are determined from CS, SiCC, SiS and some double ratios of SiS (see in the last column of Table 13). The derived results are similar to the results from Kahane et al. (1988) and so all isotopic ratios of S and Si are confirmed to be close to the solar values.

5.3.3. Abundance differences among ^{13}C isotopomers

We investigated possible abundance differences among ^{13}C substituted species of HC_3N . The integrated line intensity ratios (with the factor ν^2 corrected and 10% of relative calibration error included) $\text{H}^{13}\text{CCCN}:\text{HC}^{13}\text{CCN}:\text{HCC}^{13}\text{CN} = 1.00 : 1.19(\pm 0.14) : 1.31(\pm 0.15)$ were determined from two transitions $J = 16 - 15$ and $17 - 16$, with very similar values from the two lines. Another transition $J = 15 - 14$ was not used because this line of H^{13}CCCN was observed in poor weather (with atmospheric opacity $\tau = 0.65$). Our observations suggest that the abundances of the ^{13}C substituted species of HC_3N are not equal to each other in IRC +10216, contradicting with the results of Kahane et al. (1988) (their ratios can be reproduced from their given intensities as $1.00 : 0.94(\pm 0.16) : 0.94(\pm 0.18)$). The possible reason might be the smaller beam of IRAM 30M telescope used by Kahane et al. The abundance differentiation among the three ^{13}C variants of HC_3N is argued by Takano et al. (1998) to be enhanced in the low-temperature regions. Our observations with a larger beam probed the cooler outer parts of the CSE. Moreover, our result of the HC_3N isotopic ratios in the carbon star is in the same trend as the corresponding ratios of $1.0 : 1.0 : 1.4$ found in interstellar cloud TMC-1 by Takano et al. (1998), i.e., the ^{13}C atom is more concentrated in the C atom adjacent to the N atom.

An integrated line intensity ratio $^{13}\text{CCH}/\text{C}^{13}\text{CH} = 1.00 : 0.81(\pm 0.09)$ was determined from their $N = 3 - 2$ lines. However, the slightly higher abundance of ^{13}CCH may not be true, because not only the ^{13}CCH line in our survey was observed in a relatively worse weather (with atmospheric opacity $\tau = 0.5$), but also some of the weak hyperfine structure components may have been left out when integrating the complex blended hyperfine structure line profiles. Takano et al. (1998) mentioned the possible abundance difference between ^{13}CCH and C^{13}CH in the Orion A ridge that was found by Saleck et al. (1994) (the original paper unavailable). However, the calibration was said to be a problem in that work. Therefore, the abundance differentiation between ^{13}CCH and C^{13}CH is still inconclusive in either molecular clouds or circumstellar envelope.

5.4. Other interesting features

We have detected rotational lines from vibrationally excited states of five molecules: C₃H, C₄H, HCN, H¹³CN and SiS. C₄H shows strong rotational lines from the $\nu_7 = 1, 2^0$ and 2^2 states. The large column densities derived from rotation diagram analysis of these states in Sect. 5.2 indicate that infrared pumping could be very efficient. We have detected rotational lines from the excited bending states $\nu_2 = 1^1, 2^0, 3^1$ of HCN. The two well separated ℓ -doublets of H¹³CN in the excited $\nu_2 = 1^1$ bending mode both show clear triangular profiles, which indicates that the line emission comes from the inner acceleration region of the circumstellar envelope. The two lines from the $\nu_4 = 1$ state of C₃H are weak and their detections are tentative. The line from the $v = 1$ state of SiS is also very weak, perhaps due to large beam dilution.

Four very narrow lines have been found in the survey. One of them is the $\nu_2 = 3^{1e}, J = 3 - 2$ line of HCN, while the other three are from the $v = 0, 1$ states of SiS (see the list in Table 14). There are two possible interpretations for these narrow line widths: maser beaming effect or thermal emission from the wind acceleration zone where outflow velocity is not fully developed. For example, the peak mainbeam temperature of the narrow HCN line in our SMT beam (FWHM = 28") with a resolution of 1 MHz was 96 mK. If we assume it arises within 10 stellar radii ($\approx 4 \times 10^{14}$ cm, assuming a luminosity of $10^4 L_\odot$ and surface temperature of 2500 K for the star), with the distance of 120 pc to the star, the beam-dilution corrected brightness temperature is about 380 K, reasonable for a line thermally excited in a hot region near the photosphere. On the other hand, if the line arises from a local region smaller than the stellar size, then the brightness temperature would be $> 3.8 \times 10^4$ K, consistent with a weak maser that is magnifying the stellar continuum emission. In both cases, these lines could be varying in intensity with the pulsation of the central star. The observation dates and other parameters (observed frequency, mainbeam temperature at the peak and FWHM line width) are given in Table 14 for a follow-up study. The HCN line is the first detection from its $\nu_2 = 3^1$ vibrational state in CW Leo. The SiS, $v = 0, J = 14 - 13$ line had been observed by Fonfría Expósito et al. (2006) and was argued to be masers superposed on the top of the broad thermal line. Turner (1987) reported the detection of both SiS $v = 1$ lines (with lower S/N ratio) and argued that the $J = 13 - 12$ line may be a thermal line while the sharp peak of $J = 14 - 13$ line could be a weak maser. The blue $J = 14 - 13$ maser peak in our spectrum shows a velocity shift of about -7.4 km s^{-1} with respect to the stellar velocity of -26.5 km s^{-1} . The pumping mechanism of the SiS masers could be mid-infrared line-overlapping with C₂H₂, HCN, and their ¹³C isotopologues, as suggested by Fonfría Expósito et al. (2006).

Clear triangular line profiles were found for three lines: CCS, $N = 15 - 14, J = 15 -$

14 (234814.63 MHz) and the two well separated ℓ -doublets in the excited bending state of H^{13}CN , $\nu_2 = 1^1$, $J = 3-2$ (258936.82 and 260225.42 MHz). These triangular lines might arise from the accelerating inner shell of the circumstellar envelope where the terminal outflow velocity is not fully developed yet.

6. Summary

We have surveyed the circumstellar envelope of the archetypal carbon rich AGB star IRC +10216 in λ 1.3 and 2 mm ranges using the KP12M and SMT telescopes of ARO. In total, 377 lines were detected and 26 molecules plus 29 rare isotopic species and 2 cyclic isomers were identified to be carriers for 360 of them. Only 17 weak lines remain unidentified.

The rotational lines of two isotopic species ^{13}CCH and HN^{13}C were detected in IRC +01216 for the first time by our survey. Two rotation lines of the formaldehyde have been confirmed. Column densities of 15 extended species roughly agree with previous determinations. Isotopic ratios of C, O, S and Si confirm the conclusion that the S and Si isotopic ratios are nearly solar while the C and O isotopic ratios are non-solar. Our data suggests possible abundance differentiation among the three ^{13}C substituted isotopic isomers of HC_3N .

Modified spectroscopic parameters of alkali metal cyanide NaCN/NaNC , $\text{Na}^{13}\text{CN}/\text{NaN}^{13}\text{C}$, KCN/KNC and silacyclopropynylidene SiC_2 have been derived to help line identification. Transition frequencies from the current surveys were used to improve the spectroscopic parameters of Si^{13}CC , $^{29}\text{SiC}_2$ and $^{30}\text{SiC}_2$.

We thank the referee, Dr. M. Guélin, for many pertinent comments that have greatly improved this work. J.H. thanks Dr. H.M. Pickett for the help on understanding the JPL catalogue, Dr. William Peters for the help on the calibration of the spectral data, Dr. Mao Rui-Qing for discussions on instrumental effects in our spectra, Mr. Nico Koning for discussions on line identification, and the GILDAS help desk for the help on using CLASS. We also thank ARO telescope operators for the assistance in remote observations. H.S.P.M. and the CDMS are supported by the Bundesministerium für Bildung und Forschung (BMBF) administered through Deutsches Zentrum für Luft- und Raumfahrt (DLR; the German space agency). J.H. also thanks the projects No. 10433030 and 10503011 of the National Natural Science Foundation of China. T.H. acknowledges the support from NSC grant NSC 96-2112-M-001-018-MY3.

Facilities: HHT (), NRAO:12m ().

REFERENCES

- Avery, L. W., Amano, T., Bell, M. B., et al. 1992, *ApJS*, 83, 363
- Bieging, J. H. & Tafalla, M. 1993, *AJ*, 105, 576
- Bogey, M., Demuynck, C., Destombes, J. L., & Walters, A. D. 1991, *A&A*, 247, L13
- Brown, J. M., Hougen, J. T., Huber, K.-P., et al. 1975, *J. Mol. Spectrosc.*, 55, 500
- Cernicharo, J. & Guélin, M. 1987, *A&A*, 183, L10
- Cernicharo, J., Guélin, M., Kahane, C., Bogey, M., & Demuynck, C. 1991, *A&A*, 246, 213
- Cernicharo, J., Guélin, M., & Kahane, C. 2000, *A&AS*, 142, 181
- Cherchneff, I., Glassgold, A. E., & Mamon, G. A. 1993, *ApJ*, 410, 188
- Cummins, S. E., Linke, R. A., & Thaddeus, P. 1986, *ApJS*, 60, 819
- Fonfría Expósito, J. P., Agúndez, M., Tercero, B., Pardo, J. R., & Cernicharo, J. 2006, *ApJ*, 646, L127
- Ford, K. E. S., Neufeld, D. A., Schilke, P., & Melnick, G. J. 2004, *ApJ*, 614, 990
- Gensheimer, P. D. & Snyder, L. E. 1997, *ApJ*, 490, 819
- Gottlieb, C. A., Vrtílek, J. M., & Thaddeus, P. 1989, *ApJ*, 343, L29
- Groenewegen, M. A. T., van der Veen, W. E. C. J., & Matthews, H. E. 1998, *A&A*, 338, 491
- Groesbeck, T. D., Phillips, T. G., & Blake, G. A. 1994, *ApJS*, 94, 147
- Guélin, M., Lucas, R., & Cernicharo, J. 1993, *A&A*, 280, L19
- Guélin, M., Lucas, R., & Neri, R. 1996, in *IAU Symposium*, Vol. 170, CO: Twenty-Five Years of Millimeter-Wave Spectroscopy, ed. W. B. Latter, J. E. Radford Simon, P. R. Jewell, J. G. Mangum, & J. Bally, 359
- Johansson, L. E. B., Andersson, C., Elder, J., et al. 1985, *A&AS*, 60, 135
- Kahane, C., Cernicharo, J., Gomez-Gonzalez, J., & Guélin, M. 1992, *A&A*, 256, 235
- Kahane, C., Gomez-Gonzalez, J., Cernicharo, J., & Guélin, M. 1988, *A&A*, 190, 167
- Kawaguchi, K., Kasai, Y., Ishikawa, S.-I., & Kaifu, N. 1995, *PASJ*, 47, 853

- Kuijpers, P., Törring, T. & Dymanus A. 1976, *Chem. Phys. Lett.*, 42, 423
- Lovas, F. J. 2004, *J. Phys. Chem. Ref. Data*, 33, 177
- Lucas, R. & Guélin, M. 1999, in *IAU Symposium, Vol. 191, Asymptotic Giant Branch Stars*, ed. T. Le Bertre, A. Lebre, & C. Waelkens, 305
- Lucas, R., Guélin, M., Kahane, C., Audinos, P., & Cernicharo, J. 1995, *Ap&SS*, 224, 293
- Millar, T. J. & Herbst, E. 1994, *A&A*, 288, 561
- Millar, T. J., Herbst, E., & Bettens, R. P. A. 2000, *MNRAS*, 316, 195
- Müller, H. S. P., Schlöder, F., Stutzki, J., & Winnewisser, G. 2005, *J. Mol. Struct.*, 742, 215
- Müller, H. S. P., Thorwirth, S., Roth, D. A., & Winnewisser, G. 2001, *A&A*, 370, L49
- Pickett, H. M., Poynter, R. L., Cohen, E. A., et al. 1998, *J. Quant. Spectrosc. Radiat. Transfer*, 60, 883
- Saleck, A. H., Simon, R., Winnewisser, G., & Wouterloot, J. G. A. 1994, *Can. J. Phys.*, 72, 747
- Suenram, R. D., Lovas, F. J., & Matsumura, K. 1989, *ApJ*, 342, L103
- Takano, S., Masuda, A., Hirahara, Y., et al. 1998, *A&A*, 329, 1156
- Thaddeus, P., Cummins, S. E., & Linke, R. A. 1984, *ApJ*, 283, L45
- Törring, T., Bekooy, J. P., Meerts, L. W., Hoefft J., Tiemann, E. & Dymanus, A., 1980, *J. Chem. Phys.*, 73, 4875
- Townes, C. H. & Schawlow, A. L. 1955, *Microwave Spectroscopy* (*Microwave Spectroscopy*, New York: McGraw-Hill, 1955)
- van Vaals, J. J., Meerts, W. L., & Dymanus, A. 1984, *J. Chem. Phys.*, 86, 147
- van Vaals, J. J., Meerts, W. L., & Dymanus, A. 1984, *J. Mol. Spectrosc.*, 106, 280
- Turner, B. E. 1987, *A&A*, 183, L23

Table 1: Spectroscopic parameters^a (MHz) of alkali metal cyanides

Parameter	NaCN	Na ¹³ CN	KCN
$A - (B + C)/2$	50101.74757 (166)	48021.9343 (33)	53528.08107 (268)
$(B + C)/2$	7820.190252 (259)	7652.41519 (39)	4737.751389 (93)
$(B - C)/4$	274.1525055 (177)	272.798660 (39)	100.959727 (64)
$D_K \times 10^3$	196.52 (169)	271.79 (169)	956.79 (247)
$D_{JK} \times 10^3$	800.23 (34)	738.85 (41)	374.609 (50)
$D_J \times 10^3$	13.3361 (160)	13.2404 (186)	5.24462 (209)
$d_1 \times 10^3$	-2.34908 (34)	-2.42697 (110)	-0.51452 (78)
$d_2 \times 10^3$	-1.408951 (182)	-1.380792 (296)	-0.237559 (199)
$H_K \times 10^3$	1.428 (220)	1.354 (101)	–
$H_{KJ} \times 10^6$	155.9(184)	140.3 (73)	101.23 (107)
$H_{JK} \times 10^6$	-3.54(120)	-2.80 ^b	-7.277 (111)
$H_J \times 10^6$	0.541 (50)	0.50 ^b	–
$h_2 \times 10^9$	–	–	-5.46 (74)
$h_3 \times 10^9$	39.9 (69)	30. ^b	–

^aNumbers in parentheses are one standard deviation in units of the least significant figures. Watson’s S -reduction was used in the representation I^r .

^bEstimated and kept fixed in the fits, see section 3.

Table 2: Spectroscopic parameters^a (MHz) of SiC₂ isotopic species

Parameter	SiC ₂	Si ¹³ CC	²⁹ SiC ₂	³⁰ SiC ₂
$A - (B + C)/2$	40674.191 (100)	38928.92 (73)	40845.6 ^b	41005.5 ^b
$(B + C)/2$	11800.11861 (99)	11527.5128 (123)	11628.7544 (40)	11468.7891 (40)
$(B - C)/4$	678.41301 (130)	672.5424 (76)	659.1312 (127)	641.4564 (212)
D_K	-1.2880 (227)	-1.223 (65)	-1.288 ^b	-1.288 ^b
D_{JK}	1.624219 (88)	1.540958 (232)	1.57360 (209)	1.53715 (170)
$D_J \times 10^3$	-1.1845 (115)	-1.462 (55)	-0.554 (139)	-0.859 (203)
$d_1 \times 10^3$	-2.4392 (111)	-2.4413 (116)	-2.34 ^b	-2.24 ^b
$d_2 \times 10^3$	-7.2002 (80)	-7.0656 (146)	-6.732 (184)	-6.225 (311)
$H_{KJ} \times 10^6$	670.39 (151)	611.23 (82)	640. ^b	610. ^b
$H_{JK} \times 10^6$	-138.66 (39)	-128.14 (40)	-139. ^b	-139. ^b
$H_J \times 10^6$	1.0079 (201)	0.862 (65)	-1.0 ^b	1.0 ^b
$h_1 \times 10^9$	-180.2 (247)	-170. ^b	-170. ^b	-160. ^b
$h_2 \times 10^9$	-513.3 (301)	-493. (39)	-480. ^b	-450. ^b
$h_3 \times 10^9$	157.0 (93)	173.7 (204)	144. ^b	132. ^b
$L_{KKJ} \times 10^9$	-138.5 (80)	-118. ^b	-130. ^b	-120. ^b
$L_{JK} \times 10^9$	14.34 (266)	12. ^b	12. ^b	10. ^b
$L_{JJK} \times 10^9$	-11.06 (78)	-10. ^b	-10. ^b	-9. ^b
$P_{KKKJ} \times 10^{12}$	20. ^b	16. ^b	18.8 ^b	17. ^b

^aNumbers in parentheses are one standard deviation in units of the least significant figures. Watson’s S -reduction was used in the representation I^r .

^bEstimated and kept fixed in the fits; see section 3.

Table 3. Summary of molecular species detected in the λ 1.3 and 2 mm spectral survey towards IRC +10216.

Mol	Variants	Lines	Table	Mol	Variants	Lines	Table
AlCl	AlCl	3	8	HCN	HCN	1	10
AlCl	Al ³⁷ Cl	4	8	HCN	HCN, $\nu_2 = 1^1$	2	10
AlF	AlF	3	8	HCN	HCN, $\nu_2 = 2^0$	1	10
C ₂ H	C ₂ H	5	9	HCN	HCN, $\nu_2 = 3^1$	1	10
C ₂ H	¹³ CCH	5	9	HCN	H ¹³ CN	1	10
C ₂ H	C ¹³ CH	7	9	HCN	H ¹³ CN, $\nu_2 = 1^1$	2	10
C ₂ S	C ₂ S	7	11	HCN	HC ¹⁵ N	1	10
CH ₃ CN	CH ₃ CN	14	10	HC ₃ N	HCCCN	7	10
CN	CN	3*	10	HC ₃ N	H ¹³ CCCN	5	10
CO	CO	1	11	HC ₃ N	HC ¹³ CCN	4	10
CO	¹³ CO	1	11	HC ₃ N	HCC ¹³ CN	4	10
CO	C ¹⁷ O	1	11	HNC	HN ¹³ C	1	10
CO	C ¹⁸ O	1	11	MgNC	MgNC	6	8
CS	CS	3	11	NaCN	NaCN	9	8
CS	¹³ CS	2	11	NaCl	NaCl	5	8
CS	¹³ C ³⁴ S	1	11	NaCl	Na ³⁷ Cl	2	8
CS	C ³³ S	2	11	PN	PN	1	10
CS	C ³⁴ S	2	11	SiC	SiC, $\Omega = 1$	2	6
C ₃ H	C ₃ H	6	9	SiC	SiC, $\Omega = 2$	2	6
C ₃ H	C ₃ H, $\nu_4 = 1$	4	9	SiC ₂	SiC ₂	24	7
C ₃ H	¹³ CCCH	3	9	SiC ₂	Si ¹³ CC	33	7
C ₃ H	<i>c</i> -C ₃ H	6	9	SiC ₂	²⁹ SiC ₂	21	7
C ₃ H ₂	<i>c</i> -C ₃ H ₂	13	9	SiC ₂	³⁰ SiC ₂	20	7
C ₃ N	C ₃ N	13	10	SiN	SiN	2	6
C ₃ S	C ₃ S	2	11	SiO	SiO	1	6
C ₄ H	C ₄ H	12	9	SiO	SiO, $v = 1$	1	6
C ₄ H	C ₄ H, $\nu_7 = 1^1$	27	9	SiO	³⁰ SiO	1	6
C ₄ H	C ₄ H, $\nu_7 = 2^0$	15	9	SiS	SiS	3	6
C ₄ H	C ₄ H, $\nu_7 = 2^2$	8	9	SiS	SiS, $v = 1$	3	6
C ₄ H	¹³ CCCCH	8	9	SiS	²⁹ SiS	3	6
C ₄ H	C ¹³ CCCH	6	9	SiS	³⁰ SiS	5	6
C ₄ H	CC ¹³ CCH	3	9	SiS	Si ³³ S	2	6
C ₄ H ₂	<i>l</i> -C ₄ H ₂	9	9	SiS	Si ³⁴ S	4	6
H ₂ CO	H ₂ CO	2	11				

*The hyperfine structure components of different fine structure lines of CN are partially blended. Here, only fine structure lines are counted as lines.

Table 4. Line parameters of all detected lines in our survey. The units are MHz for ν_{obs} and ν_{cat} , K km s⁻¹ for I_{int} , mK for T_{mb} , and km s⁻¹ for V_{exp} ; the same for corresponding uncertainties.

Species	Trans	ν_{obs}	σ	ν_{cat}^{*1}	I_{int}^{*2}	σ	T_{mb}	σ	V_{exp}	σ	Note ^{*3}
U131352		131352.15	4.40		2.96	0.37	90	45	23.20	0.89	s
CCS	$N = 10 - 9, J = 11 - 10$	131551.97		131551.97	0.68	0.32	26	44	14.50		+
AIF	$J = 4 - 3$	131895.82	2.35	131899.23a	1.33	0.12	30	21	25.00	3.55	&

*The complete version of this table is in the electronic edition of the Astrophysical Journal Supplement Series. This is only a sample.

^{*1}Catalogue frequencies may be followed by an one letter coding [a, b or d]: (a) average frequency of hyperfine structure components; (b)the same as (a) but for MgNC, the hyperfine structure components of the two fine structure lines partially mix together and frequency is the average within each fine structure level; (d) average frequency of the unresolved lambda doublets of SiC.

^{*2}Entries followed by a star mark are line intensities derived by truncated parabola fitting.

^{*3}The Note column only contains coding for line blending status: (s) single line; (+)line fitted with fixed frequency and line half width of 14.5 km s⁻¹; (@)line too narrow; (*)differentiable blended lines of the same species; (\$)differentiable blended lines of different species; (&)undifferentiable blended lines of the same species (e.g., hyperfine structure or lambda doublet or some asymmetric top transitions); (#)undifferentiable blended lines of different species.

Table 5. Line parameters of unidentified lines. The units are MHz for ν_{obs} and ν_{cat} , K km s^{-1} for I_{int} , mK for T_{mb} , and km s^{-1} for V_{exp} ; the same for corresponding uncertainties.

Species	Trans	ν_{obs}	σ	ν_{cat}^{*1}	I_{int}^{*2}	σ	T_{mb}	σ	V_{exp}	σ	Note ^{*3}
U131352		131352.15	4.40		2.96	0.37	90	45	23.20	0.89	s
U141000		140999.58	4.40		0.12	0.07	2	8	14.50		+
U227219		227219.26	4.00		0.59*	0.11	20	25	17.52	5.28	s
U230601		230601.00	5.00		0.55*	0.05	18	18	8.79	6.49	@
U234078		234077.89	3.00		0.46*	0.08	14	18	12.48	3.84	s
U235017		235016.69	2.00		0.51	0.13	10	14	19.20	1.28	s
U235175		235174.70	4.00		0.22	0.28	22	10	4.97	1.27	@
U236167		236167.09	2.50		0.63	0.21	26	16	15.00	1.27	s
U236780		236780.23	4.00		0.57	0.24	23	12	6.83	1.27	@
U244608		244608.55	3.00		1.51	0.45	46	31	11.90	1.23	s
U245125		245125.22	5.00		0.88*	0.15	46	40	10.92	6.12	s
U253272		253272.58	5.00		0.30*	0.04	12	9	13.50	5.92	s
U254686		254686.06			1.06*	0.07	34	11	14.48		\$
U262251		262250.71	4.00		2.45*	0.13	78	57	13.63	4.58	s
U264072		264072.14	1.50		0.91	0.23	56	9	7.12	1.14	@
U266270		266269.17	1.00		0.90	0.11	26	9	14.60	1.13	&
U266946		266945.73	1.00		0.41	0.11	22	12	14.50		+

*1The same as *1 in Table 4.

*2The same as *2 in Table 4.

*3The same as *3 in Table 4.

Table 6. Line parameters for silicon containing species. The units are MHz for ν_{obs} and ν_{cat} , K km s⁻¹ for I_{int} , mK for T_{mb} , and km s⁻¹ for V_{exp} ; the same for corresponding uncertainties.

Species	Trans	ν_{obs}	σ	ν_{cat}^{*1}	I_{int}^{*2}	σ	T_{mb}	σ	V_{exp}	σ	Note*3
SiC	$\Omega = 1, \Lambda = 1, f, J = 6 - 5$	242968.95		242968.95	0.55	0.11	20	18	14.50		&
SiC	$\Omega = 1, \Lambda = 1, e, J = 6 - 5$	243176.94		243176.94	0.58*	0.10	30	17	14.50		\$
SiC	$\Omega = 2, \Lambda = 1, e\&f, J = 4 - 3$	157493.57	0.39	157494.09d	2.30	0.15	76	31	13.20	0.74	&
SiC	$\Omega = 2, \Lambda = 1, e\&f, J = 6 - 5$	236287.79	1.00	236287.61d	2.73	0.15	83	25	13.70	1.27	&
SiN	$N = 6 - 5, J = 11/2 - 9/2$	261648.90	1.00	261650.23a	1.85	0.16	48	25	12.40	1.15	&
SiN	$N = 6 - 5, J = 13/2 - 11/2$	262154.37	1.00	262155.46a	0.89	0.17	24	25	9.99	1.14	&
SiO	$J = 6 - 5$	260517.67	1.00	260518.02	63.90	0.10	2700	15	12.80	1.15	s
SiO	$v = 1, J = 6 - 5$	258707.39		258707.39	1.37	0.25	37	43	14.50		\$
³⁰ SiO	$J = 6 - 5$	254217.08	1.00	254216.66	4.71	0.06	170	11	13.60	1.18	s
SiS	$J = 8 - 7$	145226.91	0.39	145227.00	56.50	0.07	2310	15	13.30	0.81	s
SiS	$J = 13 - 12$	235961.15	1.00	235961.14	95.30	0.15	3960	25	13.40	1.27	s
SiS	$J = 14 - 13$	254102.82	1.00	254102.92	145.00	0.07	6350	11	11.90	1.18	s
SiS	$v = 1, J = 8 - 7$	144520.37		144520.37	0.25	0.08	13	16	14.50		+
SiS	$v = 1, J = 13 - 12$	234813.22	1.00	234812.97	0.82	0.22	66	17	7.57	1.28	@
SiS	$v = 1, J = 14 - 13$	252866.47		252866.47	2.76*	0.13	3	15	14.50		\$
Si ³³ S	$J = 8 - 7$	143175.55		143175.55	0.66*	0.06	29	13	14.50		\$
Si ³³ S	$J = 13 - 12$	232628.69	1.00	232628.58	1.43*	0.08	54	131	14.26	1.29	s
Si ³⁴ S	$J = 8 - 7$	141250.19	0.39	141250.28	3.41	0.05	122	11	13.70	0.83	s
Si ³⁴ S	$J = 9 - 8$	158903.05	0.39	158903.11	4.94	0.15	175	32	14.00	0.74	s
Si ³⁴ S	$J = 13 - 12$	229501.00	1.00	229500.87	7.08	0.10	256	15	14.30	1.31	\$
Si ³⁴ S	$J = 15 - 14$	264789.67	1.00	264789.72	7.75	0.11	288	18	13.70	1.13	s
²⁹ SiS	$J = 8 - 7$	142559.01	0.39	142558.82	4.81	0.08	164	16	13.70	0.82	s
²⁹ SiS	$J = 13 - 12$	231626.48	1.00	231626.67	7.09	0.12	269	19	13.70	1.29	s
²⁹ SiS	$J = 15 - 14$	267242.22		267242.22	12.70	0.11	544	24			#
³⁰ SiS	$J = 8 - 7$	140073.85	0.78	140073.96	2.45	0.12	87	17	14.20	1.67	s
³⁰ SiS	$J = 9 - 8$	157579.82	0.39	157579.81	3.82	0.15	134	31	14.50	0.74	s
³⁰ SiS	$J = 13 - 12$	227589.75	1.00	227589.87	5.71	0.13	197	19	13.00	1.32	s
³⁰ SiS	$J = 14 - 13$	245088.56	1.00	245088.38	5.88	0.28	222	47	14.20	1.22	s
³⁰ SiS	$J = 15 - 14$	262585.12	1.00	262585.03	5.30	0.14	194	24	14.40	1.14	s

*1 The same as *1 in Table 4.

*2 The same as *2 in Table 4.

*3 The same as *3 in Table 4.

Table 7. Line parameters SiCC lines. The units are MHz for ν_{obs} and ν_{cat} , K km s⁻¹ for I_{int} , mK for T_{mb} , and km s⁻¹ for V_{exp} ; the same for corresponding uncertainties.

Species	Trans	ν_{obs}	σ	ν_{cat}^{*1}	I_{int}^{*2}	σ	T_{mb}	σ	V_{exp}	σ	Note ^{*3}
SiCC	6 _{0,6} - 5 _{0,5}	137180.73	0.39	137180.79	24.50	0.17	884	33	13.90	0.85	s
SiCC	6 _{2,4} - 5 _{2,3}	145325.81	0.39	145325.87	20.40	0.12	716	24	13.90	0.80	s
SiCC	6 _{2,5} - 5 _{2,4}	140920.08	0.39	140920.18	20.20	0.05	705	11	13.70	0.83	s
SiCC	6 _{4,2} - 5 _{4,1}	141755.25	0.39	141755.36	19.10	0.11	371	15	14.00	0.82	*
SiCC	6 _{4,3} - 5 _{4,2}	141751.42	0.39	141751.49	19.60	0.11	424	15	13.90	0.82	*
SiCC	7 _{0,7} - 6 _{0,6}	158499.13	0.39	158499.24	27.50	0.15	916	32	13.70	0.74	s
SiCC	9 _{2,7} - 8 _{2,6}	222009.36	1.00	222009.38	24.10	0.12	842	19	14.00	1.35	s
SiCC	10 _{0,10} - 9 _{0,9}	220773.68	1.00	220773.69	24.60	0.14	984	21	13.70	1.36	s
SiCC	10 _{2,9} - 9 _{2,8}	232534.15	1.00	232534.08	22.40	0.08	770	13	13.60	1.29	s
SiCC	10 _{4,6} - 9 _{4,5}	237331.32	1.00	237331.31	14.00	0.12	470	18	13.50	1.26	s
SiCC	10 _{4,7} - 9 _{4,6}	237149.94	1.00	237150.02	13.10	0.12	457	18	13.90	1.26	s
SiCC	10 _{6,4} - 9 _{6,3}	235713.10	1.00	235713.08	16.40	0.15	564	25	13.50	1.27	&
SiCC	10 _{6,5} - 9 _{6,4}			235713.01							&
SiCC	10 _{8,2} - 9 _{8,1}	234533.92	1.00	234534.01	6.56	0.10	223	17	13.90	1.28	&
SiCC	10 _{8,3} - 9 _{8,2}			234534.01							&
SiCC	11 _{0,11} - 10 _{0,10}	241367.74	1.00	241367.71	26.10	0.10	876	16	13.70	1.24	s
SiCC	11 _{2,10} - 10 _{2,9}	254981.34	1.00	254981.49	24.80	0.06	832	11	13.60	1.18	#
SiCC	11 _{4,7} - 10 _{4,6}	261509.61	1.00	261509.33	14.90	0.15	503	25	13.80	1.15	s
SiCC	11 _{4,8} - 10 _{4,7}	261150.72	1.00	261150.70	14.10	0.09	480	15	13.80	1.15	s
SiCC	11 _{6,5} - 10 _{6,4}	259433.30	1.00	259433.31	18.80	0.26	617	43	13.50	1.16	&
SiCC	11 _{6,6} - 10 _{6,5}			259433.31							&
SiCC	11 _{8,3} - 10 _{8,2}	258065.12	1.00	258065.05	8.22	0.22	256	36	13.50	1.16	&
SiCC	11 _{8,4} - 10 _{8,3}			258065.05							&
SiCC	12 _{0,12} - 11 _{0,11}	261989.84	1.00	261990.74	23.70*	1.05	950	25	12.70	1.14	\$
Si ¹³ CC	6 _{0,6} - 5 _{0,5}	133812.94	0.39	133813.59	0.69	0.09	27	13	14.50		+
Si ¹³ CC	6 _{1,5} - 5 _{1,4}	145136.50	0.39	145136.66	0.70	0.07	27	15	14.50		+
Si ¹³ CC	6 _{2,4} - 5 _{2,3}	142138.04	0.78	142138.50	0.59*	0.05	25	15	14.50		s
Si ¹³ CC	6 _{3,4} - 5 _{3,3}	138813.80	0.78	138812.34	0.28	0.08	12	16	14.50		+
Si ¹³ CC	6 _{4,2} - 5 _{4,1}	138510.77		138512.90							\$&
Si ¹³ CC	6 _{4,3} - 5 _{4,2}			138508.63							\$&
Si ¹³ CC	6 _{5,1} - 5 _{5,0}	138219.76	3.70	138219.80	0.34	0.09	14	11	14.50		&+
Si ¹³ CC	6 _{5,2} - 5 _{5,1}			138219.78							&+
Si ¹³ CC	7 _{0,7} - 6 _{0,6}	154558.44	5.70	154558.84	0.59	0.16	14	23	14.50		+
Si ¹³ CC	7 _{1,7} - 6 _{1,6}	150383.52	0.98	150385.55	0.51	0.10	27	21	14.50		+
Si ¹³ CC	7 _{2,6} - 6 _{2,5}	160230.60	0.78	160229.69	0.84	0.14	15	29	13.50	0.73	s
Si ¹³ CC	10 _{2,8} - 9 _{2,7}	242100.88	2.00	242099.15	0.55	0.09	19	15	14.50		+
Si ¹³ CC	10 _{2,9} - 9 _{2,8}	227004.24	1.00	227004.56	0.40	0.14	9	19	10.90	1.32	s
Si ¹³ CC	10 _{3,7} - 9 _{3,6}	235101.04	5.30	235107.98	0.37	0.15	18	14	14.50		+
Si ¹³ CC	10 _{3,8} - 9 _{3,7}	231898.71	3.90	231897.91	0.33	0.18	11	11	12.30	1.29	s
Si ¹³ CC	10 _{4,6} - 9 _{4,5}	231963.87	4.90	231964.48	0.62	0.17	26	16	14.50		+
Si ¹³ CC	10 _{4,7} - 9 _{4,6}	231764.23	5.40	231764.97	0.42	0.21	5	24	9.83	1.29	s
Si ¹³ CC	10 _{6,4} - 9 _{6,3}	230345.04	9.70	230345.50	0.53	0.13	19	13	14.50		&+
Si ¹³ CC	10 _{6,5} - 9 _{6,4}			230345.41							&+
Si ¹³ CC	11 _{0,11} - 10 _{0,10}	235286.29	3.40	235284.89	0.65	0.48	12	8	15.70	1.27	&
Si ¹³ CC	11 _{1,11} - 10 _{1,10}	233669.97	3.40	233669.86	0.66	0.14	18	15	14.50	1.28	s
Si ¹³ CC	11 _{2,9} - 10 _{2,8}	266739.01	6.56	266740.96	0.73	0.11	27	17	14.50		+
Si ¹³ CC	11 _{3,9} - 10 _{3,8}	255063.41	4.00	255060.77	0.24	0.09	8	8	14.30	1.18	s
Si ¹³ CC	11 _{4,7} - 10 _{4,6}	255624.74		255624.74	0.56*	0.12	17	14	14.50	1.17	#
Si ¹³ CC	11 _{4,8} - 10 _{4,7}	255232.02	4.00	255230.50	0.29	0.06	14	11	14.50		+
Si ¹³ CC	11 _{5,6} - 10 _{5,5}	254324.42		254324.42	0.04*	0.09	1	10	14.50		*\$
Si ¹³ CC	11 _{5,7} - 10 _{5,6}	254313.25	3.00	254310.37	0.85	0.06	24	11	15.30	1.18	*\$
Si ¹³ CC	11 _{6,5} - 10 _{6,4}	253535.75	3.00	253533.77	0.41	0.07	13	11	10.80	1.18	@&
Si ¹³ CC	11 _{6,6} - 10 _{6,5}			253533.50							@&
Si ¹³ CC	11 _{7,4} - 10 _{7,3}	252856.15		252856.15	2.20*	0.02	81	10	14.50		*&
Si ¹³ CC	11 _{7,5} - 10 _{7,4}			252856.15							*\$
Si ¹³ CC	12 _{0,12} - 11 _{0,11}	255399.83	3.00	255398.38	0.49	0.07	18	11	11.70	1.17	s
Si ¹³ CC	12 _{1,12} - 11 _{1,11}	254246.05	3.00	254244.97	0.32	0.09	8	6	13.20	1.18	s
²⁹ SiCC	6 _{0,6} - 5 _{0,5}	135370.95	0.78	135371.22	1.51	0.06	50	12	13.60	0.86	s
²⁹ SiCC	6 _{2,4} - 5 _{2,3}	143061.51	0.39	143061.44	1.07	0.06	33	13	13.50	0.82	s
²⁹ SiCC	6 _{2,5} - 5 _{2,4}	138902.22	0.78	138901.83	1.24	0.08	42	16	15.40	0.84	s
²⁹ SiCC	6 _{4,2} - 5 _{4,1}	139680.02	1.56	139680.02	0.79	0.08	21	17	15.10	0.84	&
²⁹ SiCC	6 _{4,3} - 5 _{4,2}			139676.62							&
²⁹ SiCC	7 _{0,7} - 6 _{0,6}	156456.36	0.98	156456.47	1.58	0.08	59	18	14.60	0.75	s
²⁹ SiCC	10 _{2,8} - 9 _{2,7}	243657.27	1.00	243656.78	1.68	0.22	44	22	14.00	1.23	s
²⁹ SiCC	10 _{2,9} - 9 _{2,8}	229306.08	3.00	229304.82	1.22	0.11	40	17	13.70	1.31	s
²⁹ SiCC	10 _{4,6} - 9 _{4,5}	233798.78	3.00	233800.08	0.71	0.10	26	16	14.50		+
²⁹ SiCC	10 _{4,7} - 9 _{4,6}	233641.02	4.00	233640.34	0.70	0.15	23	11	14.10	1.28	s

Table 7—Continued

Species	Trans	ν_{obs}	σ	ν_{cat}^{*1}	I_{int}^{*2}	σ	T_{mb}	σ	V_{exp}	σ	Note ^{*3}
²⁹ SiCC	10 _{6,4} – 9 _{6,3}	232263.46	5.00	232266.03	0.72	0.12	20	19	14.50		&
²⁹ SiCC	10 _{6,5} – 9 _{6,4}			232265.97							&
²⁹ SiCC	10 _{8,2} – 9 _{8,1}	231128.38	7.30	231131.15	0.37	0.15	12	11	12.90	1.30	&
²⁹ SiCC	10 _{8,3} – 9 _{8,2}			231131.15							&
²⁹ SiCC	11 _{0,11} – 10 _{0,10}	238346.39	4.00	238346.98	0.95	0.12	33	20	14.50		+
²⁹ SiCC	11 _{4,7} – 10 _{4,6}	257591.49	7.60	257592.15	0.66	0.30	24	38	14.50		&
²⁹ SiCC	11 _{6,5} – 10 _{6,4}	255631.11	3.00	255631.83	1.08*	0.12	33	14	14.10	1.17	#\$
²⁹ SiCC	11 _{6,6} – 10 _{6,5}			255631.64							#\$
²⁹ SiCC	11 _{8,3} – 10 _{8,2}	254316.20		254316.20	0.22*	0.09	6	10	14.50		&\$
²⁹ SiCC	11 _{8,4} – 10 _{8,3}			254316.20							&\$
²⁹ SiCC	12 _{0,12} – 11 _{0,11}	258703.97		258703.97	0.52*	0.43	1	52	14.50		\$
³⁰ SiCC	6 _{0,6} – 5 _{0,5}	133673.03	0.78	133673.00	0.80	0.12	30	23	13.00	0.87	s
³⁰ SiCC	6 _{2,4} – 5 _{2,3}	140955.01	0.98	140955.97	0.76	0.05	25	11	13.70	0.83	s
³⁰ SiCC	6 _{2,5} – 5 _{2,4}	137016.37	1.20	137016.24	0.93	0.25	32	27	13.10	0.43	s
³⁰ SiCC	6 _{4,2} – 5 _{4,1}	137731.21	2.00	137742.77	0.50	0.19	12	22	11.20	0.43	&
³⁰ SiCC	6 _{4,3} – 5 _{4,2}			137739.75							&
³⁰ SiCC	7 _{0,7} – 6 _{0,6}	154538.55	0.58	154538.26	1.01	0.12	32	24	14.00	0.76	s
³⁰ SiCC	7 _{2,6} – 6 _{2,5}	159548.76	4.50	159552.28	0.49	0.15	25	32	14.50		+
³⁰ SiCC	7 _{6,1} – 6 _{6,0}	160129.77	2.20	160131.02	0.33	0.28	1	27	6.95	0.37	&
³⁰ SiCC	7 _{6,2} – 6 _{6,1}			160131.02							&
³⁰ SiCC	10 _{2,8} – 9 _{2,7}	240049.97	5.30	240048.86	0.70	0.32	37	24	8.58	1.25	@
³⁰ SiCC	10 _{2,9} – 9 _{2,8}	226283.87		226283.87	2.55*	0.04	78	17	14.60	0.18	*
³⁰ SiCC	10 _{4,6} – 9 _{4,5}	230509.85	6.00	230510.17	0.72	0.10	31	15	14.50		+
³⁰ SiCC	10 _{4,7} – 9 _{4,6}	230367.68	9.00	230368.29	0.50	0.13	17	14	14.50		+
³⁰ SiCC	10 _{6,4} – 9 _{6,3}	229048.17	1.50	229046.60	0.63	0.17	17	12	12.30	1.31	&
³⁰ SiCC	10 _{6,5} – 9 _{6,4}			229046.55							&
³⁰ SiCC	11 _{0,11} – 10 _{0,10}	235516.69		235516.69	0.58*	0.18	30	20	14.50		\$
³⁰ SiCC	11 _{2,9} – 10 _{2,8}	264640.61	2.00	264645.33	0.77	0.15	20	23	13.80	1.13	s
³⁰ SiCC	11 _{4,7} – 10 _{4,6}	253945.88	3.00	253945.59	0.54	0.06	14	11	14.00	1.18	s
³⁰ SiCC	11 _{4,8} – 10 _{4,7}	253662.49	2.00	253664.50	0.48	0.06	15	11	13.90	1.18	s
³⁰ SiCC	12 _{0,12} – 11 _{0,11}	255626.68		255626.41							#

*¹The same as *1 in Table 4.

*²The same as *2 in Table 4.

*³The same as *3 in Table 4.

Table 8. Line parameters for metal containing species. The units are MHz for ν_{obs} and ν_{cat} , K km s⁻¹ for I_{int} , mK for T_{mb} , and km s⁻¹ for V_{exp} ; the same for corresponding uncertainties.

Species	Trans	ν_{obs}	σ	ν_{cat}^{*1}	I_{int}^{*2}	σ	T_{mb}	σ	V_{exp}	σ	Note ^{*3}
AlCl	$J = 10 - 9$	145744.46		145744.46a	0.34*	0.06	13	13	14.50	1.21	\$&
AlCl	$J = 16 - 15$	233116.28	1.00	233116.32a	1.96	0.08	70	13	13.40	1.29	&
AlCl	$J = 18 - 17$	262220.12		262219.25a	2.29*	0.22	58	25	13.20	1.14	&\$
Al ³⁷ Cl	$J = 11 - 10$	156546.44	0.39	156547.00a	0.55	0.09	23	18	13.30	0.75	&
Al ³⁷ Cl	$J = 16 - 15$	227643.31		227643.31a	0.46	0.12	25	19	14.50		&
Al ³⁷ Cl	$J = 17 - 16$	241855.85		241854.99a	0.60	0.09	22	15	14.50		&#
Al ³⁷ Cl	$J = 18 - 17$	256063.28	1.00	256063.74a	0.72	0.08	24	14	13.50	1.17	&
AlF	$J = 4 - 3$	131895.03	2.35	131899.23a	1.33	0.12	30	21	25.00	3.55	&
AlF	$J = 7 - 6$	230793.87	1.00	230793.89a	2.39	0.10	83	15	14.00	1.30	&
AlF	$J = 8 - 7$	263749.15	1.00	263749.34a	2.69	0.11	90	19	14.10	1.14	&
MgNC	$N = 12 - 11, J = 23/2 - 21/2$	143169.51		143169.51a	0.53*	0.06	23	13	14.50		\$&
MgNC	$N = 12 - 11, J = 25/2 - 23/2$	143183.67		143183.67a	0.64*	0.05	28	13	14.50		\$&
MgNC	$N = 13 - 12, J = 25/2 - 23/2$			155097.84b							*&
MgNC	$N = 13 - 12, J = 25/2 - 23/2$	155101.12		155101.12b	0.58*	0.09	30	31	14.50		*&
MgNC	$N = 13 - 12, J = 27/2 - 25/2$			155101.12b							*&
MgNC	$N = 13 - 12, J = 27/2 - 25/2$	155097.84		155097.84b	0.06*	0.09	3	31	14.50		*&
NaCN	$9_{1,8} - 8_{1,7}$	145075.39	0.39	145075.76	0.45	0.08	19	15	11.00	0.81	\$
NaCN	$9_{1,9} - 8_{1,8}$	135303.55		135303.55	0.54	0.06	23	12	14.50		+
NaCN	$9_{2,7} - 8_{2,6}$	142410.86		142410.86	0.34	0.08	17	16	14.50		s
NaCN	$9_{3,6} - 8_{3,5}$	140936.66	1.00	140938.28	0.23	0.07	3	9	14.30	0.42	s
NaCN	$9_{3,7} - 8_{3,6}$	140854.69		140854.69	0.28	0.07	10	10	14.50		+
NaCN	$9_{4,5} - 8_{4,4}$	140666.75	3.10	140668.29	0.30	0.10	5	16	15.50	0.42	&
NaCN	$9_{4,6} - 8_{4,5}$			140667.09							&
NaCN	$10_{0,10} - 9_{0,9}$	153558.18		153558.18	0.27	0.08	15	18	14.50		+
NaCN	$10_{1,10} - 9_{1,9}$	150208.46	3.53	150210.63	0.30*	0.06	9	13	15.95	7.00	s
NaCl	$J = 11 - 10$	143238.48	0.39	143237.37	0.60	0.07	14	13	11.80	0.82	s
NaCl	$J = 12 - 11$	156248.12	0.06	156248.59	0.44	0.03	27	24	14.96	0.13	s
NaCl	$J = 17 - 16$	221260.16		221260.16	0.95	0.13	36	21	14.50		+
NaCl	$J = 18 - 17$	234251.83		234251.83	0.61	0.10	22	16	14.50		+
NaCl	$J = 20 - 19$			260223.11							#
Na ³⁷ Cl	$J = 20 - 19$	254663.46		254663.46	0.32*	0.04	5	11	14.48		\$
Na ³⁷ Cl	$J = 21 - 20$	267365.84		267365.84	0.29	0.11	16	13	14.50		+

*1The same as *1 in Table 4.

*2The same as *2 in Table 4.

*3The same as *3 in Table 4.

Table 9. Line parameters for hydrocarbon compounds. The units are MHz for ν_{obs} and ν_{cat} , K km s⁻¹ for I_{int} , mK for T_{mb} , and km s⁻¹ for V_{exp} ; the same for corresponding uncertainties.

Species	Trans	ν_{obs}	σ	ν_{cat}^{*1}	I_{int}^{*2}	σ	T_{mb}	σ	V_{exp}	σ	Note*3
CCH	$(N, J, F) = (3, \frac{5}{2}, 3) - (2, \frac{5}{2}, 3)$	262208.59	1.00	262208.44	5.33*	0.25	129	25	13.80	1.14	\$
CCH	$(N, J, F) = (3, 2) - (2, \frac{5}{2}, 2)$	262079.60	1.00	262078.78	6.54*	0.57	226	25	13.80	1.14	*
CCH	$(N, J, F) = (3, 2) - (2, \frac{5}{2}, 1)$	262065.62	1.00	262067.33	69.60*	0.75	2390	25	13.90	1.14	*&
CCH	$(N, J, F) = (3, \frac{7}{2}, 3) - (2, \frac{5}{2}, 2)$			262064.84							*&
CCH	$(N, J) = (3, \frac{7}{2}) - (2, \frac{5}{2})$	262004.73	1.00	262005.32a	96.20*	1.08	3520	25	13.90	1.14	\$&
¹³ CCH	$(N, J, F_1, F) = (3, \frac{5}{2}, 2, \frac{5}{2}) - (2, \frac{5}{2}, 1, \frac{5}{2})$	252480.92		252480.92	1.39*	0.25	35	43	14.50		*
¹³ CCH	$(N, J, F_1, F) = (3, \frac{3}{2}, 3, \frac{3}{2}) - (2, \frac{3}{2}, 2, \frac{3}{2})$	252468.78		252468.78	0.02*	0.02	2	44	14.50		*
¹³ CCH	$(N, J, F_1, F) = (3, \frac{3}{2}, 3, \frac{3}{2}) - (2, \frac{3}{2}, 2, \frac{3}{2})$	252457.86		252457.86	0.74*	0.29	19	43	14.50		*
¹³ CCH	$(N, J, F_1) = (3, \frac{7}{2}, 3) - (2, \frac{5}{2}, 2)$	252448.62		252448.62a	1.92*	0.32	49	43	14.50		*&
¹³ CCH	$(N, J, F_1) = (3, \frac{7}{2}, 4) - (2, \frac{5}{2}, 3)$	252423.54		252423.54a	2.43*	0.25	62	43	14.50		*&
C ¹³ CH	$(N, J, F_1, F) = (3, \frac{5}{2}, 2, \frac{5}{2}) - (2, \frac{5}{2}, 1, \frac{5}{2})$	255815.39		255816.16	0.04*	0.07	1	14	14.50		*
C ¹³ CH	$(N, J, F_1, F) = (3, \frac{5}{2}, 2, \frac{5}{2}) - (2, \frac{5}{2}, 1, \frac{5}{2})$	255809.64		255810.41	0.28*	0.07	10	14	14.50		*
C ¹³ CH	$(N, J, F_1, F) = (3, \frac{5}{2}, 2, \frac{5}{2}) - (2, \frac{5}{2}, 1, \frac{5}{2})$	255803.79		255805.41	1.02*	0.04	36	14	14.50		*&
C ¹³ CH	$(N, J, F_1, F) = (3, \frac{3}{2}, 3, \frac{3}{2}) - (2, \frac{3}{2}, 2, \frac{3}{2})$			255803.72							*&
C ¹³ CH	$(N, J, F_1, F) = (3, \frac{3}{2}, 3, \frac{3}{2}) - (2, \frac{3}{2}, 2, \frac{3}{2})$	255794.09		255794.86	0.86*	0.10	31	14	14.50		*
C ¹³ CH	$(N, J, F_1) = (3, \frac{7}{2}, 3) - (2, \frac{5}{2}, 2)$	255758.19	1.00	255757.40a	1.32*	0.08	45	14	13.60	1.17	*&
C ¹³ CH	$(N, J, F_1) = (3, \frac{7}{2}, 4) - (2, \frac{5}{2}, 3)$	255746.61	1.00	255746.68a	1.87*	0.08	60	14	14.30	1.17	*&
C ₃ H	X ² Π, (N, J) = (6, $\frac{13}{2}$) - (5, $\frac{11}{2}$), e	141636.09	0.39	141636.12a	4.50	0.07	151	14	14.10	0.83	&
C ₃ H	X ² Π, (N, J) = (6, $\frac{13}{2}$) - (5, $\frac{11}{2}$), f	141708.97	0.39	141709.12a	4.13	0.07	130	14	13.30	0.83	&
C ₃ H	X ² Π, (N, J) = (7, $\frac{13}{2}$) - (6, $\frac{11}{2}$), e	149212.54	0.39	149212.67a	1.96	0.06	61	11	13.50	0.78	&
C ₃ H	X ² Π, (N, J) = (7, $\frac{13}{2}$) - (6, $\frac{11}{2}$), f	149106.79	0.39	149106.97a	2.04	0.06	63	11	13.70	0.78	&
C ₃ H	X ² Π, (N, J) = (10, $\frac{21}{2}$) - (9, $\frac{19}{2}$), e	229433.07		229433.07	0.62	0.15	19	16	14.50		+
C ₃ H	X ² Π, (N, J) = (10, $\frac{21}{2}$) - (9, $\frac{19}{2}$), f	229213.88		229213.88	0.52*	0.14	8	16	14.50	1.31	\$
C ₃ H	$\nu_4 = 1, \mu^2\Sigma, (N, J) = (6, \frac{11}{2}) - (5, \frac{9}{2})$	134628.08		134628.08a	0.16	0.07	9	10	14.50		&
C ₃ H	$\nu_4 = 1, \mu^2\Sigma, (N, J) = (6, \frac{13}{2}) - (5, \frac{11}{2})$	134604.19		134604.19a	0.16	0.07	9	9	14.50		&
C ₃ H	$\nu_4 = 1, \mu^2\Sigma, (N, J) = (7, \frac{13}{2}) - (6, \frac{11}{2})$	157061.67	1.50	157061.15	0.42	0.15	14	17	12.40	0.37	s
C ₃ H	$\nu_4 = 1, \mu^2\Sigma, (N, J) = (7, \frac{13}{2}) - (6, \frac{11}{2})$	157039.26	1.50	157038.93	0.46	0.14	9	17	13.30	0.37	s
¹³ CCCH	X ² Π, (N, J) = (11, $\frac{23}{2}$) - (10, $\frac{21}{2}$), e			241856.03a							&#
¹³ CCCH	X ² Π, (N, J) = (12, $\frac{21}{2}$) - (11, $\frac{19}{2}$), e	252718.74	2.54	252721.23a	0.16*	0.05	4	9	14.00	1.19	\$&
¹³ CCCH	X ² Π, (N, J) = (12, $\frac{23}{2}$) - (11, $\frac{21}{2}$), f	252954.97	3.00	252964.72	0.19	0.08	7	7	14.60	1.19	s
c-C ₃ H	3 _{1,3} - 2 _{1,2} , J = 5/2 - 3/2	133187.09		133187.09a	0.62	0.17	14	36	14.50		&
c-C ₃ H	3 _{1,3} - 2 _{1,2} , J = 7/2 - 5/2	132994.32		132994.32a	0.76	0.17	12	33	14.50		&
c-C ₃ H	4 _{3,1} - 3 _{3,0} , J = 7/2 - 5/2	238688.96		238688.96a	0.74*	0.17	31	22	14.50		*
c-C ₃ H	4 _{3,1} - 3 _{3,0} , J = 9/2 - 7/2	238637.10		238637.10a	1.06	0.14	34	22	14.50		&
c-C ₃ H	5 _{1,4} - 4 _{1,3} , J = 11/2 - 9/2	252697.52	1.00	252697.78a	0.71*	0.03	16	5	14.00	1.19	\$&
c-C ₃ H	5 _{1,4} - 4 _{1,3} , J = 9/2 - 7/2	252881.32		252881.32a	1.60*	0.12	2	15	14.50		\$&
c-C ₃ H ₂	2 _{2,0} - 1 _{1,1}	150436.55		150436.55	0.74	0.10	26	21	14.50		+
c-C ₃ H ₂	3 _{1,2} - 2 _{2,1}	145089.61	0.39	145089.59	2.20	0.07	75	15	13.80	0.81	\$
c-C ₃ H ₂	3 _{2,1} - 2 _{1,2}	244222.08	3.90	244222.13	0.78	0.22	32	23	14.50		&
c-C ₃ H ₂	3 _{2,2} - 2 _{1,1}	155518.66	0.39	155518.30	1.18	0.15	38	30	12.50	0.75	s
c-C ₃ H ₂	4 _{0,4} - 3 _{1,3}	150820.64	0.39	150820.67	1.26	0.07	35	14	13.60	0.78	s
c-C ₃ H ₂	4 _{1,4} - 3 _{0,3}	150851.78	0.39	150851.91	3.79	0.07	122	14	13.80	0.78	s
c-C ₃ H ₂	4 _{3,2} - 3 _{2,1}	227169.33	1.00	227169.13	1.02	0.12	24	19	13.80	1.32	s
c-C ₃ H ₂	4 _{4,1} - 3 _{3,0}	265759.26	1.00	265759.44	2.26	0.11	72	13	14.40	1.13	s
c-C ₃ H ₂	5 _{3,3} - 4 _{2,2}	254987.64		254987.64	24.80	0.09	832	11	13.60	0.03	#
c-C ₃ H ₂	6 _{2,5} - 5 _{1,4}	251527.15	4.00	251527.30	1.15	0.37	33	40	14.20	1.19	s
c-C ₃ H ₂	7 _{3,4} - 7 _{2,5}	150283.48		150283.48	0.57	0.14	20	16	14.50		s
c-C ₃ H ₂	7 _{4,4} - 7 _{3,5}	150584.62		150584.62	0.08*	0.14	4	24	14.50		+
C ₄ H	N = 14 - 13, J = 27/2 - 25/2	133252.07	0.39	133252.14a	13.40	0.12	424	23	14.00	0.88	&
C ₄ H	N = 14 - 13, J = 29/2 - 27/2	133213.54	0.39	133213.65a	10.30	0.17	335	33	13.90	0.88	&
C ₄ H	N = 15 - 14, J = 29/2 - 27/2	142767.15	0.39	142767.28a	16.50	0.06	521	13	13.90	0.82	&
C ₄ H	N = 15 - 14, J = 31/2 - 29/2	142728.76	0.39	142728.77a	14.90	0.08	471	16	13.80	0.82	&
C ₄ H	N = 16 - 15, J = 31/2 - 29/2	152282.04	0.39	152282.09a	13.60	0.12	408	18	14.00	0.77	&
C ₄ H	N = 16 - 15, J = 33/2 - 31/2	152243.57	0.39	152243.62a	13.40	0.07	408	15	14.00	0.77	&
C ₄ H	N = 24 - 23, J = 47/2 - 45/2	228386.78	1.00	228386.92a	15.50	0.13	402	19	13.30	1.31	&
C ₄ H	N = 24 - 23, J = 49/2 - 47/2	228348.46	1.00	228348.59a	11.30	0.13	327	19	13.80	1.31	&
C ₄ H	N = 25 - 24, J = 49/2 - 47/2	237897.91	1.00	237898.02a	13.00	0.13	358	20	13.80	1.26	&
C ₄ H	N = 25 - 24, J = 51/2 - 49/2	237859.77	1.00	237859.69a	9.93	0.13	286	20	13.90	1.26	&
C ₄ H	N = 28 - 27, J = 55/2 - 53/2	266428.14	1.00	266428.06a	11.40	0.11	288	25	13.70	1.13	&
C ₄ H	N = 28 - 27, J = 57/2 - 55/2	266389.83	1.00	266389.81a	9.60	0.11	250	25	14.00	1.13	&
C ₄ H	$\nu_7 = 1^1e, (N, J) = (14, \frac{27}{2}) - (13, \frac{25}{2})$	132179.06	0.78	132178.98	2.82	0.16	95	21	13.80	1.77	s
C ₄ H	$\nu_7 = 1^1f, (N, J) = (14, \frac{27}{2}) - (13, \frac{25}{2})$	132586.99	0.78	132586.98	3.07	0.15	103	20	13.80	1.77	s
C ₄ H	$\nu_7 = 1^1e, (N, J) = (14, \frac{29}{2}) - (13, \frac{27}{2})$	134415.64	0.78	134415.87	2.41	0.07	79	10	13.60	1.74	s
C ₄ H	$\nu_7 = 1^1f, (N, J) = (14, \frac{29}{2}) - (13, \frac{27}{2})$	134023.57	0.78	134023.70	3.14	0.10	104	13	13.60	1.75	s
C ₄ H	$\nu_7 = 1^1e, (N, J) = (15, \frac{29}{2}) - (14, \frac{27}{2})$	141783.67	0.39	141783.70	2.41	0.07	76	15	13.90	0.82	s
C ₄ H	$\nu_7 = 1^1f, (N, J) = (15, \frac{29}{2}) - (14, \frac{27}{2})$	142223.81	0.39	142223.58	2.82	0.07	74	15	14.00	0.82	*
C ₄ H	$\nu_7 = 1^1e, (N, J) = (15, \frac{31}{2}) - (14, \frac{29}{2})$	143870.08	0.39	143870.37	2.57	0.07	80	14	13.40	0.81	s

Table 9—Continued

Species	Trans	ν_{obs}	σ	ν_{cat}^{*1}	I_{int}^{*2}	σ	T_{mb}	σ	V_{exp}	σ	Note ^{*3}
C ₄ H	$\nu_7 = 1^1_f, (N, J) = (15, \frac{31}{2}) - (14, \frac{29}{2})$	143446.43	0.39	143446.61	2.34	0.10	74	20	13.90	0.82	s
C ₄ H	$\nu_7 = 1^1_e, (N, J) = (16, \frac{31}{2}) - (15, \frac{29}{2})$	151375.81	0.39	151375.80	2.97	0.08	102	17	13.70	0.77	s
C ₄ H	$\nu_7 = 1^1_f, (N, J) = (16, \frac{31}{2}) - (15, \frac{29}{2})$	151847.29	0.39	151847.22	3.03	0.07	92	15	13.70	0.77	s
C ₄ H	$\nu_7 = 1^1_e, (N, J) = (16, \frac{33}{2}) - (15, \frac{31}{2})$	153334.71	0.39	153335.05	3.21	0.09	95	18	13.30	0.76	s
C ₄ H	$\nu_7 = 1^1_f, (N, J) = (16, \frac{33}{2}) - (15, \frac{31}{2})$	152879.82	0.39	152879.97	2.79	0.09	86	19	13.50	0.76	s
C ₄ H	$\nu_7 = 1^1_e, (N, J) = (23, \frac{47}{2}) - (22, \frac{45}{2})$	219767.50	1.00	219767.33	1.91	0.09	57	14	14.20	1.36	s
C ₄ H	$\nu_7 = 1^1_e, (N, J) = (24, \frac{47}{2}) - (23, \frac{45}{2})$	227824.35	1.00	227824.28	3.28	0.13	95	19	13.70	1.32	s
C ₄ H	$\nu_7 = 1^1_f, (N, J) = (24, \frac{47}{2}) - (23, \frac{45}{2})$	228539.45	1.00	228539.42	2.78	0.11	86	17	13.90	1.31	s
C ₄ H	$\nu_7 = 1^1_e, (N, J) = (24, \frac{49}{2}) - (23, \frac{47}{2})$	229273.87	1.00	229273.31	2.14	0.11	64	17	14.10	1.31	s
C ₄ H	$\nu_7 = 1^1_f, (N, J) = (24, \frac{49}{2}) - (23, \frac{47}{2})$	228575.27	1.00	228575.52	2.05	0.11	58	17	13.70	1.31	s
C ₄ H	$\nu_7 = 1^1_e, (N, J) = (25, \frac{49}{2}) - (24, \frac{47}{2})$	237357.69	1.00	237357.42	2.40	0.12	72	18	13.70	1.26	s
C ₄ H	$\nu_7 = 1^1_f, (N, J) = (25, \frac{49}{2}) - (24, \frac{47}{2})$	238101.91	1.00	238102.19	2.55	0.13	73	20	13.80	1.26	s
C ₄ H	$\nu_7 = 1^1_e, (N, J) = (25, \frac{51}{2}) - (24, \frac{49}{2})$	238781.60	1.00	238781.55	3.57	0.14	118	22	13.80	1.26	s
C ₄ H	$\nu_7 = 1^1_f, (N, J) = (25, \frac{51}{2}) - (24, \frac{49}{2})$	238053.41	1.00	238054.12	1.97	0.14	55	20	12.00	1.26	s
C ₄ H	$\nu_7 = 1^1_e, (N, J) = (27, \frac{53}{2}) - (26, \frac{51}{2})$	256414.03	1.00	256414.11	2.87	0.08	91	14	13.60	1.17	s
C ₄ H	$\nu_7 = 1^1_e, (N, J) = (27, \frac{55}{2}) - (26, \frac{53}{2})$	257802.98	1.00	257803.36	2.51	0.22	67	36	13.90	1.16	s
C ₄ H	$\nu_7 = 1^1_e, (N, J) = (28, \frac{55}{2}) - (27, \frac{53}{2})$	265938.58	1.00	265938.28	3.52	0.11	102	28	14.10	1.13	s
C ₄ H	$\nu_7 = 1^1_f, (N, J) = (28, \frac{55}{2}) - (27, \frac{53}{2})$	266770.86	1.00	266771.19	3.97	0.11	102	10	13.90	1.12	s
C ₄ H	$\nu_7 = 1^1_e, (N, J) = (28, \frac{57}{2}) - (27, \frac{55}{2})$	266500.42	1.00	266500.88	2.71	0.11	71	13	13.60	1.12	s
C ₄ H	$\nu_7 = 1^1_f, (N, J) = (28, \frac{57}{2}) - (27, \frac{55}{2})$	267316.20	1.00	267316.34	3.06	0.11	92	13	13.70	1.12	s
C ₄ H	$\nu_7 = 2^0, (N, J) = (14, \frac{27}{2}) - (13, \frac{25}{2})$	133918.35	0.78	133919.22	2.33	0.10	68	13	13.60	1.75	s
C ₄ H	$\nu_7 = 2^0, (N, J) = (14, \frac{29}{2}) - (13, \frac{27}{2})$	133862.49	0.78	133862.20	2.04	0.09	62	13	14.00	1.75	s
C ₄ H	$\nu_7 = 2^0, (N, J) = (15, \frac{27}{2}) - (14, \frac{25}{2})$	143480.74	0.39	143481.14	2.03	0.10	62	20	14.10	0.81	s
C ₄ H	$\nu_7 = 2^0, (N, J) = (15, \frac{29}{2}) - (14, \frac{27}{2})$	143424.54	0.39	143424.31	1.74	0.10	58	20	14.30	0.82	s
C ₄ H	$\nu_7 = 2^0, (N, J) = (16, \frac{27}{2}) - (15, \frac{25}{2})$	153042.24	0.39	153042.72	2.17	0.09	63	19	13.90	0.76	s
C ₄ H	$\nu_7 = 2^0, (N, J) = (16, \frac{29}{2}) - (15, \frac{27}{2})$	152986.34	0.39	152986.09	1.86	0.09	61	19	14.00	0.76	s
C ₄ H	$\nu_7 = 2^0, (N, J) = (23, \frac{45}{2}) - (22, \frac{43}{2})$	219962.46	1.00	219962.48	1.80	0.09	51	14	14.00	1.36	s
C ₄ H	$\nu_7 = 2^0, (N, J) = (23, \frac{47}{2}) - (22, \frac{45}{2})$	219907.90	1.00	219907.64	1.38	0.09	38	14	14.10	1.36	s
C ₄ H	$\nu_7 = 2^0, (N, J) = (24, \frac{47}{2}) - (23, \frac{45}{2})$	229521.69	1.00	229520.53	1.77	0.10	69	15	11.90	1.31	\$
C ₄ H	$\nu_7 = 2^0, (N, J) = (24, \frac{49}{2}) - (23, \frac{47}{2})$	229465.26	1.00	229466.03	1.34	0.11	52	17	12.80	1.31	s
C ₄ H	$\nu_7 = 2^0, (N, J) = (25, \frac{49}{2}) - (24, \frac{47}{2})$	239078.11		239078.11	2.13*	0.12	60	22	14.50		*\$
C ₄ H	$\nu_7 = 2^0, (N, J) = (25, \frac{51}{2}) - (24, \frac{49}{2})$	239023.58	1.00	239023.89	1.67	0.14	47	22	14.60	1.25	s
C ₄ H	$\nu_7 = 2^0, (N, J) = (27, \frac{53}{2}) - (26, \frac{51}{2})$	258190.57	1.00	258191.55	1.69	0.23	25	36	12.60	1.16	s
C ₄ H	$\nu_7 = 2^0, (N, J) = (27, \frac{55}{2}) - (26, \frac{53}{2})$	258137.80	1.00	258137.98	1.48*	0.22	32	36	15.10	1.16	\$
C ₄ H	$\nu_7 = 2^2, (N, J) = (14, \frac{29}{2}) - (13, \frac{27}{2})$	134921.19		134921.19	0.21	0.07	8	15	14.50		+
C ₄ H	$\nu_7 = 2^2, (N, J) = (15, \frac{27}{2}) - (14, \frac{25}{2})$	142214.23		142214.23	0.12*	0.07	3	15	14.50		+
C ₄ H	$\nu_7 = 2^2, (N, J) = (15, \frac{29}{2}) - (14, \frac{27}{2})$	144375.97		144375.97	0.20	0.11	6	16	14.50		*
C ₄ H	$\nu_7 = 2^2, (N, J) = (16, \frac{27}{2}) - (15, \frac{25}{2})$	151868.89		151868.89	0.16	0.07	5	15	14.50		+
C ₄ H	$\nu_7 = 2^2, (N, J) = (16, \frac{29}{2}) - (15, \frac{27}{2})$	153841.58		153841.58	0.38	0.08	17	18	14.50		+
C ₄ H	$\nu_7 = 2^2, (N, J) = (27, \frac{53}{2}) - (26, \frac{51}{2})$	257539.94		257539.94	0.67*	0.29	25	36	14.50		\$
C ₄ H	$\nu_7 = 2^2, (N, J) = (27, \frac{55}{2}) - (26, \frac{53}{2})$	258375.76	3.00	258376.49	0.74	0.33	7	28	12.70	1.16	s
C ₄ H	$\nu_7 = 2^2, (N, J) = (28, \frac{55}{2}) - (27, \frac{53}{2})$	267116.17	1.00	267116.97	2.05*	0.12	106	14	14.50	1.12	\$
¹³ CCCCH	$(N, J, F) = (15, \frac{29}{2}, 14) - (14, \frac{27}{2}, 13)$	137843.61		137843.61	0.16	0.09	10	11	14.50		&
¹³ CCCCH	$(N, J, F) = (15, \frac{29}{2}, 15) - (14, \frac{27}{2}, 14)$	137839.78		137839.78	0.16	0.09	10	11	14.50		&
¹³ CCCCH	$(N, J, F) = (15, \frac{31}{2}, 15) - (14, \frac{29}{2}, 14)$	137810.85		137810.85	0.14*	0.09	8	13	14.50		*
¹³ CCCCH	$(N, J, F) = (15, \frac{31}{2}, 16) - (14, \frac{29}{2}, 15)$	137806.92		137806.92	0.05*	0.09	2	13	14.50		*
¹³ CCCCH	$(N, J, F) = (16, \frac{31}{2}, 15) - (15, \frac{29}{2}, 14)$	147030.34		147030.34	0.20	0.14	1	12	9.34	0.40	&
¹³ CCCCH	$(N, J, F) = (16, \frac{31}{2}, 16) - (15, \frac{29}{2}, 15)$	147026.75		147026.75	0.20	0.14	1	12	9.34	0.40	&
¹³ CCCCH	$(N, J, F) = (16, \frac{33}{2}, 16) - (15, \frac{31}{2}, 15)$	146997.29		146997.29	0.19	0.11	8	15	14.50		&
¹³ CCCCH	$(N, J, F) = (16, \frac{33}{2}, 17) - (15, \frac{31}{2}, 16)$	146993.60		146993.60	0.19	0.11	8	15	14.50		&
C ¹³ CCCH	$(N, J) = (14, \frac{27}{2}) - (13, \frac{25}{2})$	132579.25		132579.25	0.12*	0.17	6	16	14.50		\$
C ¹³ CCCH	$(N, J) = (14, \frac{29}{2}) - (13, \frac{27}{2})$	132542.76	4.70	132541.49	0.46	0.20	9	11	17.60	0.88	s
C ¹³ CCCH	$(N, J) = (15, \frac{29}{2}) - (14, \frac{27}{2})$	142046.75	1.90	142046.38	0.34	0.10	13	12	15.70	0.41	s
C ¹³ CCCH	$(N, J) = (15, \frac{31}{2}) - (14, \frac{29}{2})$	142009.50	3.00	142008.59a	0.34	0.08	14	15	12.70	6.54	&
C ¹³ CCCH	$(N, J) = (16, \frac{31}{2}) - (15, \frac{29}{2})$	151513.08		151513.08	0.19	0.12	8	11	14.50		+
C ¹³ CCCH	$(N, J) = (16, \frac{33}{2}) - (15, \frac{31}{2})$	151475.30	4.80	151475.35	0.36	0.12	9	14	14.60	0.39	s
CC ¹³ CCH	$(N, J) = (15, \frac{29}{2}) - (14, \frac{27}{2})$	142263.62		142263.62	0.27	0.11	4	14	14.50		+
CC ¹³ CCH	$(N, J) = (16, \frac{31}{2}) - (15, \frac{29}{2})$	151744.87		151744.87	0.31	0.12	3	22	14.50		+
CC ¹³ CCH	$(N, J) = (16, \frac{33}{2}) - (15, \frac{31}{2})$	151706.57		151706.57	0.28	0.12	5	18	14.50		+
<i>l</i> -C ₄ H ₂	15 _{1,14} - 14 _{1,13}	134526.49	1.20	134525.23	0.35	0.08	7	7	11.70	1.74	+
<i>l</i> -C ₄ H ₂	15 _{1,15} - 14 _{1,14}	133405.29	1.00	133405.26	0.55	0.18	21	11	12.50	0.44	s
<i>l</i> -C ₄ H ₂	15 _{3,12} - 14 _{3,11}			133931.28							\$&
<i>l</i> -C ₄ H ₂	15 _{3,13} - 14 _{3,12}	133931.68		133931.28	0.50*	0.09	14	12	14.50		\$&
<i>l</i> -C ₄ H ₂	16 _{0,16} - 15 _{0,15}	142891.77		142891.69	0.23*	0.08	7	11	14.50		*&
<i>l</i> -C ₄ H ₂	16 _{2,14} - 15 _{2,13}			142891.85							*&
<i>l</i> -C ₄ H ₂	16 _{2,15} - 15 _{2,14}	142881.87		142881.87	0.10*	0.08	3	11	14.50		*&
<i>l</i> -C ₄ H ₂	16 _{3,13} - 15 _{3,12}			142859.14							&

Table 9—Continued

Species	Trans	ν_{obs}	σ	ν_{cat} ^{*1}	I_{int} ^{*2}	σ	T_{mb}	σ	V_{exp}	σ	Note ^{*3}
<i>l</i> -C ₄ H ₂	16 _{3,14} – 15 _{3,13}	142859.77	1.80	142859.12	0.22	0.10	3	11	11.50	0.41	&

^{*1}The same as *1 in Table 4.

^{*2}The same as *2 in Table 4.

^{*3}The same as *3 in Table 4.

Table 10. Line parameters for nitrogen containing species. The units are MHz for ν_{obs} and ν_{cat} , K km s⁻¹ for I_{int} , mK for T_{mb} , and km s⁻¹ for V_{exp} ; the same for corresponding uncertainties.

Species	Trans	ν_{obs}	σ	ν_{cat}^*1	I_{int}^*2	σ	T_{mb}	σ	V_{exp}	σ	Note*3
CN	$(N, J, F) = (2, \frac{1}{2}, \frac{1}{2}) - (1, \frac{1}{2}, \frac{1}{2})$	226286.81	1.00	226287.42	2.55*	0.13	78	17	14.60	1.32	*&
CN	$(N, J, F) = (2, \frac{3}{2}, \frac{3}{2}) - (1, \frac{3}{2}, \frac{3}{2})$	226301.21	1.00	226298.92	2.37*	0.16	65	17	16.40	1.32	*&
CN	$(N, J, F) = (2, \frac{5}{2}, \frac{5}{2}) - (1, \frac{5}{2}, \frac{5}{2})$	226314.84	1.00	226314.55	3.26*	0.14	101	17	14.40	1.32	*&
CN	$(N, J, F) = (2, \frac{7}{2}, \frac{7}{2}) - (1, \frac{7}{2}, \frac{7}{2})$			226303.08							*&
CN	$(N, J, F) = (2, \frac{9}{2}, \frac{9}{2}) - (1, \frac{9}{2}, \frac{9}{2})$	226341.45	1.00	226332.53	3.52*	0.12	113	17	13.90	1.32	*&
CN	$(N, J, F) = (2, \frac{11}{2}, \frac{11}{2}) - (1, \frac{11}{2}, \frac{11}{2})$	226359.79	1.00	226359.87	6.43*	0.12	213	17	13.50	1.32	*&
CN	$(N, J, F) = (2, \frac{13}{2}, \frac{13}{2}) - (1, \frac{13}{2}, \frac{13}{2})$			226341.94							*&
CN	$(N, J, F) = (2, \frac{15}{2}, \frac{15}{2}) - (1, \frac{15}{2}, \frac{15}{2})$	226661.71	1.00	226663.70	7.29*	0.06	267	19	13.10	1.32	*
CN	$(N, J, F) = (2, \frac{17}{2}, \frac{17}{2}) - (1, \frac{17}{2}, \frac{17}{2})$	226615.65	1.00	226616.56	1.15*	0.26	38	19	13.90	1.32	*
CN	$(N, J, F) = (2, \frac{19}{2}, \frac{19}{2}) - (1, \frac{19}{2}, \frac{19}{2})$	226631.85	1.00	226632.19	6.54*	0.25	220	19	13.50	1.32	*
CN	$(N, J, F) = (2, \frac{21}{2}, \frac{21}{2}) - (1, \frac{21}{2}, \frac{21}{2})$	226678.63	1.00	226679.37	8.33*	0.06	274	19	14.60	1.32	*
CN	$(N, J, F) = (2, \frac{23}{2}, \frac{23}{2}) - (1, \frac{23}{2}, \frac{23}{2})$	226658.23	1.00	226659.58	12.50*	0.06	482	19	12.50	1.32	*
CN	$(N, J, F) = (2, \frac{25}{2}, \frac{25}{2}) - (1, \frac{25}{2}, \frac{25}{2})$	226887.36		226887.36	3.66*	0.17	160	19	14.50		*&
CN	$(N, J, F) = (2, \frac{27}{2}, \frac{27}{2}) - (1, \frac{27}{2}, \frac{27}{2})$			226875.89							*&
CN	$(N, J, F) = (2, \frac{29}{2}, \frac{29}{2}) - (1, \frac{29}{2}, \frac{29}{2})$	226892.12		226892.12	13.40*	0.15	584	19	14.50		*
CN	$(N, J, F) = (2, \frac{31}{2}, \frac{31}{2}) - (1, \frac{31}{2}, \frac{31}{2})$	226873.79	1.00	226874.17	44.70*	0.11	1980	19	14.30	1.32	*&
CN	$(N, J, F) = (2, \frac{33}{2}, \frac{33}{2}) - (1, \frac{33}{2}, \frac{33}{2})$			226874.75							*&
C ₃ N	$(N, J) = (14, \frac{27}{2}) - (13, \frac{25}{2})$	138534.29	0.39	138534.48a	10.10	0.07	330	14	13.80	0.84	&
C ₃ N	$(N, J) = (14, \frac{29}{2}) - (13, \frac{27}{2})$	138515.68	0.39	138515.72a	9.30	0.07	310	14	13.80	0.84	&
C ₃ N	$(N, J) = (15, \frac{29}{2}) - (14, \frac{27}{2})$	148427.70	0.39	148427.97a	10.70	0.05	340	10	13.80	0.79	&
C ₃ N	$(N, J) = (15, \frac{31}{2}) - (14, \frac{29}{2})$	148409.02	0.39	148408.94a	9.45	0.05	307	10	14.00	0.79	&
C ₃ N	$(N, J) = (16, \frac{31}{2}) - (15, \frac{29}{2})$	158320.90	0.39	158321.04a	10.60	0.15	313	32	13.90	0.74	&
C ₃ N	$(N, J) = (16, \frac{33}{2}) - (15, \frac{31}{2})$	158302.13	0.39	158302.02a	9.30	0.15	279	32	13.90	0.74	&
C ₃ N	$(N, J) = (23, \frac{43}{2}) - (22, \frac{41}{2})$	227562.86		227562.86a	0.84*	0.25	29	19	14.50		*&
C ₃ N	$(N, J) = (23, \frac{45}{2}) - (22, \frac{43}{2})$	227544.97		227544.97a	1.30*	0.25	45	19	14.50		*&
C ₃ N	$(N, J) = (24, \frac{47}{2}) - (23, \frac{45}{2})$	237453.53		237453.53	0.55*	0.13	13	15	14.50		*
C ₃ N	$(N, J) = (24, \frac{49}{2}) - (23, \frac{47}{2})$	237434.78		237434.78	0.28*	0.13	6	15	14.50		*
C ₃ N	$(N, J) = (27, \frac{53}{2}) - (26, \frac{51}{2})$	267121.62		267121.62a	0.06*	0.12	3	14	14.50		&\$
C ₃ N	$(N, J) = (27, \frac{55}{2}) - (26, \frac{53}{2})$	267102.88		267102.88a	0.31*	0.12	16	14	14.50		&\$
HCN	$J = 3 - 2$	265884.55	1.00	265886.44	619.00	0.11	31200	487	13.10	1.13	s
HCN	$\nu_2 = 1^1e, J = 3 - 2$	265852.20	1.00	265852.72	22.50	0.11	1070	30	12.60	1.13	s
HCN	$\nu_2 = 1^1f, J = 3 - 2$	267200.20	1.00	267199.28	19.90	0.11	1120	122	12.60	1.12	s
HCN	$\nu_2 = 2^0, J = 3 - 2$	267242.23	1.00	267243.15	12.70	0.11	544	24	13.70	1.12	#
HCN	$\nu_2 = 3^1e, J = 3 - 2$	266540.82	1.00	266540.97	0.62	0.21	85	5	4.33	1.12	s
H ¹³ CN	$J = 3 - 2$	259010.96	1.00	259011.80	251.00	0.25	12700	43	14.60	1.16	s
H ¹³ CN	$\nu_2 = 1^1e, J = 3 - 2$	258936.05		258936.05	1.44	0.25	83	43	14.50		+
H ¹³ CN	$\nu_2 = 1^1f, J = 3 - 2$	260223.86	1.00	260224.81	1.59	0.13	81	21	13.80	1.15	#
HC ¹⁵ N	$J = 3 - 2$	258156.90	1.00	258157.09	4.06*	0.20	102	36	12.80	1.16	\$
HN ¹³ C	$J = 3 - 2$	261263.97	1.00	261263.31	1.02	0.09	36	15	13.50	1.15	s
HCCCN	$J = 15 - 14$	136464.23	0.39	136464.41	38.60	0.08	1590	16	13.80	0.86	s
HCCCN	$J = 16 - 15$	145560.81	0.39	145560.95	31.80	0.12	1280	24	13.50	0.80	s
HCCCN	$J = 17 - 16$	154657.25	0.39	154657.28	29.50	0.12	1170	24	13.80	0.76	s
HCCCN	$J = 25 - 24$	227418.96	1.00	227418.91	5.34	0.12	202	19	13.40	1.32	s
HCCCN	$J = 26 - 25$	236512.48	1.00	236512.78	4.38	0.12	158	18	13.40	1.27	s
HCCCN	$J = 28 - 27$	254699.33	1.00	254699.50	3.34*	0.07	110	11	13.60	1.18	\$
HCCCN	$J = 29 - 28$	263792.27	1.00	263792.31	2.24*	0.12	86	19	13.02	0.11	\$
H ¹³ CCCN	$J = 15 - 14$	132246.26	0.78	132246.36	1.78	0.16	54	21	13.90	1.77	s
H ¹³ CCCN	$J = 16 - 15$	141061.87	0.39	141061.78	0.71	0.05	25	11	13.70	0.83	s
H ¹³ CCCN	$J = 17 - 16$	149876.78	0.39	149876.98	0.67	0.07	20	13	13.10	0.78	s
H ¹³ CCCN	$J = 18 - 17$	158692.00		158692.00	0.46	0.15	21	17	14.50		@
H ¹³ CCCN	$J = 26 - 25$	229203.10		229203.10	0.39*	0.14	6	16	14.50		\$
HC ¹³ CCN	$J = 15 - 14$	135885.29	0.39	135885.52	1.15	0.08	37	14	13.00	0.86	s
HC ¹³ CCN	$J = 16 - 15$	144943.61	0.39	144943.47	0.91	0.08	24	15	12.30	0.81	\$
HC ¹³ CCN	$J = 17 - 16$	154001.15	0.39	154001.22	0.84	0.09	26	18	13.00	0.76	\$
HC ¹³ CCN	$J = 26 - 25$	235509.49		235509.49	0.44*	0.18	23	20	14.50		\$
HCC ¹³ CN	$J = 15 - 14$	135898.51	0.39	135898.63	1.22	0.07	36	14	14.50	0.86	s
HCC ¹³ CN	$J = 16 - 15$	144957.67	0.39	144957.45	0.86	0.07	24	15	13.10	0.81	\$
HCC ¹³ CN	$J = 17 - 16$	154015.93	0.39	154016.08	0.87	0.09	28	18	13.70	0.76	\$
HCC ¹³ CN	$J = 26 - 25$	235532.21		235532.21	0.38*	0.18	19	20	14.50		\$
CH ₃ CN	8 ₀ - 7 ₀	147174.63		147174.63a	1.26*	0.12	44	16	14.50		&
CH ₃ CN	8 ₁ - 7 ₁	147171.81		147171.81a	1.22*	0.13	42	16	14.50		&
CH ₃ CN	8 ₂ - 7 ₂	147163.32		147163.32a	0.69*	0.07	24	16	14.50		&
CH ₃ CN	8 ₃ - 7 ₃	147149.10		147149.10a	0.82*	0.06	28	16	14.50		&
CH ₃ CN	12 ₀ - 11 ₀	220746.01		220747.26a	2.42*	0.14	93	21	14.50		*&\$#
CH ₃ CN	12 ₁ - 11 ₁			220743.01a							*&\$#
CH ₃ CN	12 ₂ - 11 ₂	220730.28		220730.28a	1.28*	0.14	43	22	14.50		*&
CH ₃ CN	12 ₃ - 11 ₃	220707.10	2.65	220709.08a	1.39*	0.14	49	22	13.90	1.36	*&

Table 10—Continued

Species	Trans	ν_{obs}	σ	$\nu_{\text{cat}}^{\ast 1}$	$I_{\text{int}}^{\ast 2}$	σ	T_{mb}	σ	V_{exp}	σ	Note ^{*3}
CH ₃ CN	13 ₀ – 12 ₀	239137.94		239137.94a	1.76*	0.13	50	22	14.50		*&
CH ₃ CN	13 ₁ – 12 ₁	239133.34		239133.34a	0.20*	0.11	6	22	14.50		*&
CH ₃ CN	13 ₂ – 12 ₂	239119.54		239119.54a	0.95*	0.12	27	22	14.50		*&
CH ₃ CN	13 ₃ – 12 ₃	239096.52		239096.52a	1.41*	0.12	40	22	14.50		*&\$
CH ₃ CN	14 ₀ – 13 ₀	257522.45		257527.40a	2.77*	0.30	102	36	14.50		\$&
CH ₃ CN	14 ₁ – 13 ₁			257522.45a							\$&
PN	$J = 3 - 2$	140967.75	3.34	140967.75a	0.14*	0.04	5	9	12.20	0.83	\$&

(to be continued)

Table 11. Line parameters for oxygen and sulfur containing species. The units are MHz for ν_{obs} and ν_{cat} , K km s^{-1} for I_{int} , mK for T_{mb} , and km s^{-1} for V_{exp} ; the same for corresponding uncertainties.

Species	Trans	ν_{obs}	σ	$\nu_{\text{cat}}^{\text{*1}}$	$I_{\text{int}}^{\text{*2}}$	σ	T_{mb}	σ	V_{exp}	σ	Note ^{*3}
CO	$J = 2 - 1$	230537.32	1.00	230538.00	561.00	0.10	26600	15	13.60	1.30	s
¹³ CO	$J = 2 - 1$	220398.48	1.00	220398.67	56.30	0.09	1650	14	14.20	1.36	s
C ¹⁷ O	$J = 2 - 1$	224714.37	1.00	224714.39	3.45	0.11	78	18	14.20	1.33	s
C ¹⁸ O	$J = 2 - 1$	219560.23	1.00	219560.36	2.94	0.09	64	14	14.40	1.37	s
H ₂ CO	$2_{1,1} - 1_{1,0}$	150498.33		150498.33	0.15	0.14	3	18	14.50		+
H ₂ CO	$2_{1,2} - 1_{1,1}$	140839.50		140839.50	0.22	0.07	21	10	14.50		+
CS	$J = 3 - 2$	146968.79	0.39	146969.03	113.00	0.08	4900	16	13.00	0.80	s
CS	$J = 5 - 4$	244934.91	1.00	244935.64	220.00	0.30	9910	47	12.50	1.22	s
CS	$v = 1, J = 5 - 4$	243160.77		243160.77	0.48*	0.07	25	11	14.50		\$
¹³ CS	$J = 3 - 2$	138739.22	0.39	138739.33	4.32	0.07	155	14	13.50	0.84	s
¹³ CS	$J = 5 - 4$	231220.85	1.00	231221.00	7.09	0.10	275	15	14.10	1.30	s
C ³³ S	$J = 3 - 2$	145755.61	0.20	145755.73	1.13*	0.05	43	10	14.90	4.02	\$
C ³³ S	$J = 5 - 4$	242913.52	1.00	242913.61	3.30	0.11	123	18	14.30	1.23	s
C ³⁴ S	$J = 3 - 2$	144617.13	0.39	144617.11	8.69	0.08	306	16	13.80	0.81	s
C ³⁴ S	$J = 5 - 4$	241015.87	1.00	241016.19	16.30	0.10	598	16	13.70	1.24	s
¹³ C ³⁴ S	$J = 5 - 4$	227300.50		227300.50	0.17	0.12	8	19	14.50		+
CCS	$N = 10 - 9, J = 11 - 10$	131551.97		131551.97	0.68	0.32	26	44	14.50		+
CCS	$N = 11 - 10, J = 10 - 9$	140180.74		140180.74	0.42	0.17	19	22	14.50		+
CCS	$N = 11 - 10, J = 11 - 10$	142500.85	0.39	142501.70	0.70	0.07	22	16	17.50	0.82	s
CCS	$N = 11 - 10, J = 12 - 11$	144245.19	0.39	144244.84	0.97	0.08	37	14	11.90	0.81	s
CCS	$N = 12 - 11, J = 11 - 10$	153449.78		153449.78	0.46	0.08	13	18	14.50		+
CCS	$N = 12 - 11, J = 12 - 11$	155451.35	2.00	155454.49	0.37	0.21	13	23	13.80	0.38	s
CCS	$N = 12 - 11, J = 13 - 12$	156981.67		156981.67	0.87	0.09	35	20	14.50		+
C ₃ S	$J = 24 - 23$	138725.84		138725.84a	0.22	0.07	12	14	14.50		&
C ₃ S	$J = 25 - 24$	144504.36	0.39	144504.99	0.54	0.07	14	16	17.30	0.81	s

*¹The same as *1 in Table 4.

*²The same as *2 in Table 4.

*³The same as *3 in Table 4.

Table 12. Column density and excitation temperature of extended species and some results from the literature. The unit is 10^{14}cm^{-2} for column density and K for temperature.

Mol	T_{ex}	σ^\dagger	N_{col}	σ^\dagger	θ_s	Lit. θ	$T_{\text{ex,lit}}$	N_{lit}	Lit. T,N	Notes on our results
C ₃ H	25	5	1.32	0.35	30''	1	20	0.7	7	
							8.5	0.56	8	
C ₄ H	53	3	81	11	30''	1	35	30	7	($v = 0$)
							48	56	9	
							15	24	8	
C ₄ H	53	4	59	21	30''	2				($\nu_7 = 1$)
C ₄ H	51	3	77	65	30''	2				($\nu_7 = 2^0$)
<i>c</i> -C ₃ H ₂	8	6	1.22	2.03	30''	2	20	0.16	8	(para)
<i>c</i> -C ₃ H ₂	5.7	1.4	4.82	4.14	30''	2				(ortho)
C ₃ N	35	10	4.54	2.13	36''	3	20	2.5	7	
							15	4.1	8	
HC ₃ N	28	1	8.0	1.5	30''	4	26	17	8	
H ¹³ CCCN	27		0.2		30''	2				
HC ¹³ CCN	18	16	0.5	1.4	30''	2				
HCC ¹³ CN	17	14	0.6	1.6	30''	2				
CH ₃ CN	35	4	0.26	0.06	30''	2	16	0.06	10	
SiC	33	13	0.49	0.23	30''	5	13	0.6	5	
SiCC	96	38	23.5	3.6	27''	6	16	2.2	8	($J_{\text{up}} = 6, 7, K_{\text{a}} = 0, 2, 4$)
							106	3.7	11	
							140	1.5	12	
							14	9.5	9	
							60	19	9	
SiCC	54	5.7	5.4	0.88	27''	6				($J_{\text{up}} = 9, 10, 11, 12, K_{\text{a}} = 0, 2, 4$)
SiCC	49		10.4		27''	6				($J_{\text{up}} = 10, 11, K_{\text{a}} = 6$)
SiCC	36		53		27''	6				($J_{\text{up}} = 10, 11, K_{\text{a}} = 8$)
Si ¹³ CC	25	2	0.99	0.17	27''	2				
²⁹ SiCC	25	2	1.06	0.19	27''	2				
³⁰ SiCC	33	3	0.73	0.12	27''	2				
MgNC	8.6		0.78		30''	1	15	0.25	8	

[†]Results without uncertainty are derived by two-point fitting in the rotation diagram. Note that the 1σ uncertainty of T_{ex} of C₃H, *c*-C₃H₂, C₃N, H¹³CCCN, HC¹³CCN, HCC¹³CN, SiCC (all 4 entries) and MgNC only includes the 10% relative calibration uncertainty because they only have reliable line intensities from one of our two telescopes, while that of the other entries and the uncertainty of all N_{col} values include the 20% absolute calibration uncertainty.

References. — (1) Guélin et al. 1993; (2) assumed to the same as its main isotopomer; (3) Bieging & Taffala 1993; (4) Guélin et al. 1996; (5) Cernicharo et al. 1989; (6) Lucas et al. 1995; (7) Cernicharo et al. 2000; (8) Kawaguchi et al. 1995; (9) very et al. 1992; (10) Guélin et al. 1991; (11) Groesbeck et al. 1994; (12) Thaddeus et al. 1984.

Table 13: Isotopic ratios determined from intensity ratios of optically thin lines for the circumstellar envelope of IRC +10216. The 1σ uncertainty includes the relative calibration uncertainty of 10%.

Ratios	Our results	Literature	Solar	Our method
12C/13C	34.7 [†] ±4.3 [†]	47 (+6,-5) ^a	89	SiCC
17O/18O	1.14 ±0.17	1.47 (+0.33,-0.25) ^b	0.18	CO
16O/17O	967 ±157	840 (+230,-170) ^b	2695	[13CO/C17O]*[12C/13C]
16O/18O	1172 ±348	1260 (+315,-240) ^b	490	[13CO/C18O]*[12C/13C]
32S/33S	93 ±10	100 (+23,-16) ^a	125	[13CS/C33S]*[12C/13C], [29SiS/Si33S]*[28Si/29Si], [30SiS/Si33S]*[28Si/30Si]
32S/34S	18.9 ±1.3	20.2 (+2.6-2.1) ^a	22.5	[29SiS/Si34S]*[28Si/29Si], [30SiS/Si34S]*[28Si/30Si]
34S/33S	5.17 ±0.44	5.7 (+0.8,-0.6) ^a	5.5	CS
28Si/29Si	17.2 ±1.1	18.7 (+1.3,-1.0) ^a	19.6	SiCC
28Si/30Si	24.7 ±1.8	28.6 (+1.8,-1.5) ^a	29.8	SiCC
29Si/30Si	1.46 ±0.11	1.47 (+0.11,-0.09) ^a	1.52	SiS,SiCC

^aKahane et al. 1988

^bKahane et al. 1992

[†]The uncertainty does not take into account line saturation effect and the value could be underestimated.

Table 14: List of narrow lines. Frequency is in MHz, T_{mb} is in mK, FWHM is in km s^{-1} and observation date is in Y/M/D format.

Transition	Freq	$T_{\text{mb}}^{\text{peak}}$	FWHM	Obs.date	Notes
HCN, $\nu_2 = 3^1e$, $J = 3 - 2$	266540.82	96 ± 5	7	2007/01/07	
SiS, $v = 0$, $J = 14 - 13$	254102.82	9070 ± 11		2007/01/08	blue peak on the top of thermal line
SiS, $v = 1$, $J = 13 - 12$	234813.22	92 ± 17	8.2	2005/12/15	
SiS, $v = 1$, $J = 14 - 13$	252866.47	295 ± 15	10.2	2007/01/23	blended with <i>c</i> -C ₃ H, $5_{1,4} - 4_{1,3}$, $9/2 - 7/2$ and Si ¹³ CC, ($11_{7,5} - 10_{7,4}$)&($11_{7,4} - 10_{7,3}$)

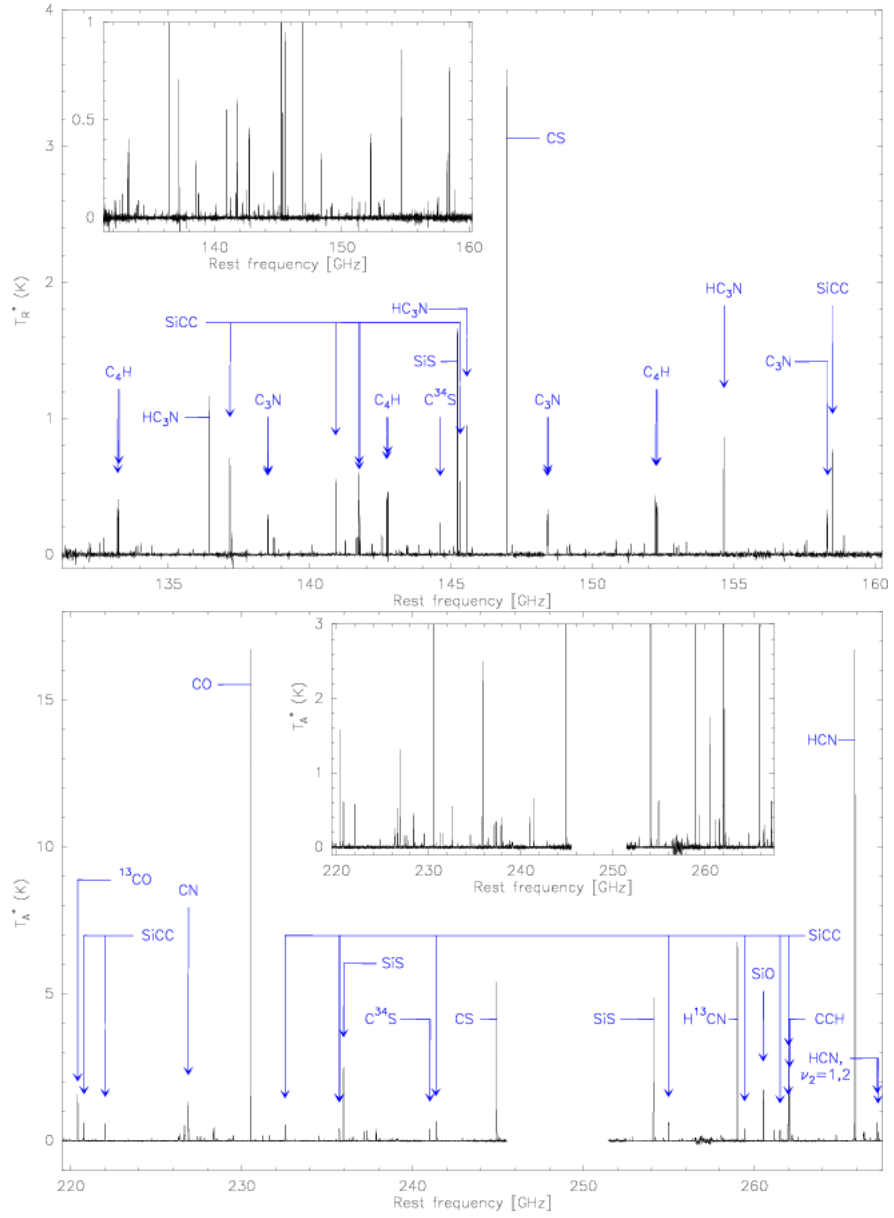


Fig. 1.— Over view of strong lines detected in the λ 1.3 and 2 mm surveys.

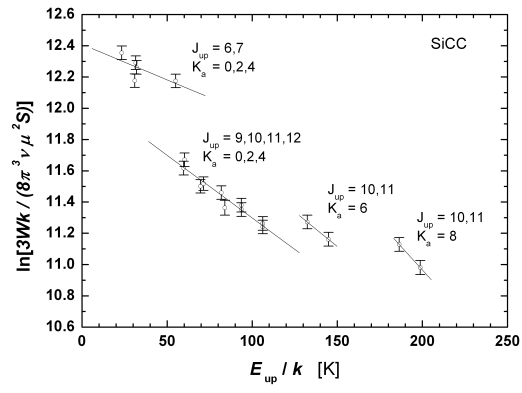


Fig. 2.— Rotation diagram of SiCC lines. A relative calibration uncertainty of 10% has been included in the error bar.

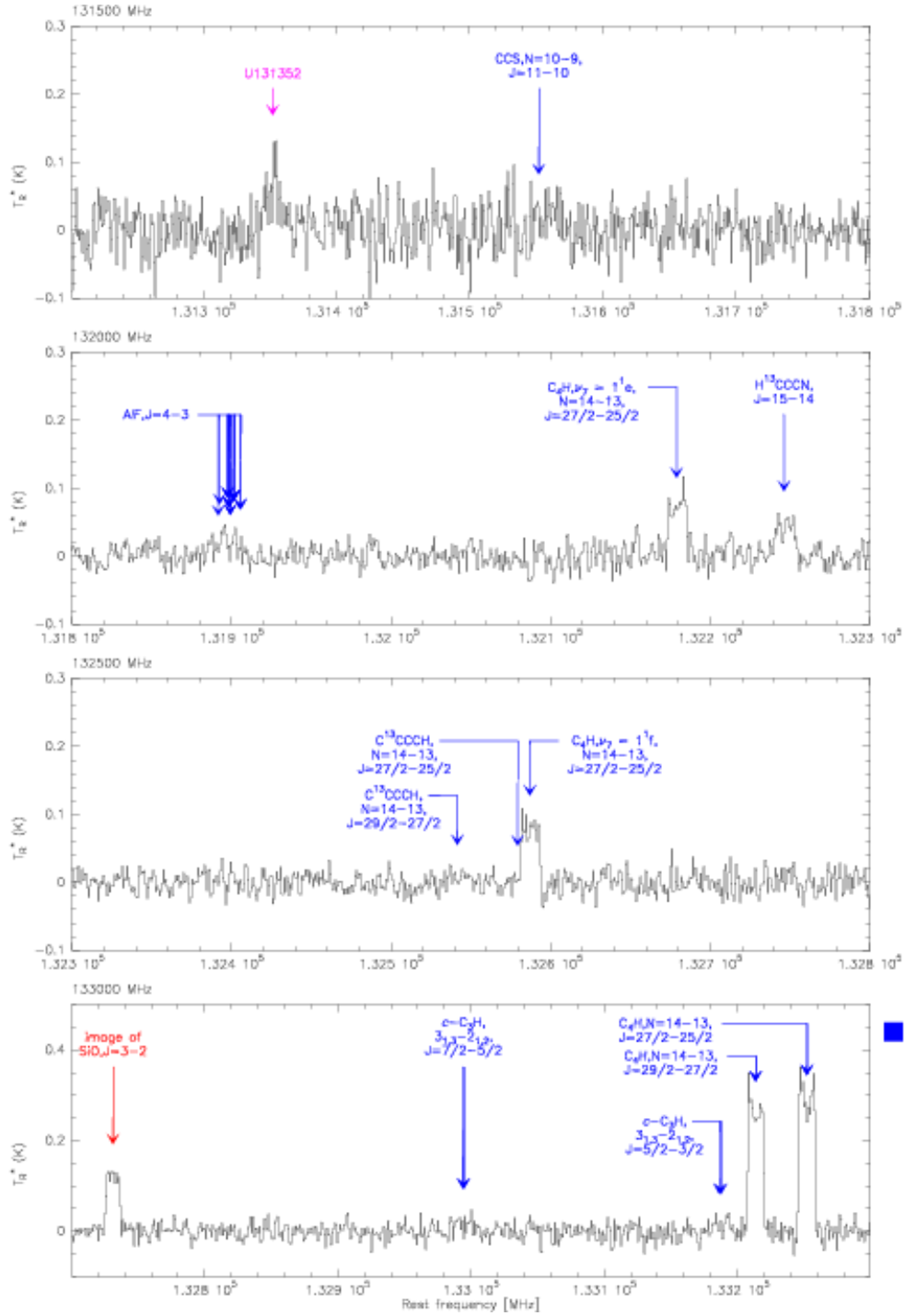


Fig. 3.— Spectra of IRC +10216 in the frequency ranges: 131.2-160.3, 219.5-245.5 and 251.5-267.5 GHz. T_R^* and T_A^* are plotted for KP12M (< 200 GHz) and SMT (> 200 GHz) data respectively. Resolution is 1 MHz in all plots. Temperature is usually plotted in -0.1 to 0.3K range, with exceptional plots marked by a blue square to the upper-right corner. Vertical arrows mark archival frequencies. (In an online color version, blue, magenta and red labels and arrows are used for identified, unidentified and image contamination lines, respectively, while zoom-in plots are placed in red boxes.)

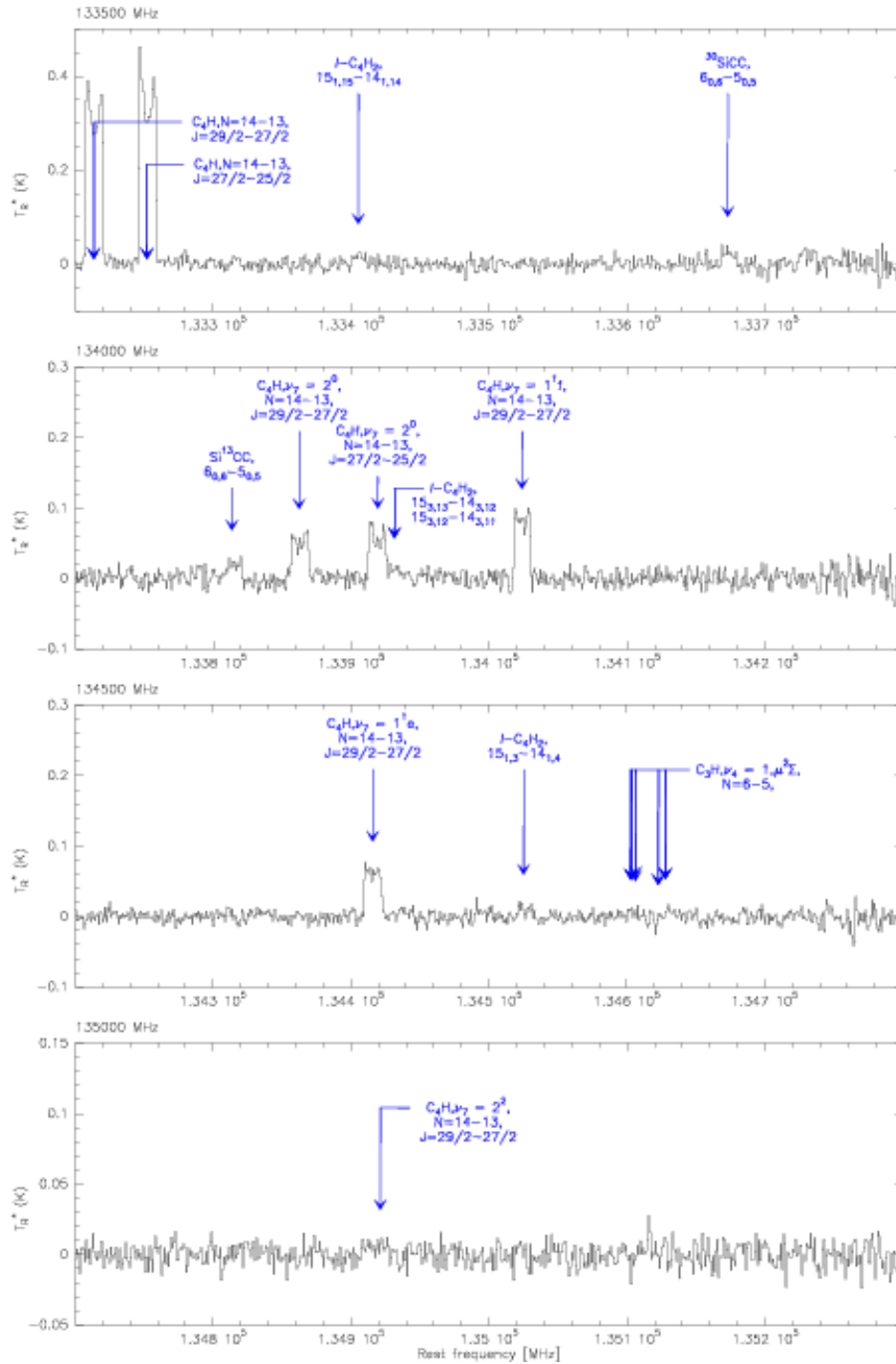


Fig. 3. — Continued.

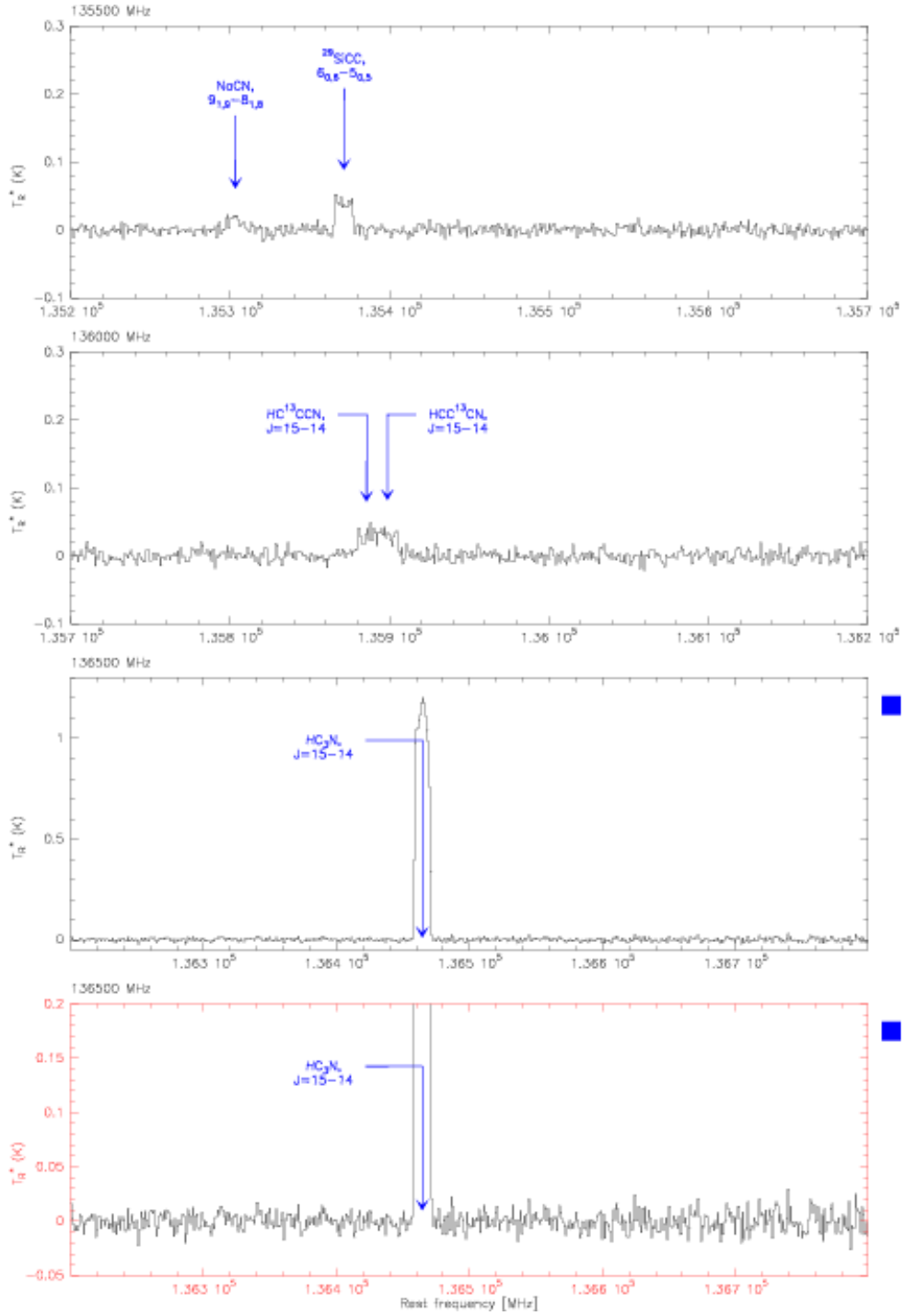


Fig. 3. — Continued.

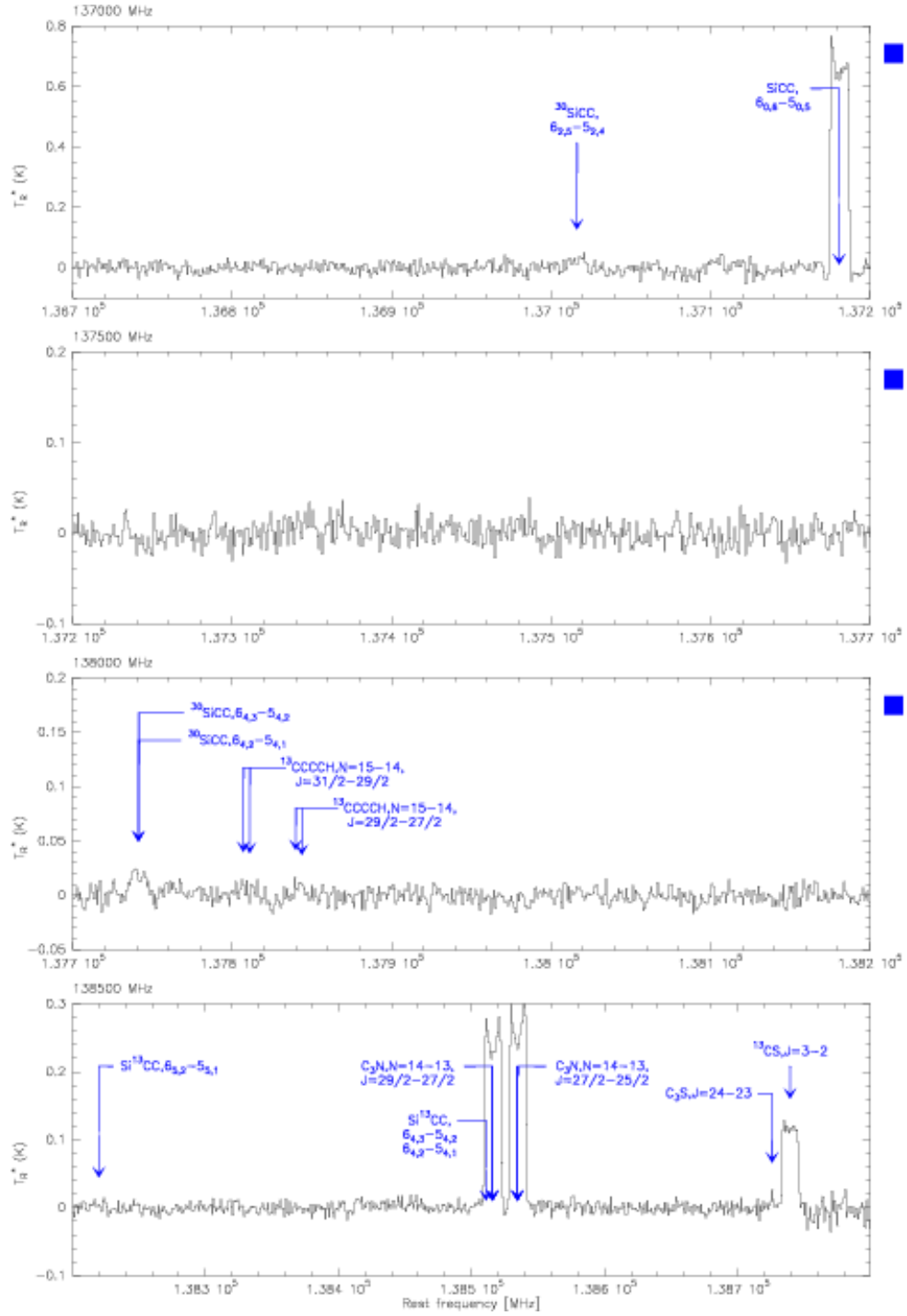


Fig. 3. — Continued.

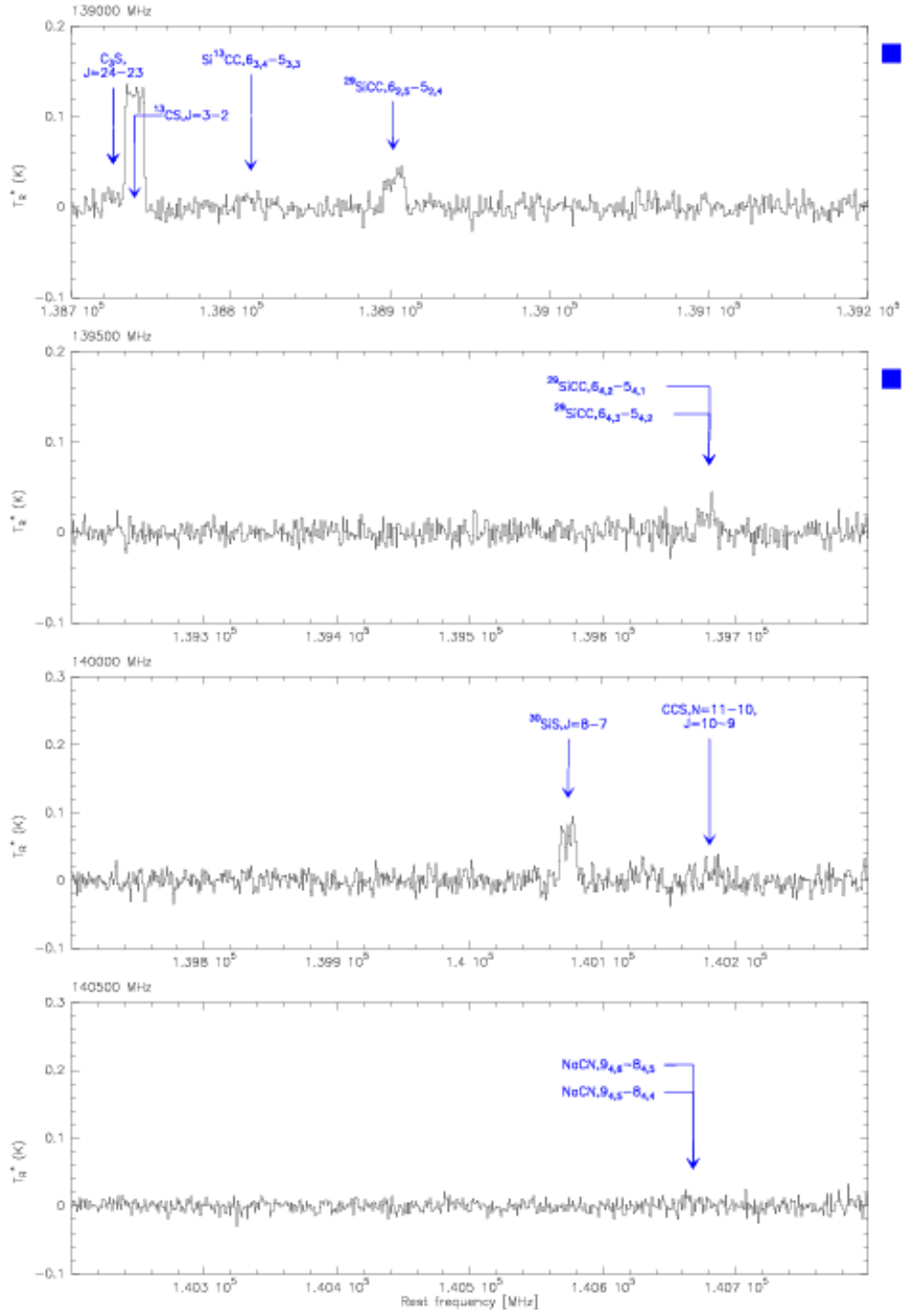


Fig. 3. — Continued.

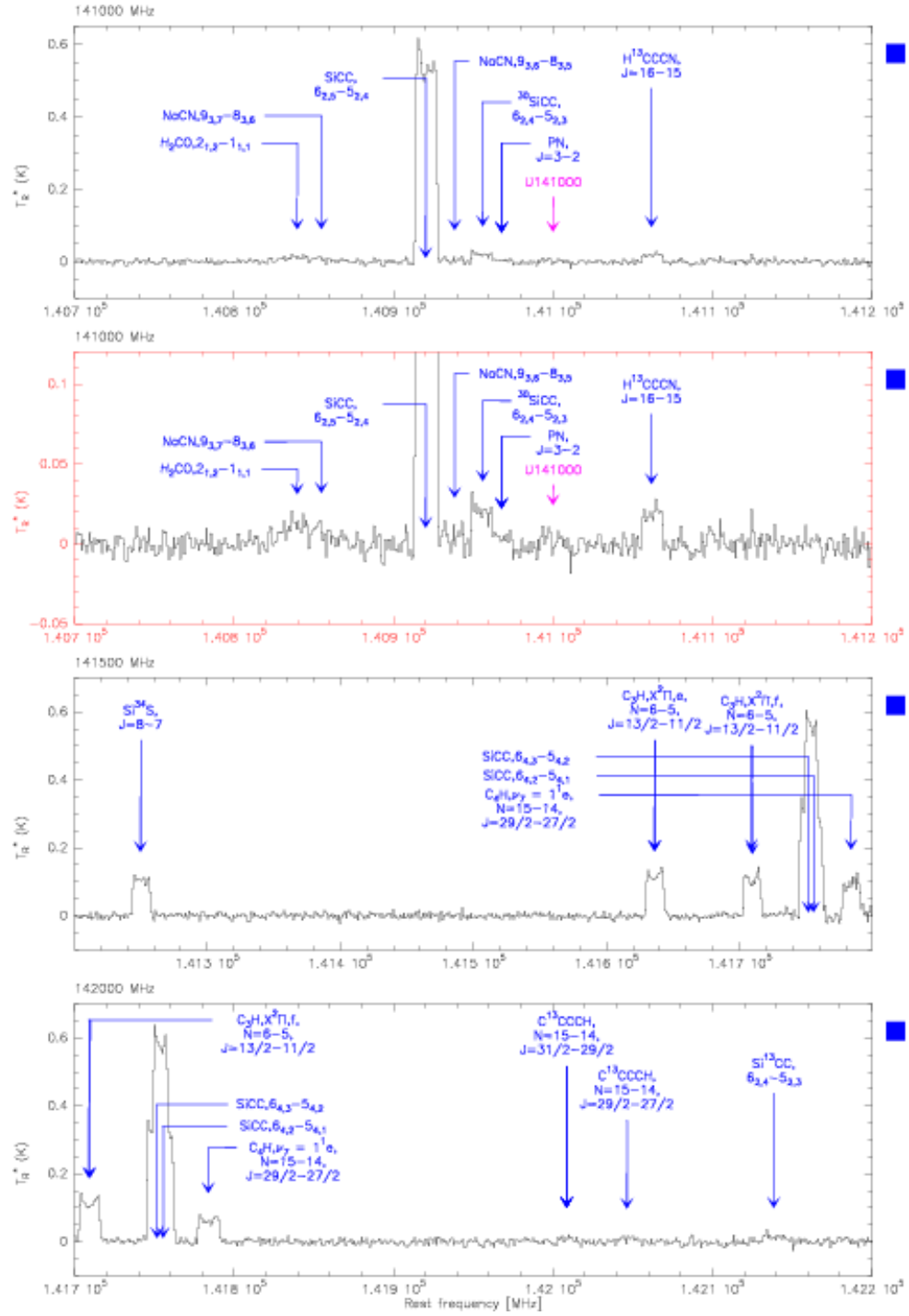


Fig. 3. — Continued.

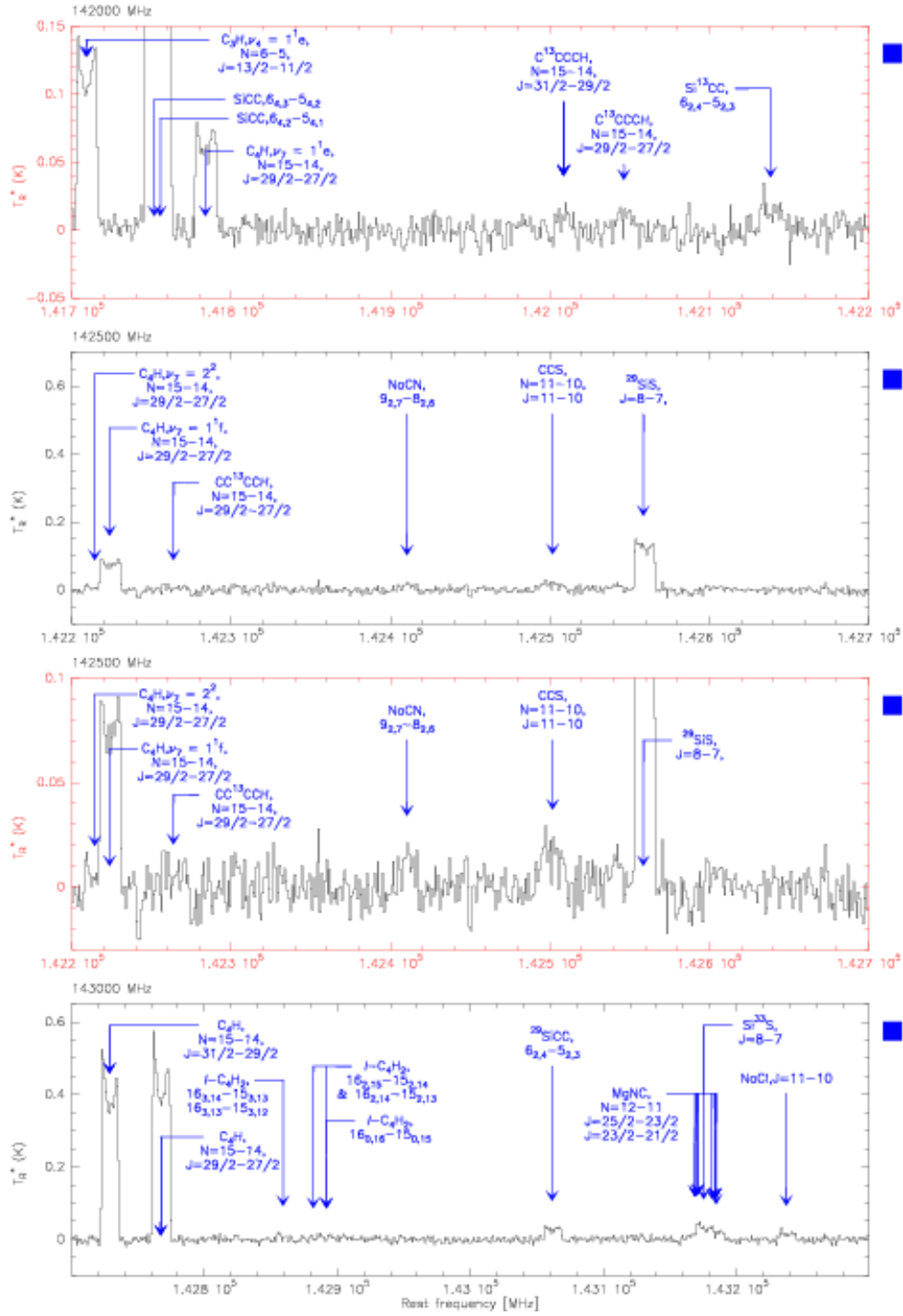


Fig. 3. — Continued.

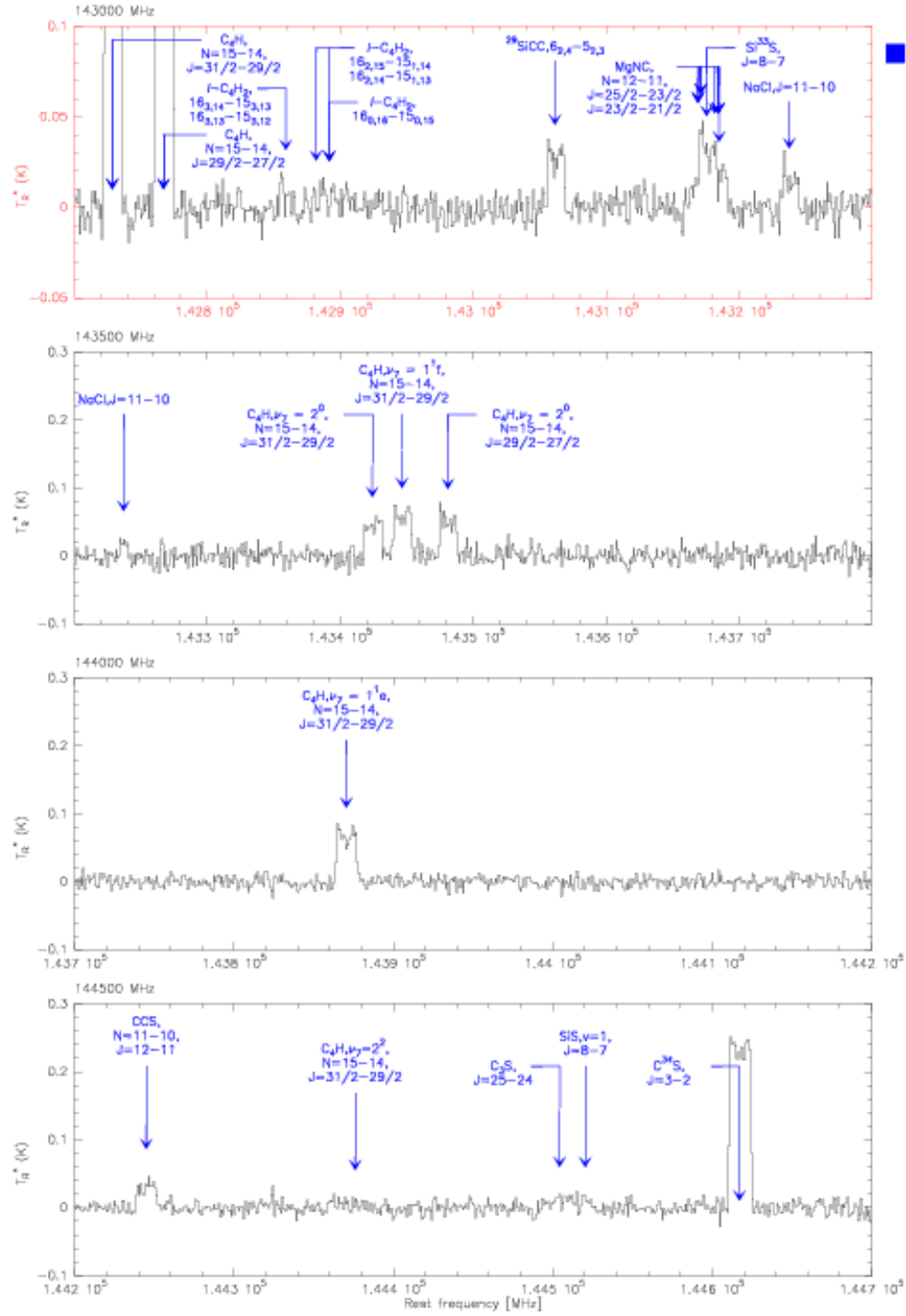


Fig. 3. — Continued.

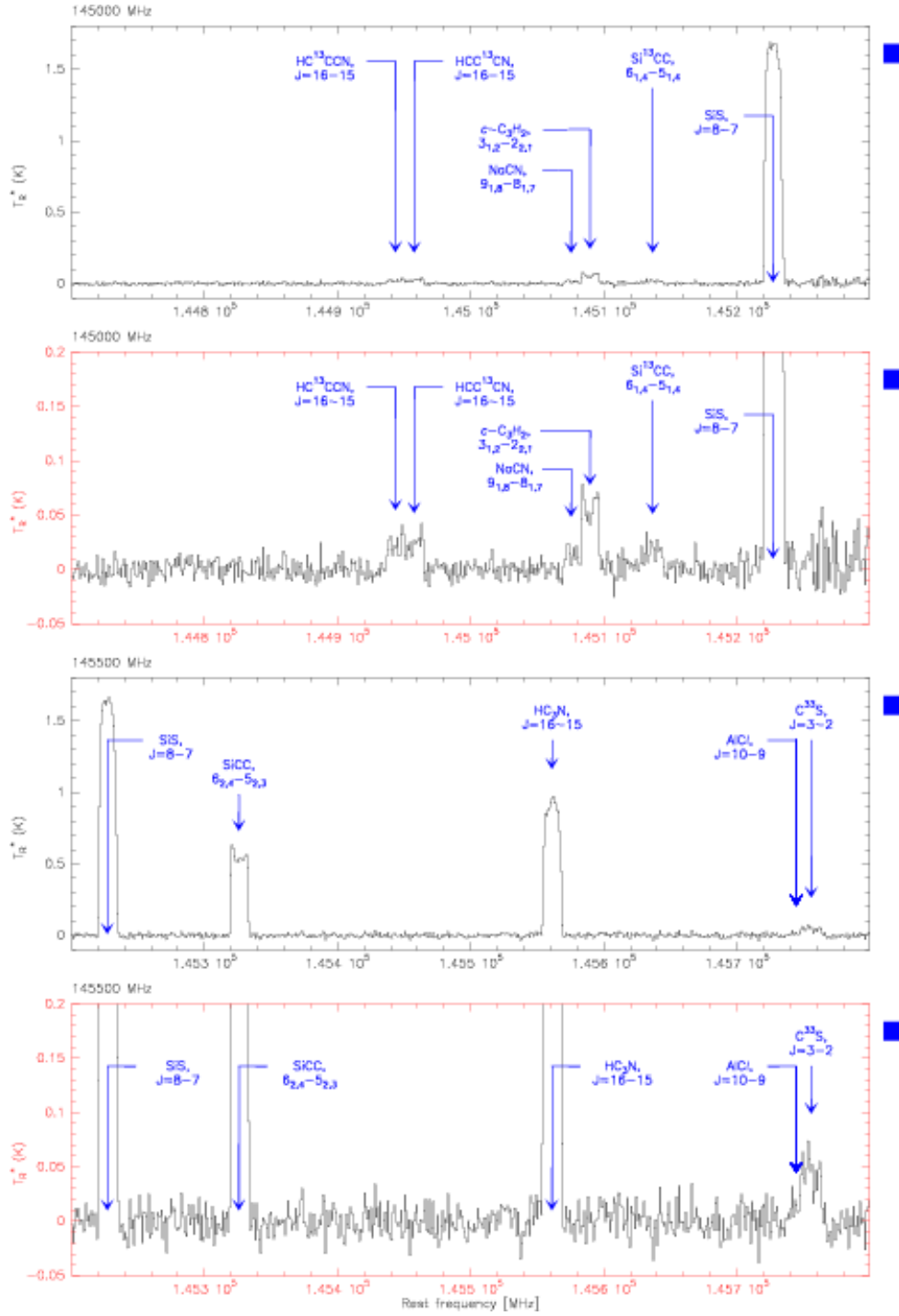


Fig. 3. — Continued.

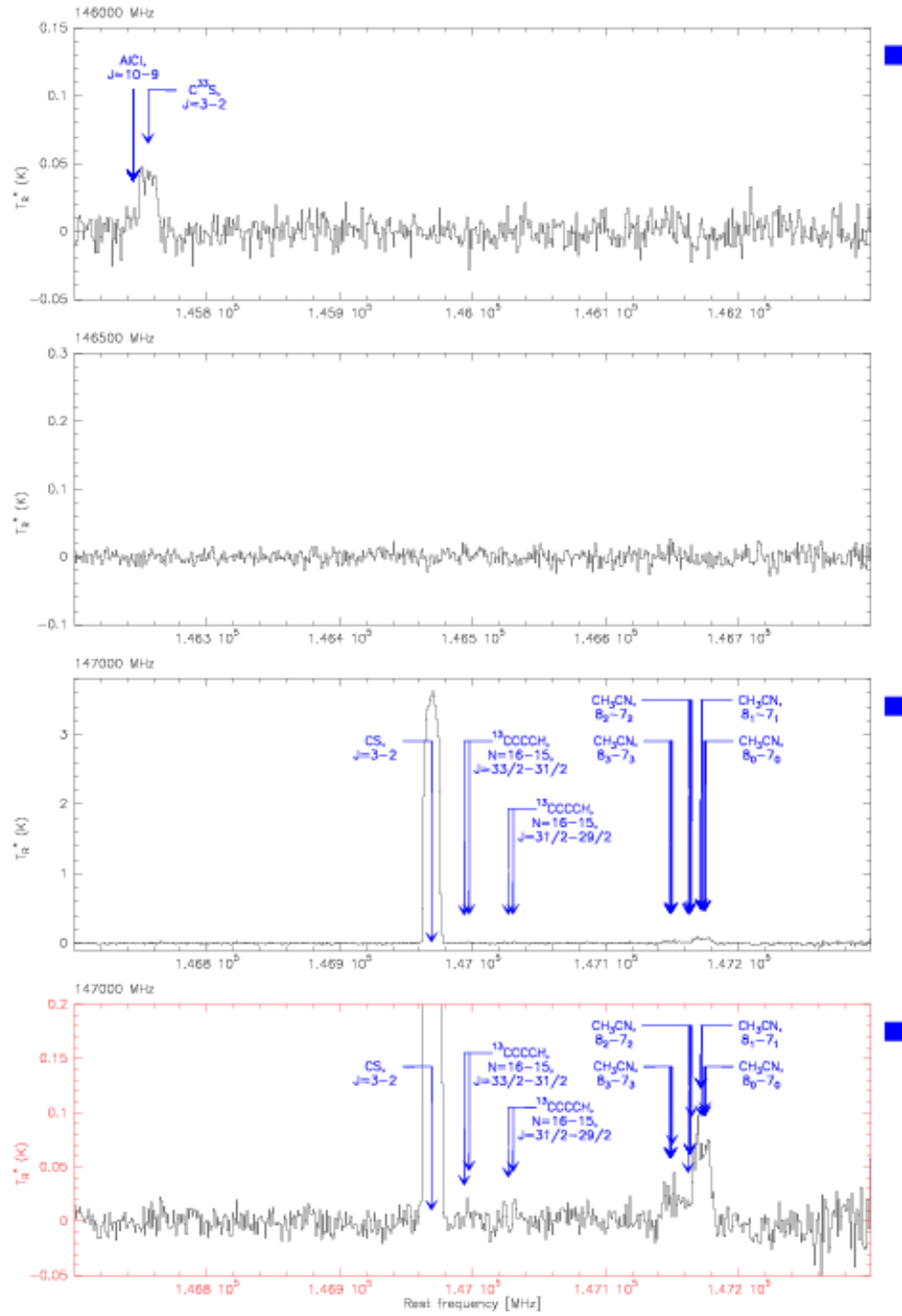


Fig. 3. — Continued.

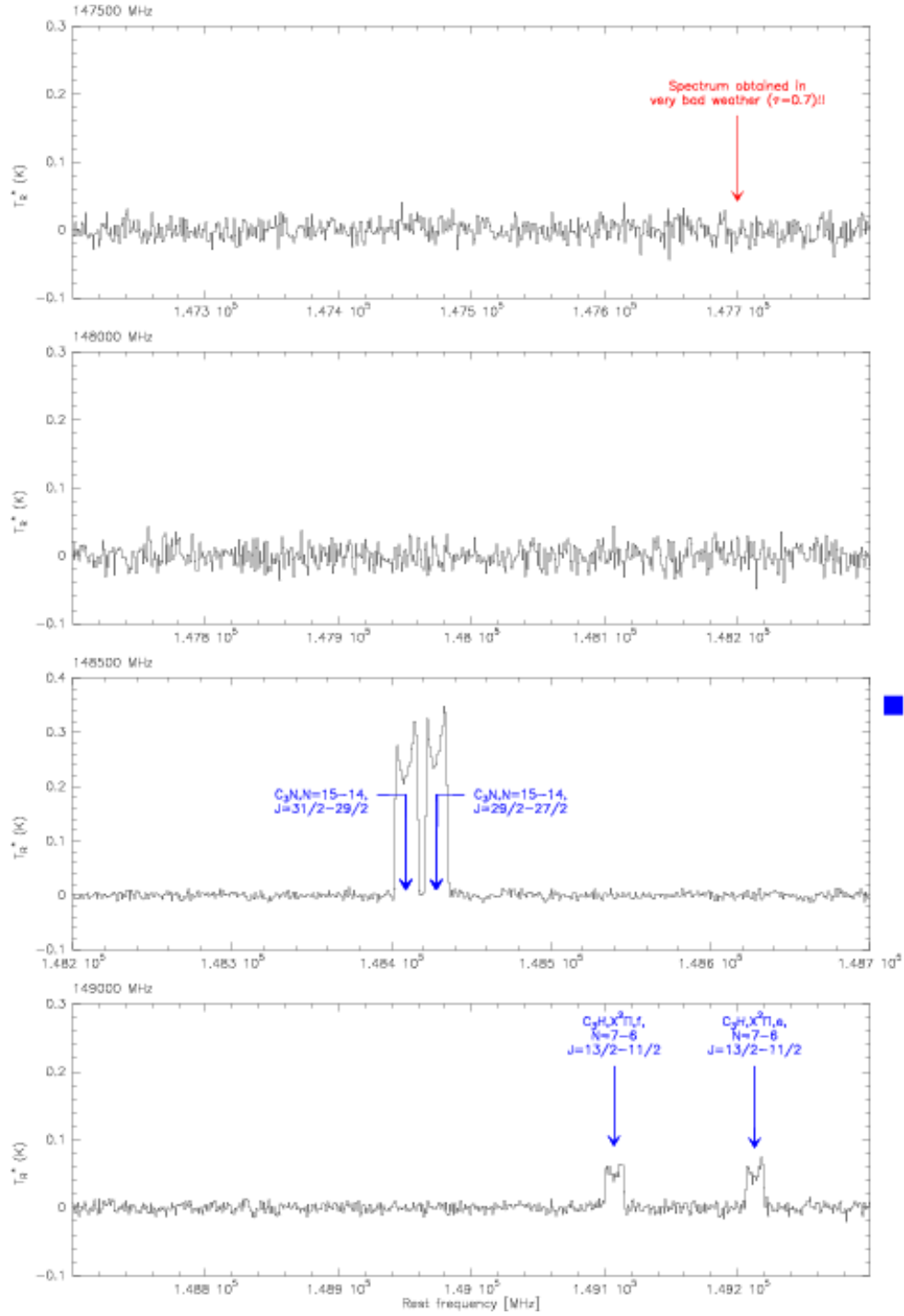


Fig. 3. — Continued.

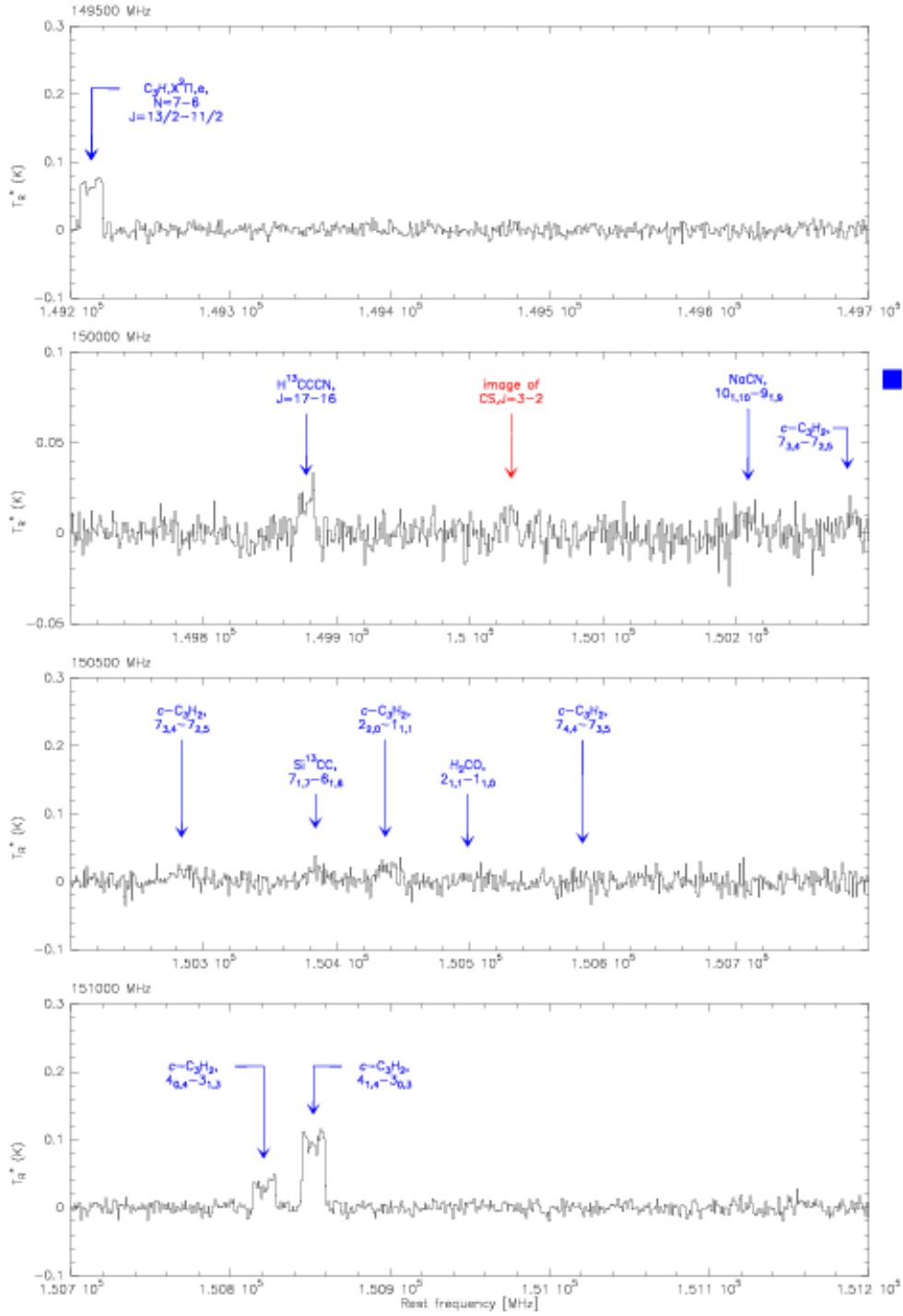


Fig. 3. — Continued.

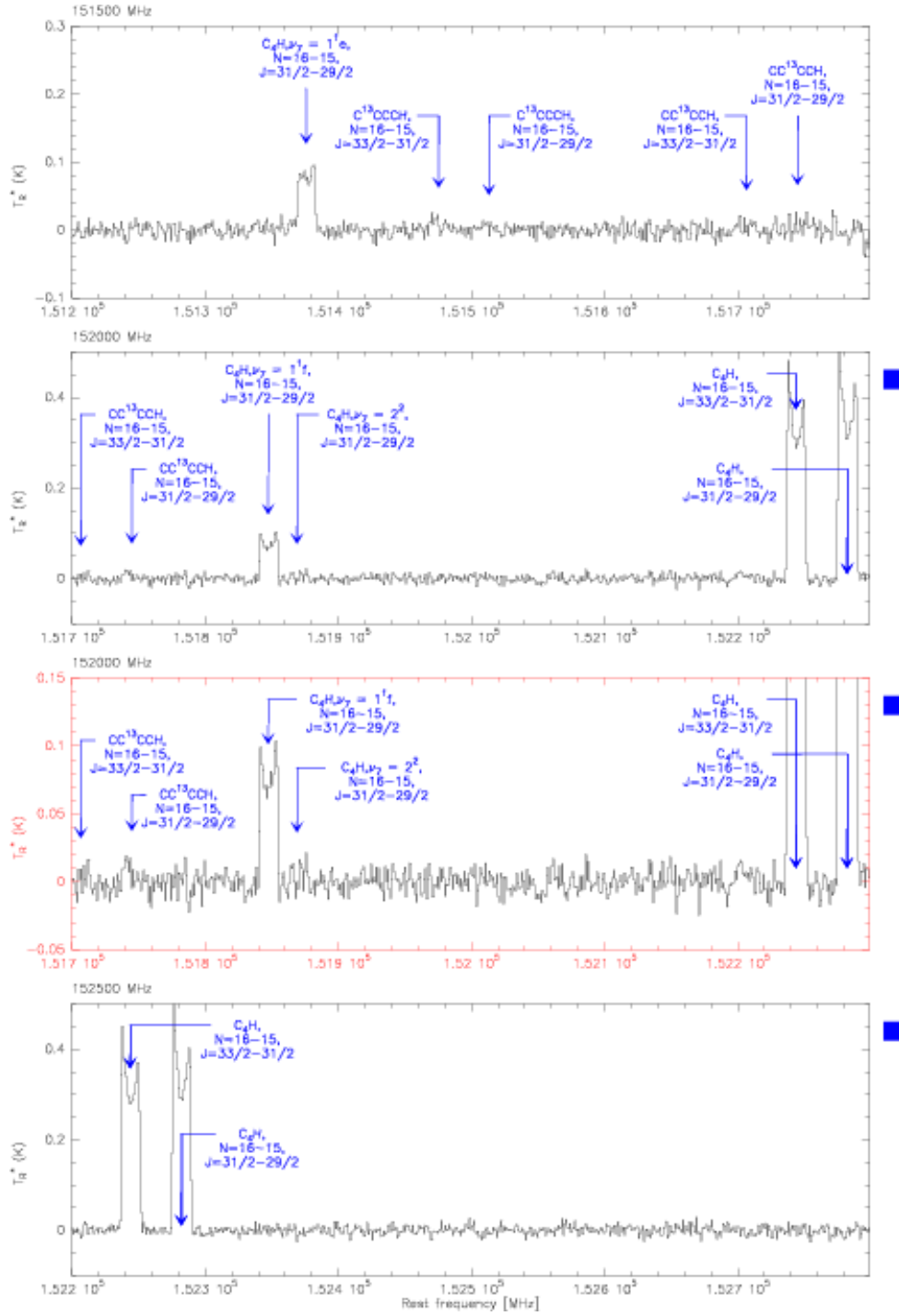


Fig. 3. — Continued.

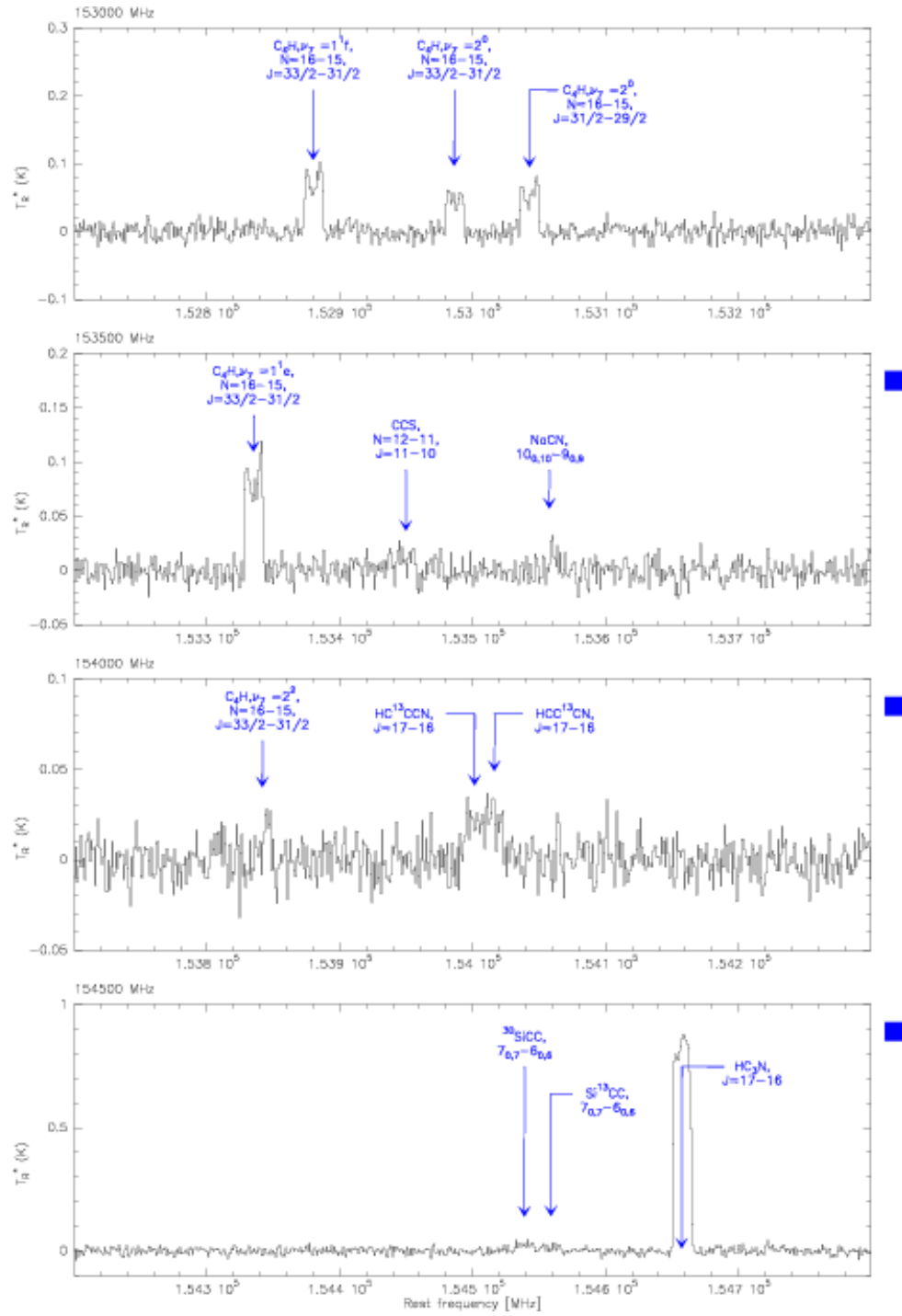


Fig. 3. — Continued.

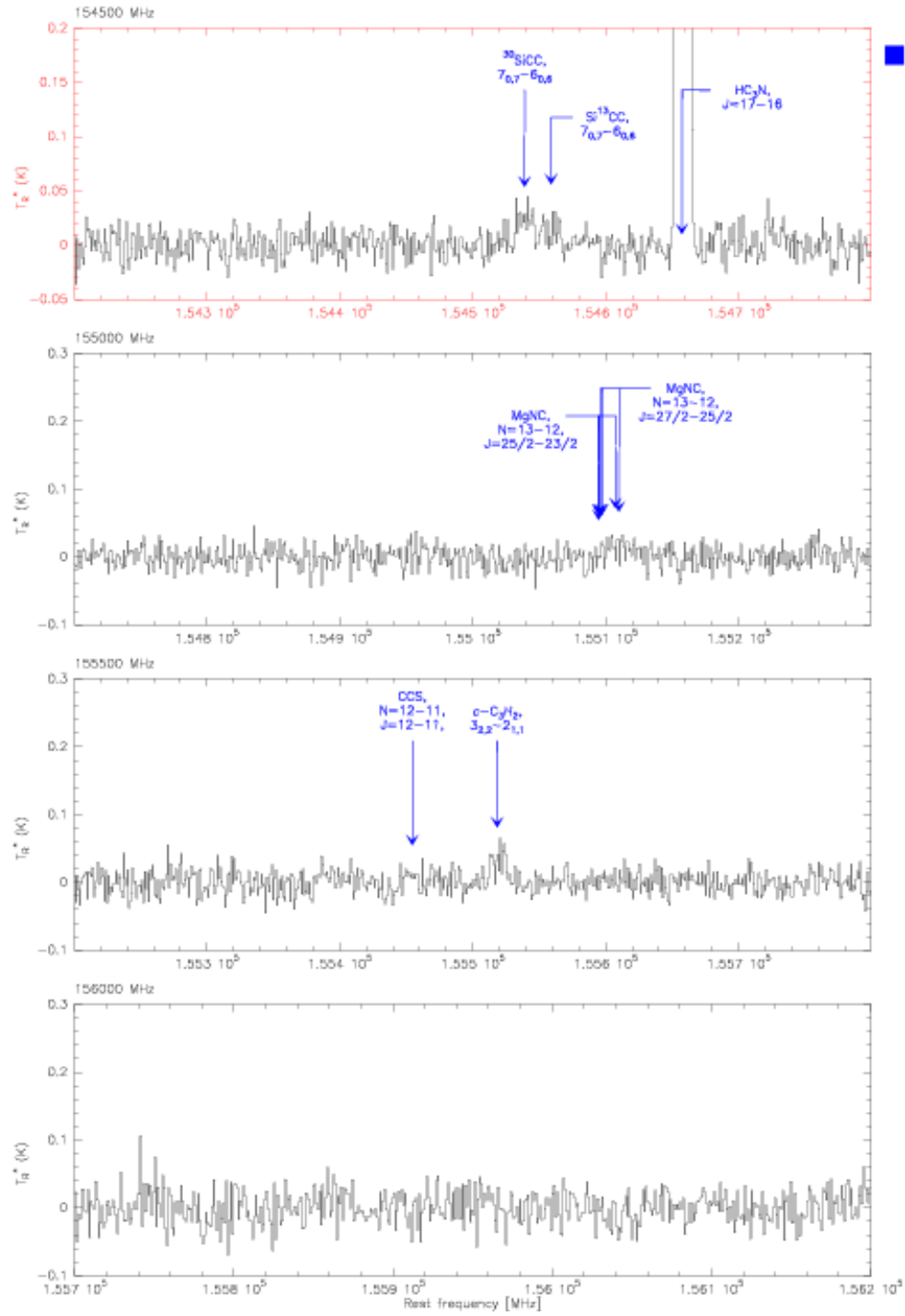


Fig. 3. — Continued.

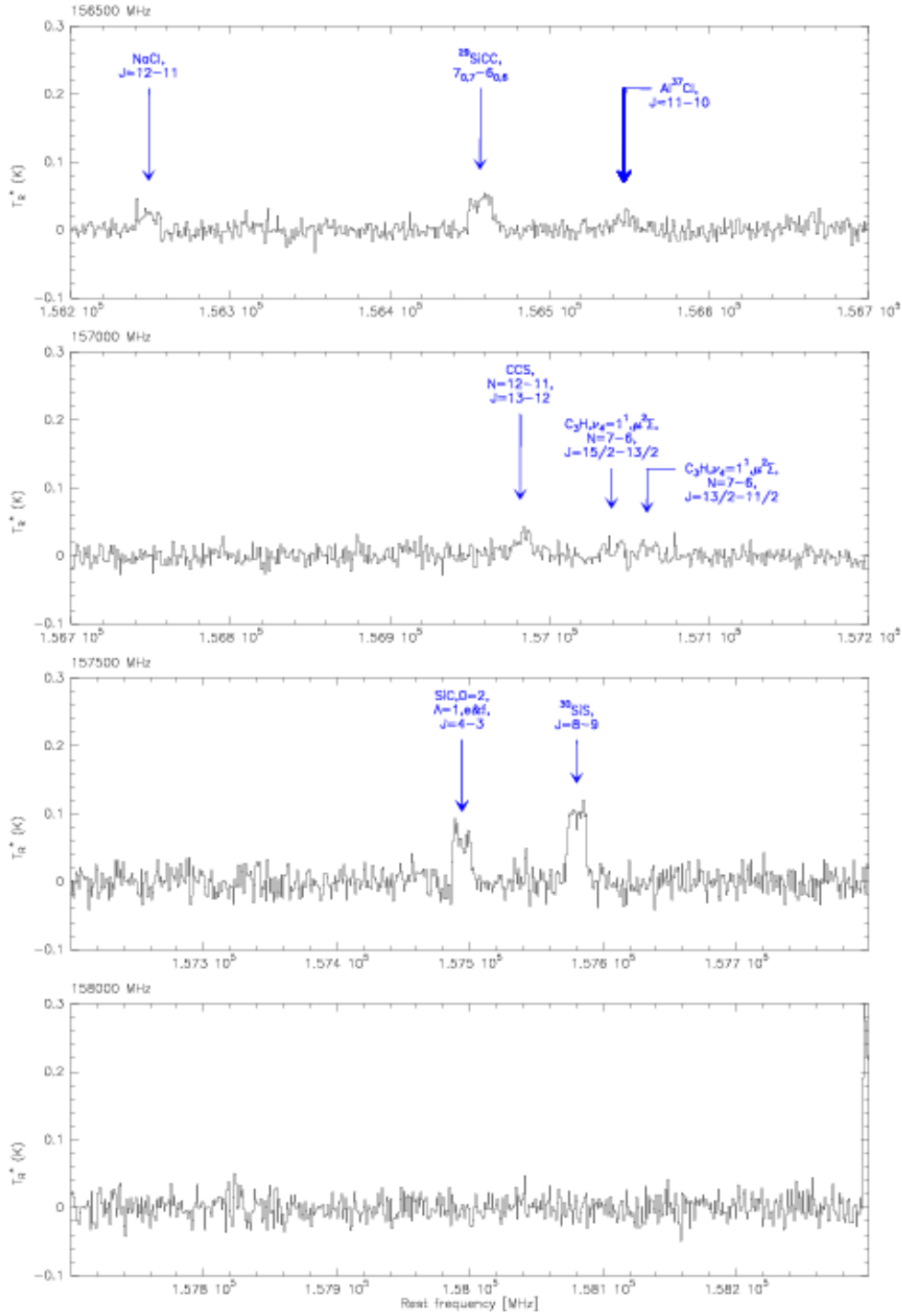


Fig. 3. — Continued.

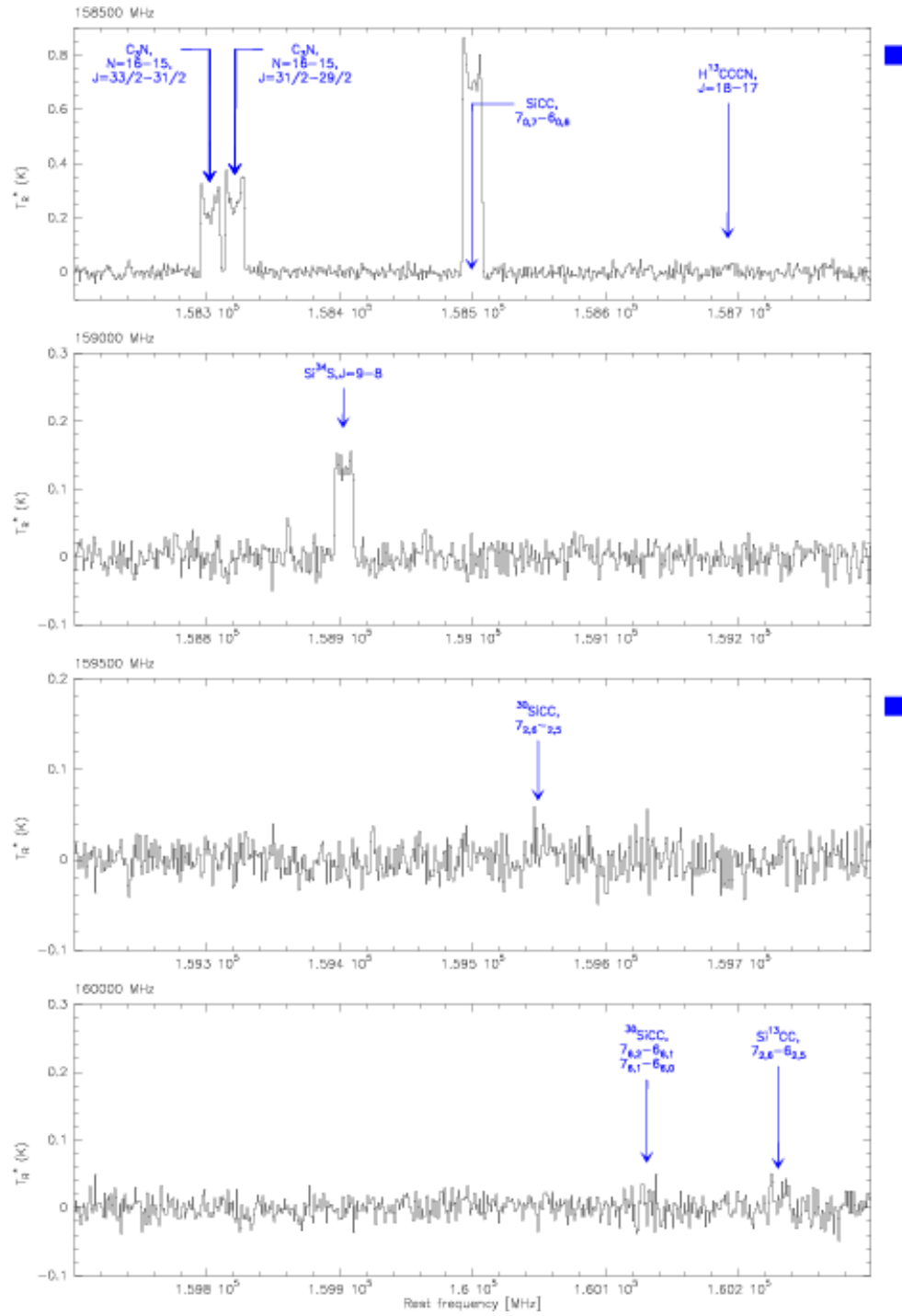


Fig. 3. — Continued.

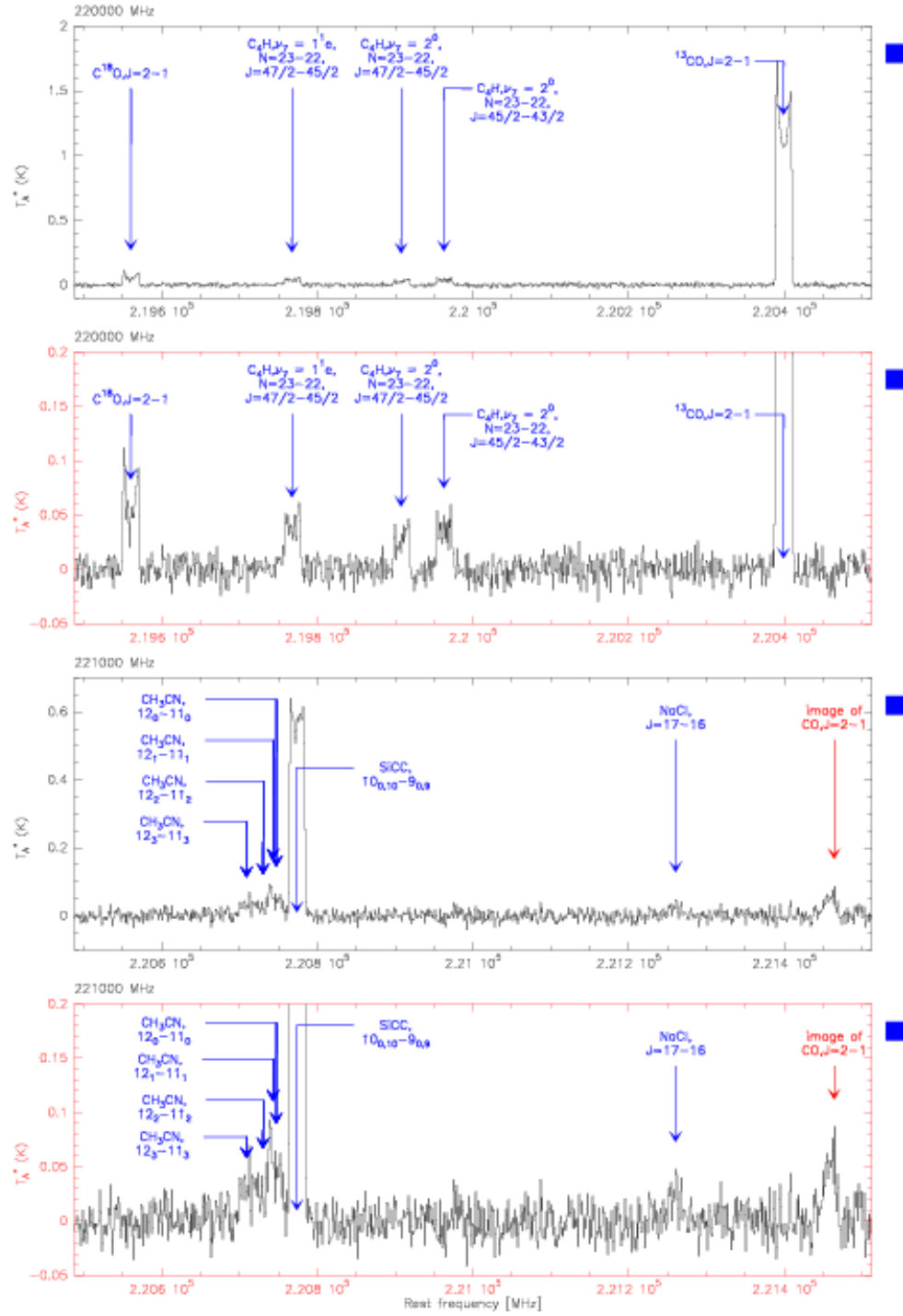


Fig. 3. — Continued.

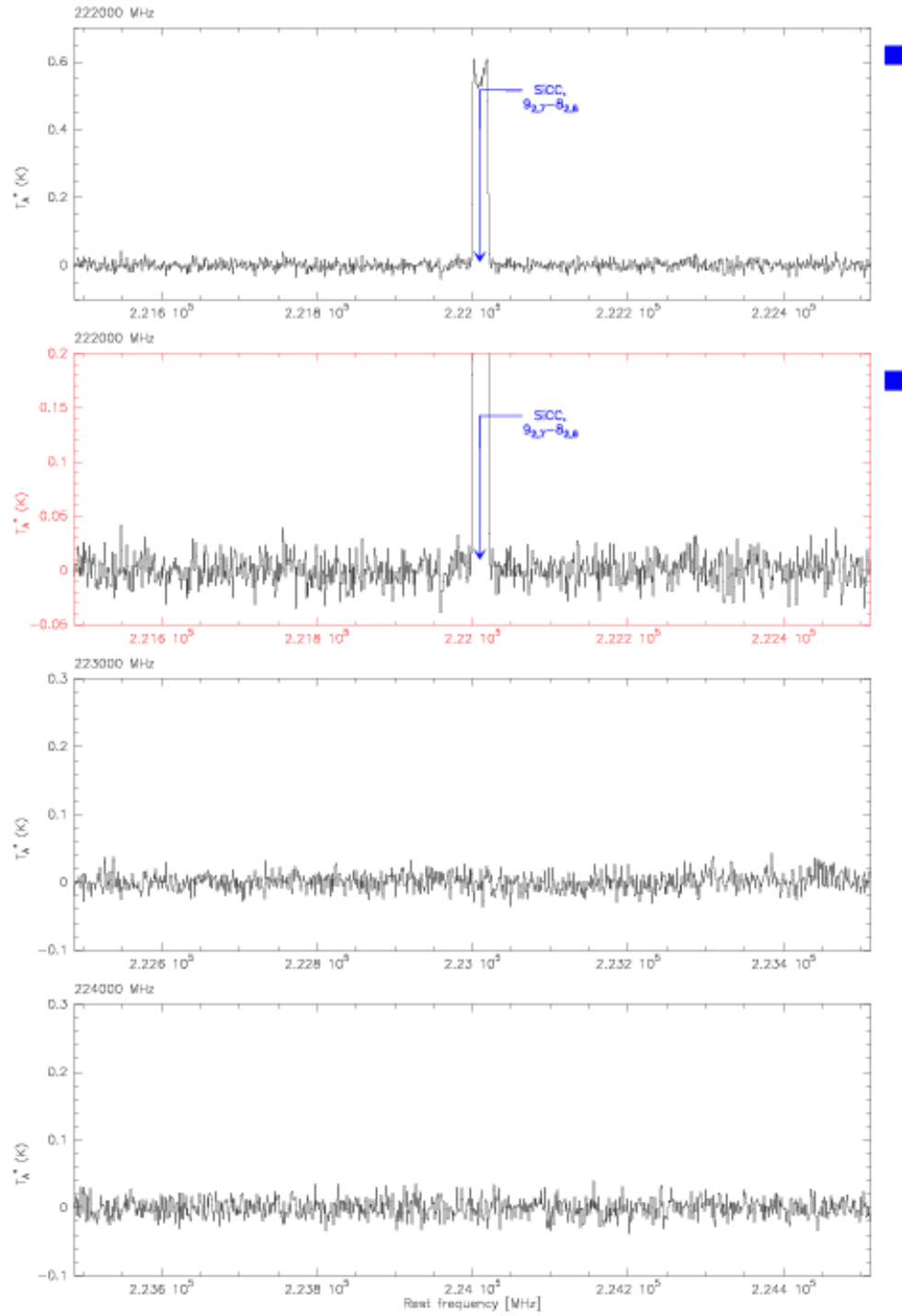


Fig. 3. — Continued.

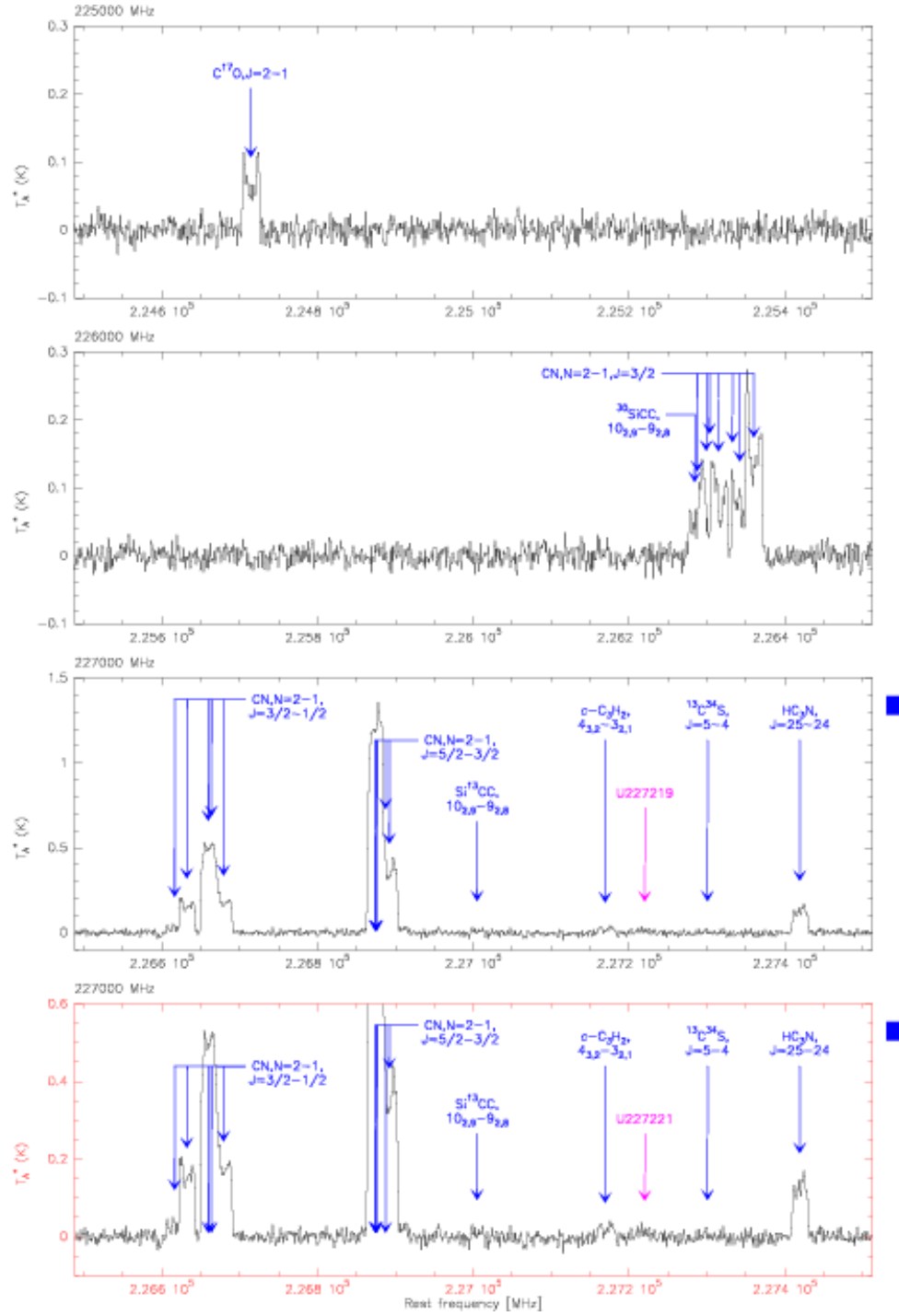


Fig. 3. — Continued.

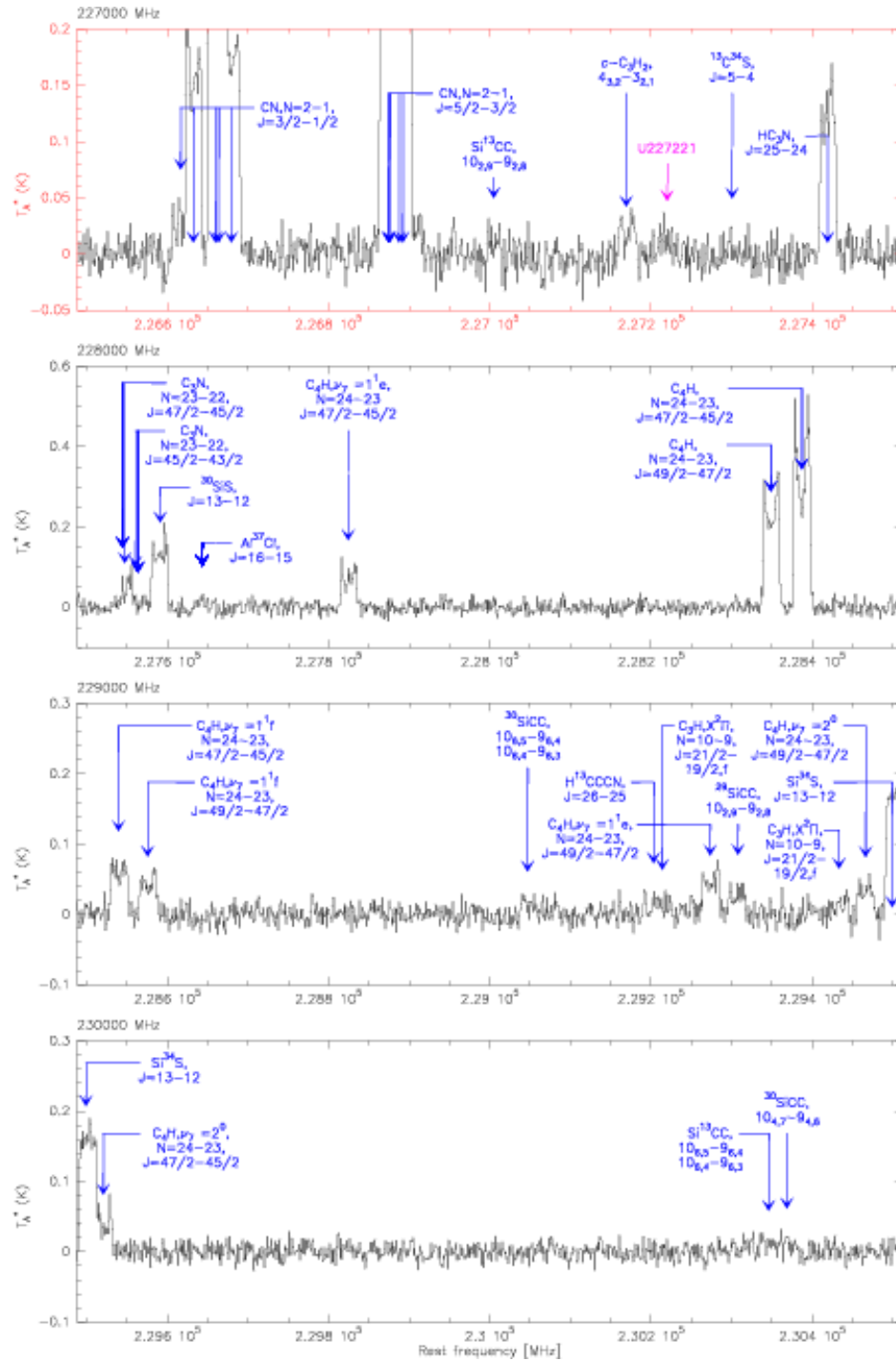


Fig. 3. — Continued.

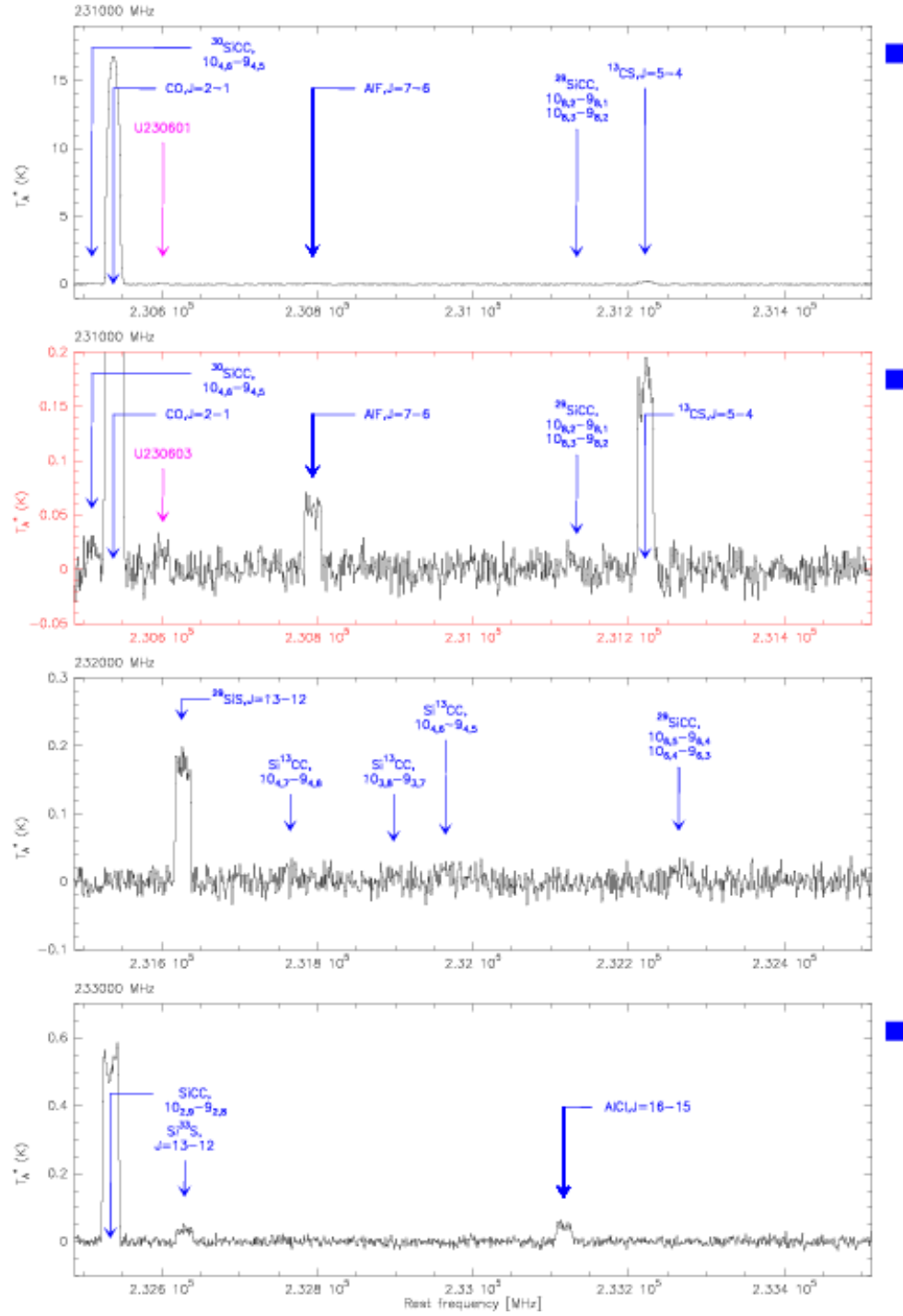


Fig. 3. — Continued.

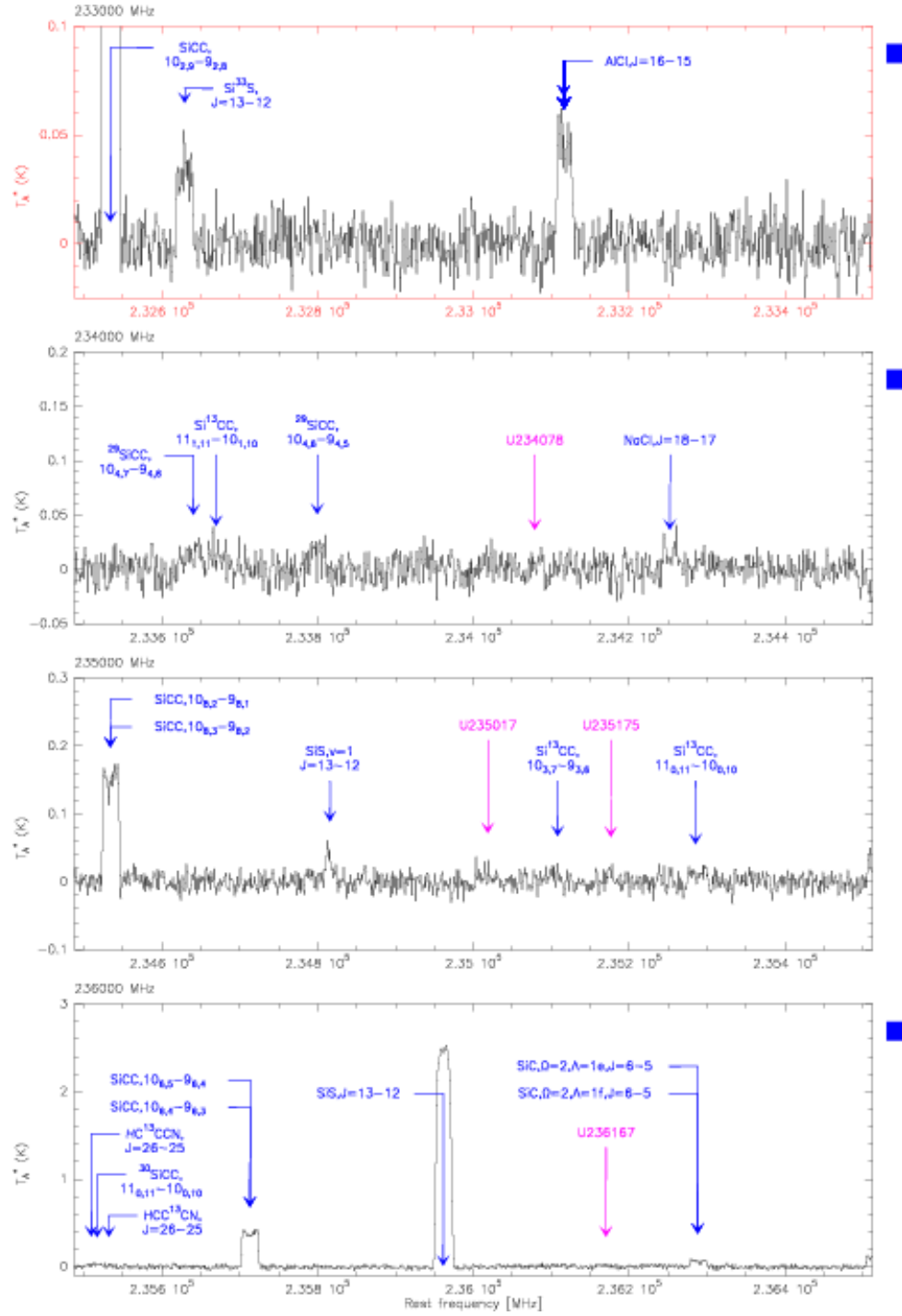


Fig. 3. — Continued.

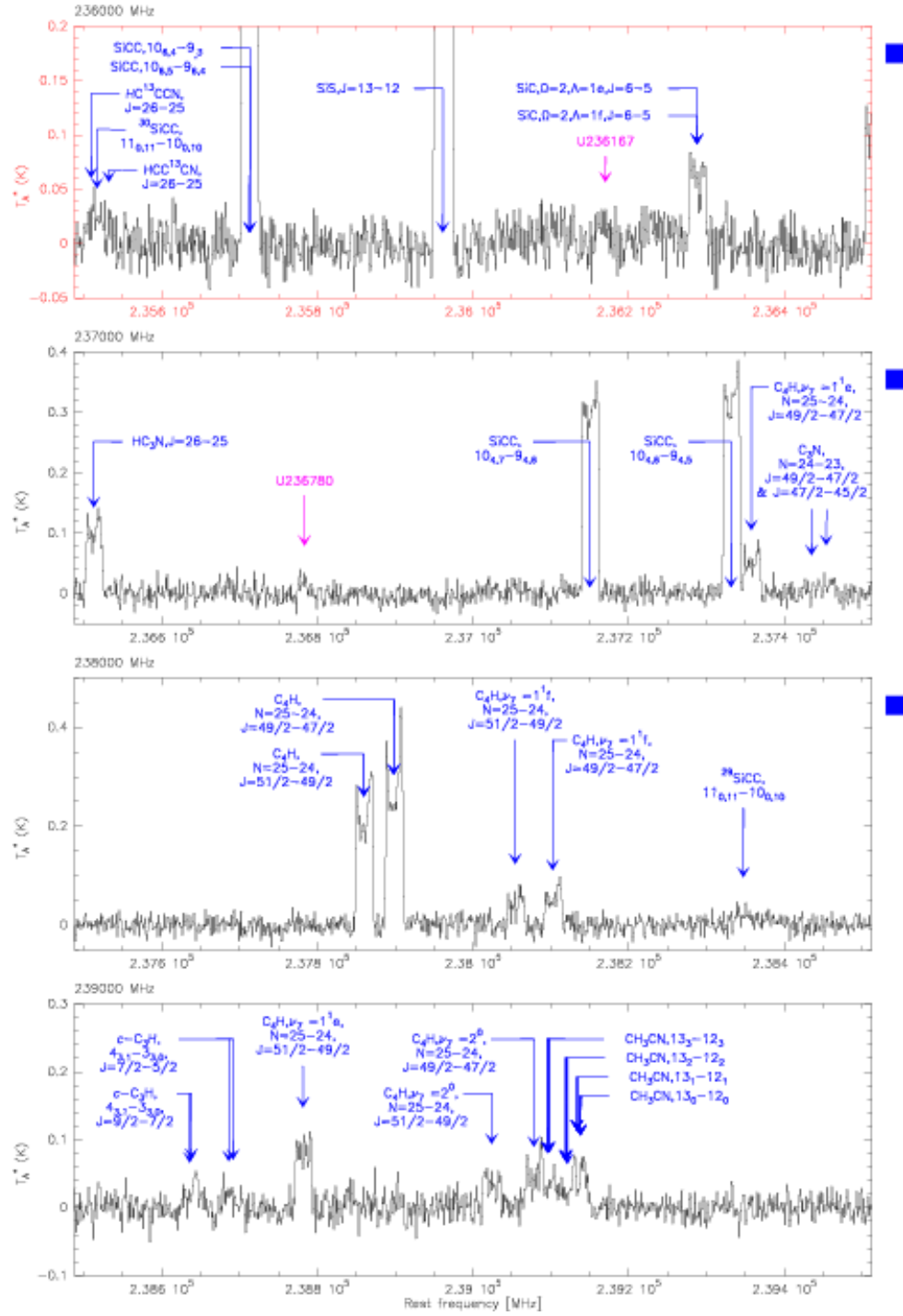


Fig. 3. — Continued.

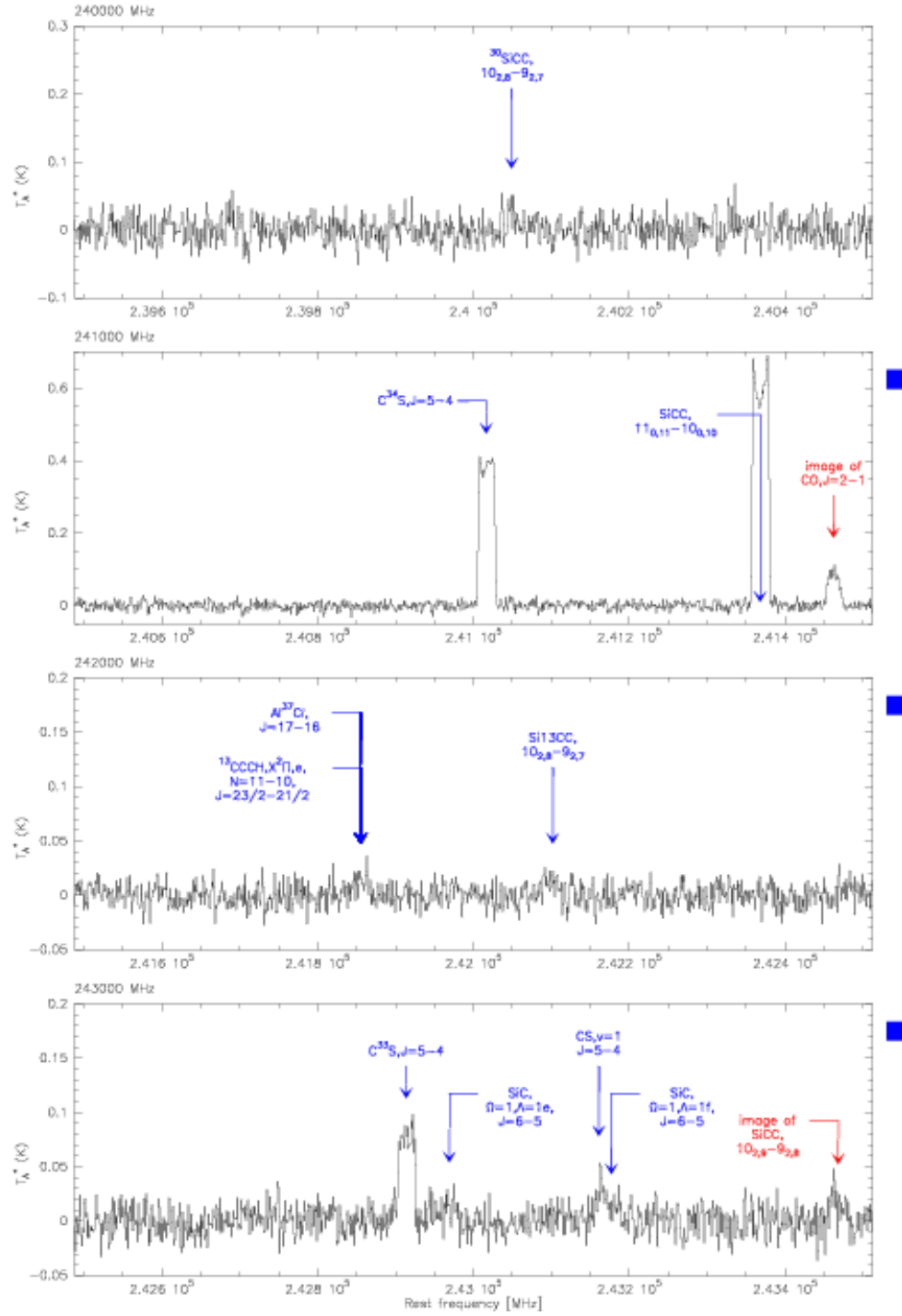


Fig. 3. — Continued.

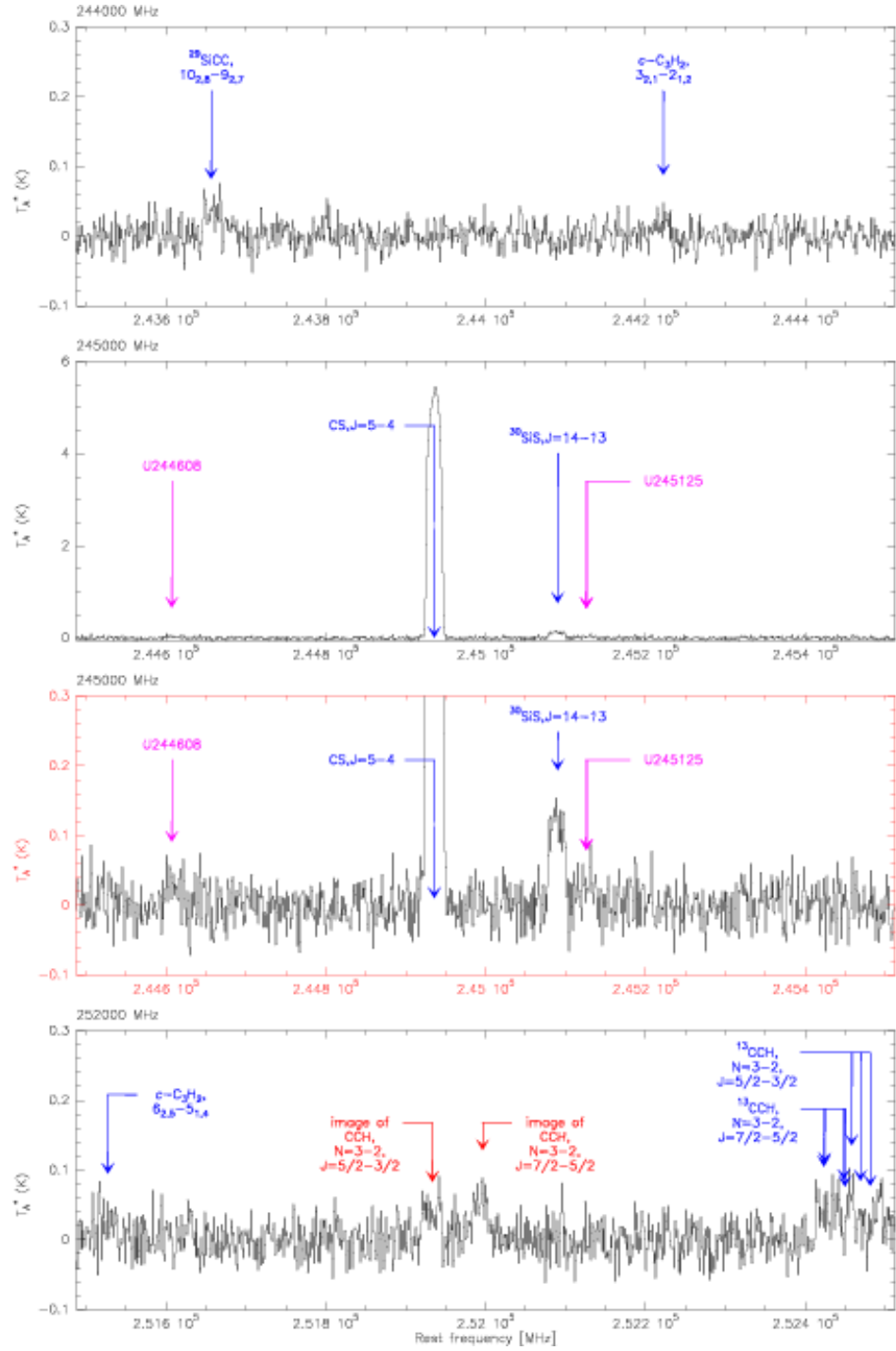


Fig. 3. — Continued.

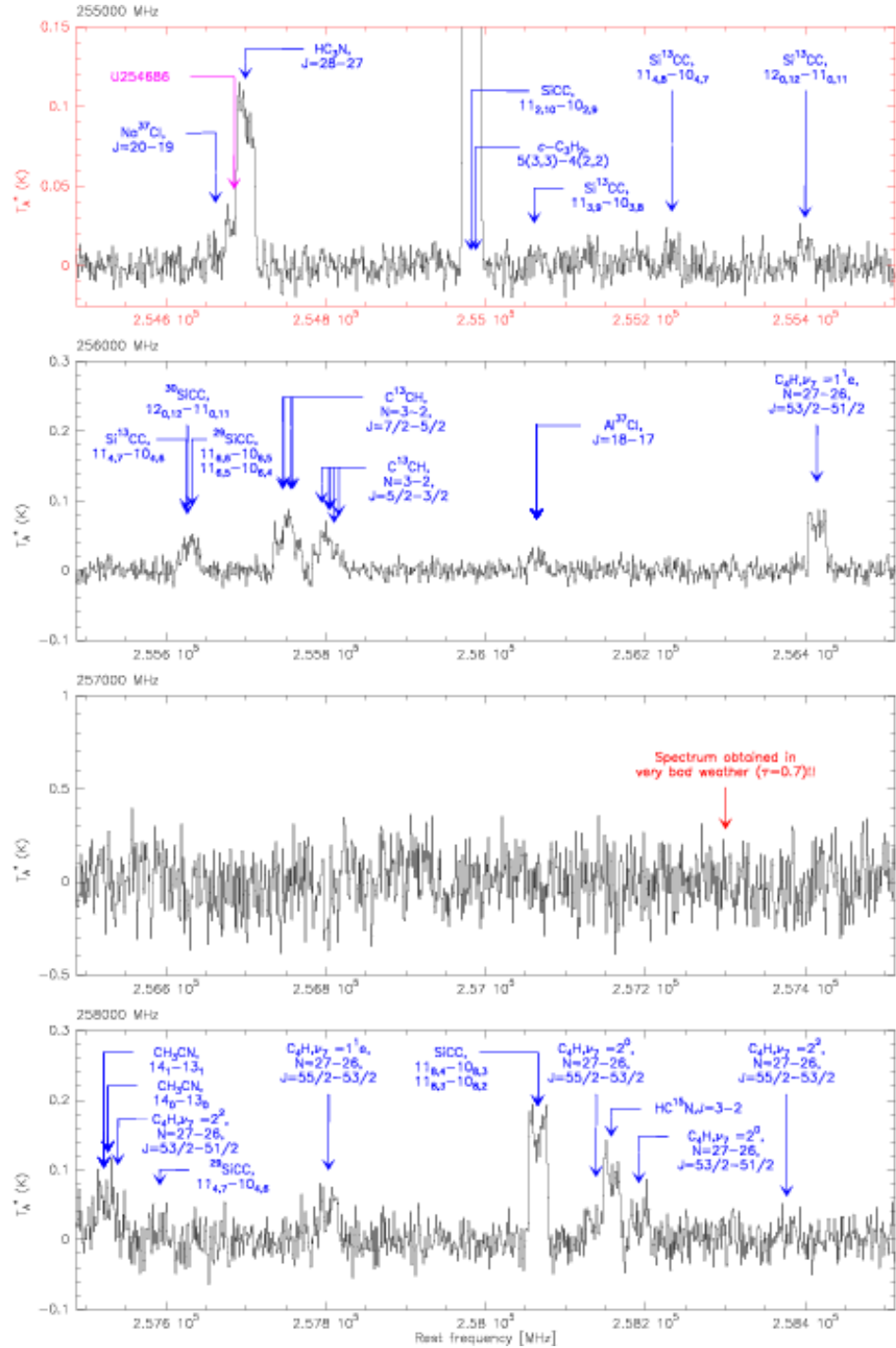


Fig. 3. — Continued.

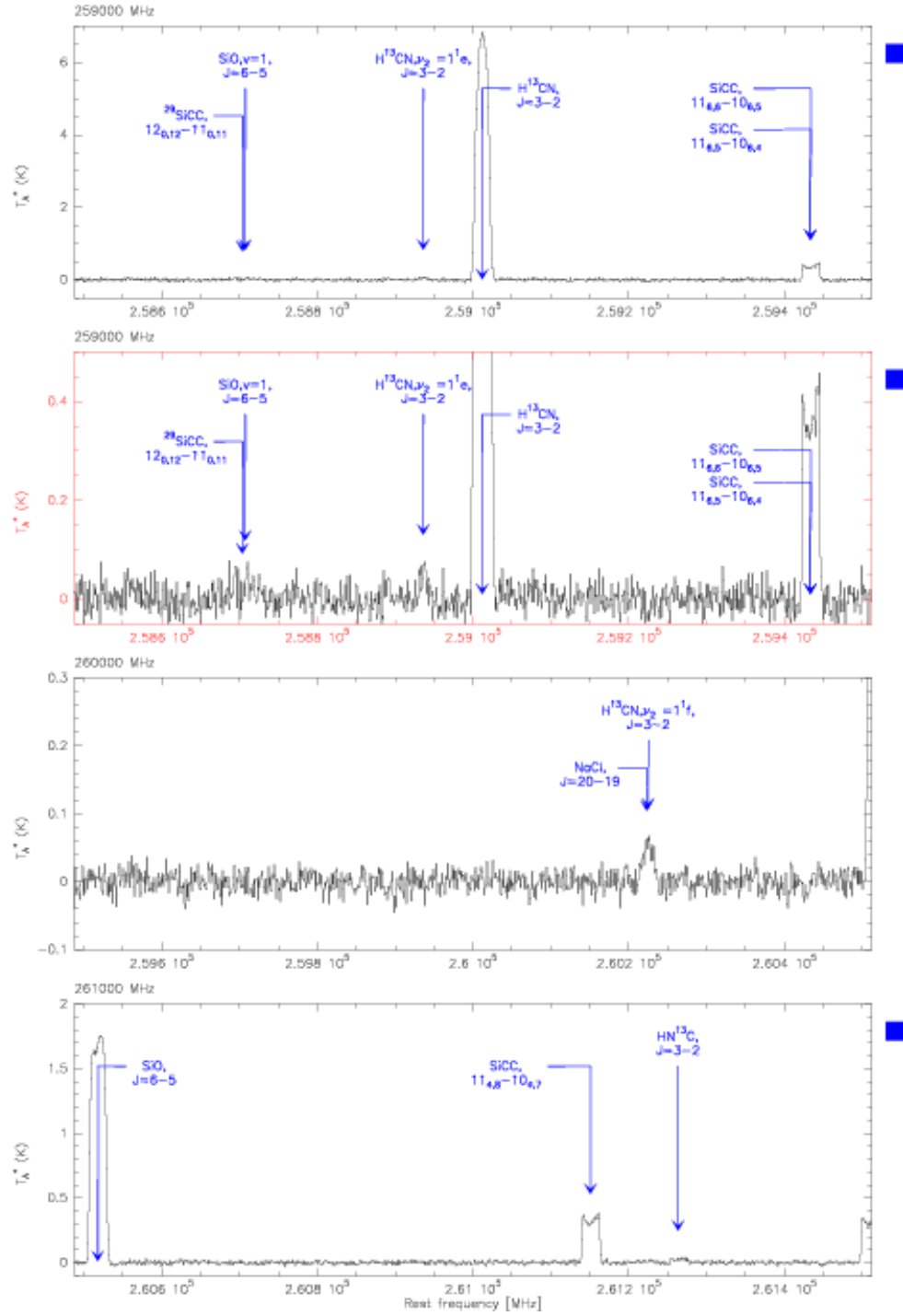


Fig. 3. — Continued.

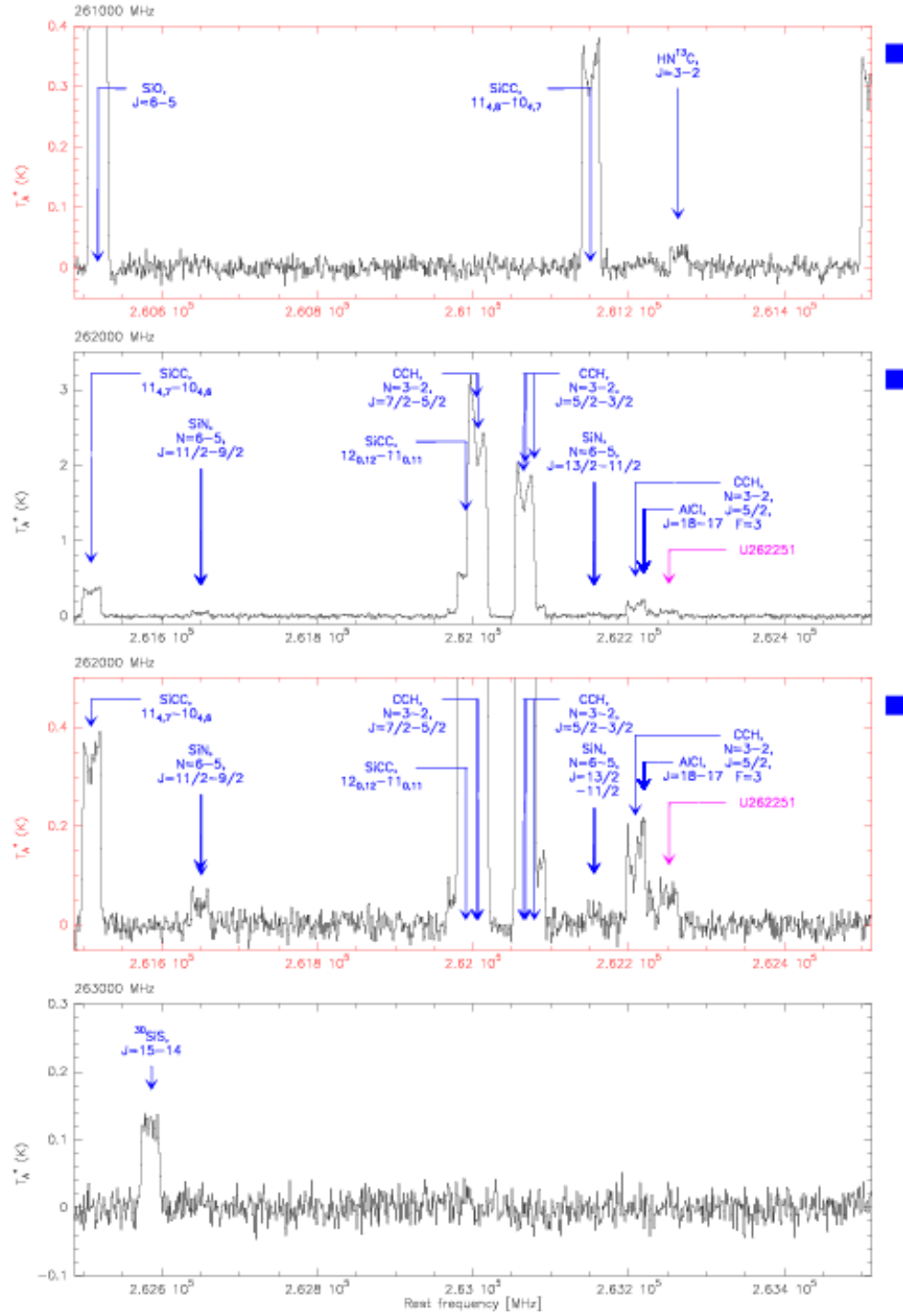


Fig. 3. — Continued.

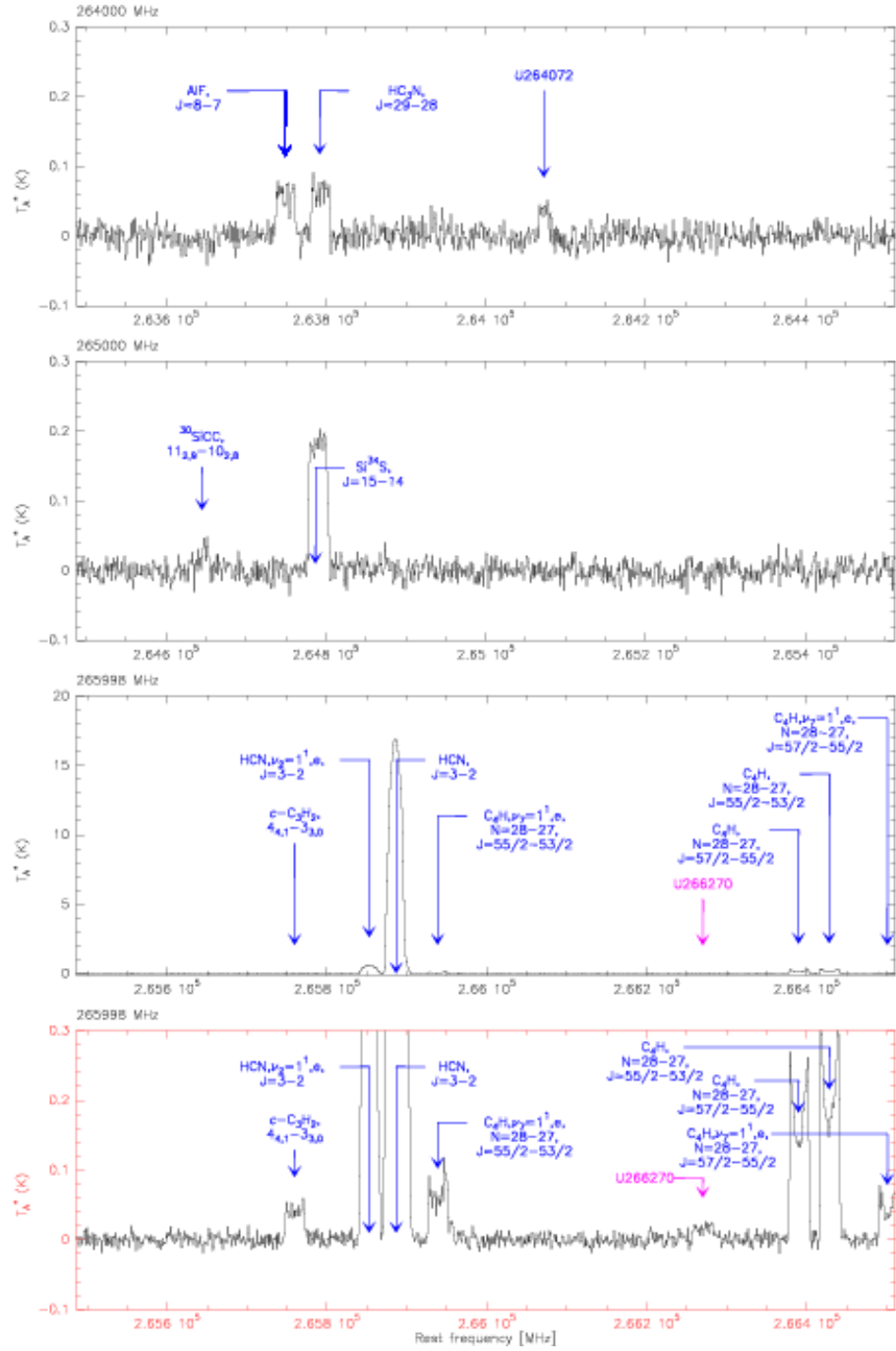


Fig. 3. — Continued.

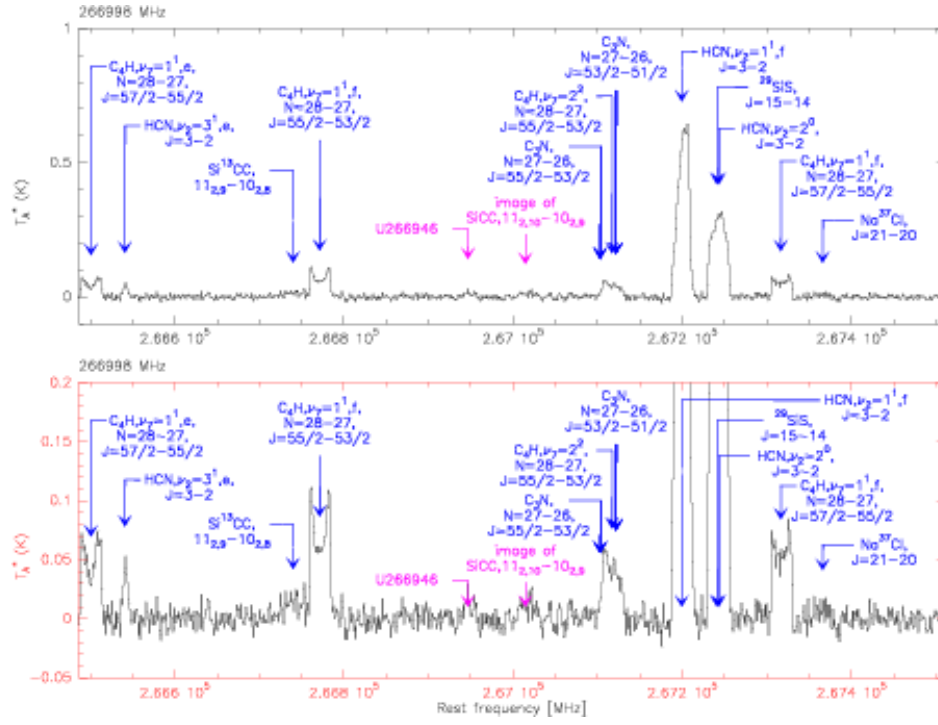


Fig. 3. — Continued.

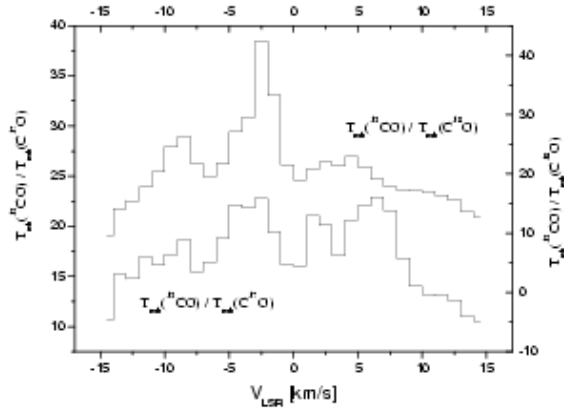


Fig. 4.— The channel-by-channel $J = 2 - 1$ line intensity ratios $T_{\text{mb}}(^{13}\text{CO})/T_{\text{mb}}(\text{C}^{17}\text{O})$ and $T_{\text{mb}}(^{13}\text{CO})/T_{\text{mb}}(\text{C}^{18}\text{O})$ against LSR velocity ($-14.5, +14.5$) km s^{-1} that show opacity effects on both edges of the profile (the drop-down trends).